ISBN 978-82-471-1911-2 (printed ver.)
ISBN 978-82-471-1912-9 (electronic ver.)
ISSN 1503-8181

Doctoral theses at NTNU, 2009:250

Kristian Berbom Dahl

# Mechanical properties of clear wood from Norway spruce

NTNU
Norwegian University of
Science and Technology

Kristian Berbom Dahl

Doctoral Thesis

NTNU
Norwegian University of
Science and Technology

Thesis for the degree of
philosophiae doctor

Faculty of Engineering Science and Technology
Department of Structural Engineering

Doctoral theses at NTNU, 2009:250

NTNU

NTNU
Norwegian University of
Science and Technology

Kristian Berbom Dahl

# Mechanical properties of clear wood from Norway spruce

Thesis for the degree of philosophiae doctor

Trondheim, December 2009

Norwegian University of
Science and Technology
Faculty of Engineering Science and Technology
Department of Structural Engineering

NTNU
Norwegian University of
Science and Technology

NTNU
Norwegian University of Science and Technology

Thesis for the degree of philosophiae doctor

Faculty of Engineering Science and Technology
Department of Structural Engineering



ISBN 978-82-471-1911-2 (printed ver.)
ISBN 978-82-471-1912-9 (electronic ver.)
ISSN 1503-8181

Doctoral Theses at NTNU, 2009:250

Printed by Tapir Uttrykk

*Isn't it good - Norwegian wood?*

The Beatles (1965)

# Preface

This doctoral thesis is submitted to the Norwegian University of Science and Technology (NTNU) for the degree Philosophiae Doctor (PhD). The work has been carried out at the Department of Structural Engineering, Faculty of Engineering Science and Technology at NTNU, with Professor Kjell Arne Malo as the main supervisor and Professor Kolbein Bell as co-supervisor. The project was started in August 2003 and completed for submission in August 2009, including approximately one year of leave to conduct external projects. The thesis is presented on an article based form containing eight papers and an introductory part with theoretical background and conclusions.

# Abstract

This thesis reports mechanical properties of clear wood from Norway spruce, comprising each orthotropic material direction and plane over the complete loading range till failure. The material properties are quantified in a set of linear, nonlinear and failure parameters. In addition, statistical distributions and inter-parametric correlations are presented. Several quantities have hardly been studied for Norway spruce earlier, and are also scarcely documented for spruce softwood in general.

The properties were determined by means of experimental tests in conjunction with numerical analyses. In order to obtain accurate and applicable results suitable for input in numerical simulations, the tests were mostly based on non-standardized procedures. Normal stress behaviour was investigated by means of compressive and tensile tests, whereas shear properties were based on the Arcan method. Constant climatic conditions and loading rates were applied and no effects from variation in humidity, temperature, size, loading rate or load duration were studied. The wood comprises graded and ungraded material from the spruce subspecies *Picea Abies* (L.) Karst., with provenance Southern Norway. The use of material from the outer part of wooden stems enabled suitable specimens of various categories with material axes complying with a Cartesian coordinate system. Video extensometry was used for contact free strain measurements. All combinations of load directions and orthotropic measurement planes were tested. The 12 linear elastic orthotropic parameters were based on both loading and unloading, and were, in general, found to correspond relatively well with values reported for other spruce species. Characterization of the upper stress ranges was also emphasized, as accurate predictions of ultimate deformations and capacities are crucial in many analyses. Nonlinearity and ductility were, as normally assumed, found in compression, especially transversely. A more peculiar finding was the observation of a varying degree of nonlinearity in tension, and particularly in shear. The nonlinearity was adapted to bilinear models for each stress component, and for the case of shear, to exponential Voce models. The failure parameters were adapted to the ultimate stress and the Tsai-Wu failure criteria. In order to remove configuration and measurement effects, potentially distorting the material parameters, numerical FEM models were used to modify nominal values.

The relatively large quantity of parametric observations enabled investigation of statistical distributions for each material parameter. Moreover, correlations between values determined from the same test could be estimated. Hence, the work constitutes a basis for deterministic and probabilistic numerical analyses of spruce softwood on the macro scale level (0.1–1.0 m), suitable for general three-dimensional studies of details and joints in timber constructions.

# Acknowledgements

This work has been funded by the Norwegian Research Council through the Strategic University Program *Wood as a building material* coordinated by Professor Per Jostein Hovde at NTNU. It has moreover been supported by the engineering company Multiconsult AS in Oslo, where I have been employed since before this work was commenced. Their contributions and patience are kindly acknowledged, and I would like to express my deepest gratitude to them for making the project possible.

I would like to thank Professor Kjell Arne Malo for valuable guidance, many constructive discussions and manuscript readings in addition to taking care of administrative issues. His introduction to the topic, feedback on experimental and numerical work and critical review has been important. The fact that I was allowed to pursue a more fundamental study on the mechanical properties of clear wood, even though the plans initially seemed too time-consuming, is appreciated.

I'm also grateful to Professor Kolbein Bell and colleagues at the Department of Structural Engineering for a nice working environment and social atmosphere. The subject and social gathering among the many PhD students over the years have been highly appreciated. I would especially thank Knut B. Lunde for many canteen dinners with accompanying discussions and practical feedback on statistics, software and research papers. The research comprises a substantial amount of experimental work, and the collaboration with the staff in the laboratory has been appreciated. I'm also grateful to the former master students Nathan Betts, Jon Aksel Brynildsen, Vicente Canós, Pål Ellingsbø, Edith Voksøy and Jeffrey Walters for assisting parts of the experimental work, and to Professor Emeritus Fridtjov Irgens for proof reading parts of the thesis. Moreover, Per Horn in Multiconsult deserves his name in this context, without the early interest, encouragement and the practical arrangements he initiated, the work would probably not have been started. Thanks also go to Lynette Wermager, Colorado; and Anna and Angus McLean, London, for reading English proofs of nearly all written material. Finally, I'm grateful to all friends for cheerful support, and to my family at Gunstad for kind understanding over these years.

Trondheim in August 2009

*Kristian B. Dahl*

# Table of Contents

# Introduction

Wood is historically one of the oldest and most important materials used by humankind. Since ancient times, it has been utilized for tools, art, furnishing, handicraft and structural purposes in constructions like boats, buildings and bridges. Its extensive use has been governed by good mechanical properties, easy workability, carpentry traditions and availability nearly everywhere in the world.

Wood is today one of the principal materials with an extraordinarily large amount of consumption. The total volume harvested annually, including wood for fuel, pulp and paper, is nearly 3500 million $m^3$ globally, and exceeds the volume of cement, steel, plastics and aluminium combined. Approximately 45% is used for industrial materials, which approximates that of cement and steel. Both because of a growing world population, and the many advantages of wood, it is reasonable to expect that its use will grow even further (Haygreen and Bowyer 1996, Sasaki and Yamasaki 2004).

The characteristics of wooden material originate from nature since wood is a naturally grown material. The behaviour is designed and optimized to meet the demands in the forest, where the struggle for light has resulted in stems with a distinct length orientation vertically. Its longitudinal direction is stiff and strong in order to withstand vertical gravity loads from branches, stem, ice and snow, and to resist bending moment effects from horizontal wind forces, whereas the direction perpendicular to grain is considerably weaker. Other adaptations have resulted in more local phenomena known as juvenile wood and compression and tension wood. It should be noted that the basic material properties are hardly affected by harvesting and industrial processing into wooden products and structural components.

Wood as a material is characterized by:

- Orthotropy – directional dependent mechanical properties
- Heterogeneity – significant property variation
- Hygroscopicity – moisture interaction
- Viscoelasticity – time dependent deformations (creep)
- Load duration affecting strengths
- Ductility in compression, brittleness in tension and shear
- High strength and stiffness relative to its own weight

The ratio between longitudinal strength and density is quite remarkable, and ranges from 70–150 in compression and 100–300 in tension for clear wood. This is significantly higher than other building materials; steel ranges from 50–130 in both tension and compression, whereas the ratio for concrete in compression is in the range of 10–50. Even for structural lumber, where natural defects like knots

and cracks are present, the ratio compares well with steel. Its low weight, compared to strength, is generally advantageous as less structural capacity is required to carry dead load. Moreover, foundation systems can in many cases be simplified. Another advantage is low inertia forces, making structures less vulnerable to earthquakes. Hence, timber structures have in many cases proved to be an economic alternative, with potential for even further cost reductions in lightweight building systems (Thelandersson 2003).

Wood is relatively versatile with respect to manufacture and workability. It can be sawn into lumber or sliced into veneer, separated into fibre or basic chemical constituents, which again can be processed into finished products with relatively little energy consumption (Haygreen and Bowyer 1996). The aesthetic qualities of wooden surfaces, and the variety of shapes and structural forms for instance glulam may be given, offer good architectural possibilities. Worldwide, many large buildings and timber bridges are excellent examples of good architecture, as illustrated in Figure 1.

**Figure 1:** Evenstad Bridge in Norway (1996) is designed for full traffic load and has a length of 180 m

Apparent drawbacks of wood are low stiffness and strengths perpendicular to grain, and relatively high variability in mechanical properties, making accurate predictions of deformations and capacities difficult. The influence on mechanical properties from load duration and moisture also represent challenges. Other issues are fire safety and sound insulation. The risk of biological decay in outdoor surroundings requires treatment with chemical preservatives or, preferably, careful detailing. The Norwegian stave churches are excellent examples of wooden buildings for which these issues were adequately solved centuries ago, see Figure 2. They prove that wooden constructions can endure for hundreds of years if properly designed and maintained. It should also be noted that wood used in buildings constitutes a natural material with good influence on human health (Thelandersson and Larsen 2003).

**Figure 2:** The stave church in Ringebu is an impressive timber building dating partly back to 1220

Another aspect that will probably be even more important in the future is the environmentally friendly properties of wood. Since the carbon dioxide ($CO_2$) that the trees absorb from the atmosphere will remain in the material until combustion or decay, any wooden construction will, in reality, be storage of carbon. The storage capabilities are considerable when it is taken into account that each $m^3$ of spruce absorbs approximately 0.75 tons of $CO_2$, of which the carbon retaining in the material constitutes roughly 50% of the dry wood density (CRFR 2008). With a total growth of roughly 30 million $m^3$ annually in Norway, approximately 50% of the $CO_2$ emission is absorbed by the forests. Although the net effect is lower due to decay and combustion, the remaining storage of carbon is considerable. This effect can be enhanced by increasing the standing forest volume, or the wood consumption for more permanent applications such as buildings. Moreover, as the energy consumption during manufacture of wooden products is low compared to other building materials, the positive effects are even higher. If this is taken into account, the $CO_2$ emission is reduced by approximately 1 ton per $m^3$ wood replacing brick, steel or concrete, making wood an ecologically sound alternative. As a direct consequence, the Norwegian government agreed to increase the wood consumption per capita from 0.65 $m^3$ annually in 2006 to 0.75 $m^3$ in 2010 (FOEN 2009, LMD 2008–2009).

# 1. Background

A fundamental requirement for efficient use of wood as a competitive and applicable structural material is accurate knowledge of its mechanical behaviour. However, despite extensive and worldwide use in many structural applications, the understanding of its general mechanical properties remains insufficient. The design and use of timber has traditionally been based on inherited experience and craftsmanship instead of engineering principles. Wood has consequently been considered as a low-tech material with insufficient control and documentation. Hence, there is a need for more knowledge of its mechanical properties. The only way to obtain this is by experimental testing, although inhomogeneities, high variability and direction dependency complicate experiments on wood. This probably explains why wood has been less scientifically studied than other building materials. Most publications are typically focusing on specific structural details instead of the general material behaviour. Moreover, research is often limited to linear elastic behaviour, or ultimate capacities, without taking nonlinearity or failure criteria into account. Safety and reliability assessments are also of increasing interest for a material of high variability such as wood. Progress, however, is hampered by the lack of probabilistic material data, although probabilistic analyses nowadays can be handled quite effectively by many numerical codes.

Of the studies focusing on the general mechanical behaviour of wood, much has been reported on uniaxial longitudinal loading in bending and compression, whereas tension seems to be somewhat less studied (Bodig and Jayne 1993). The directions perpendicular to grain are often neglected as the longitudinal properties usually are of main interest. The fact that perpendicular specimens can be hard to manufacture from sawn lumber can also be a reason for the lack of reported work. Regarding shear, the property determination seems somewhat impeded by difficulties in obtaining a state of pure and uniform shear in test specimens, making estimation of shear properties complicated (Xavier et al. 2004). The fact that many standardized tests incorporate several limitations and drawbacks is hampering a more detailed knowledge, see PAPER II and VI (Dahl and Malo 2009a, b). It is also interesting to note that most general studies on the orthotropic parameters of softwoods are relatively old, and that the subspecies Norway spruce has hardly been studied in this sense, see Ch. 3.5. Another topic which deserves more attention is nonlinearity in compression; this influences joint ductility and other highly stressed regions. Biaxial and triaxial stress situations, which can occur in many real cases, have also, in general, received less attention (Yamasaki and Sasaki 2003).

## 1.1. Motivation

The use of wood in bigger and more complex structures, and the availability of more sophisticated and powerful numerical tools for structural analysis, accentuates the need for an accurate and generalized material model for wood. This is particularly true for macro scale analyses (0.1–1.0 m), where a three-dimensional material model comprising nonlinearity and failure prediction is desirable. However, it appears that no constitutive models have been suggested that comprise the complete stress-strain range up to failure in three dimensions of wood. A generalized and robust model would enable prediction of the behaviour of numerous applications in timber engineering, without the reliance on extensive and costly experiments. This would enable better designs and innovative development of details in structural systems of wood and wooden composites. In particular, numerical studies of the complex and often highly stressed joints in timber structures are

desired. Whereas the free spans of a structure are characterized by a relatively uniform state of uniaxial stresses, a complex three-dimensional state of stresses can occur in the joint regions; these cannot be analysed with sufficient accuracy by hand calculations alone. In addition to more exact predictions of stiffness and strengths, a comprehensive numerical model enables quite detailed conceptual studies where, for instance, dowels may be placed in more complex patterns, or the geometry and material parameters may be altered. Moreover, problematic capacities perpendicular to grain and complicated loading situations resulting from eccentricities or inertia forces can be analysed. Hence, through better control and documentation, the potential of more efficient and reliable solutions is believed to be significant. Wood could consequently be used more in large scale timber systems such as multi storey buildings and large bridges.

## 1.2. Joints in timber structures

Joints constitute the connections between various members in a structure. They are located where the members are intersecting geometrically, or where splicing is required in members being shorter than the span width. The joints comprise the most critical and complex parts of a timber structure. Failure and even collapse of buildings are often initiated as a local failure at, or in the vicinity, of a joint. In particular, the low tensile capacities perpendicular to grain require special attention (Larsen 2003). Figure 1-1 shows the dramatic consequences of a joint failure in one of the biggest glulam halls in Europe. The collapse occurred two years after erection, and was mainly caused by design errors. Several similar catastrophic failures of large structures indicate the need for improved joint design in timber constructions. The trend towards bigger and more complex timber structures also stresses the necessity of robust joint design (Sjödin 2008). Another aspect is that efficient jointing techniques are important for competitiveness of timber structures, both with respect to mechanical performance and erection time.

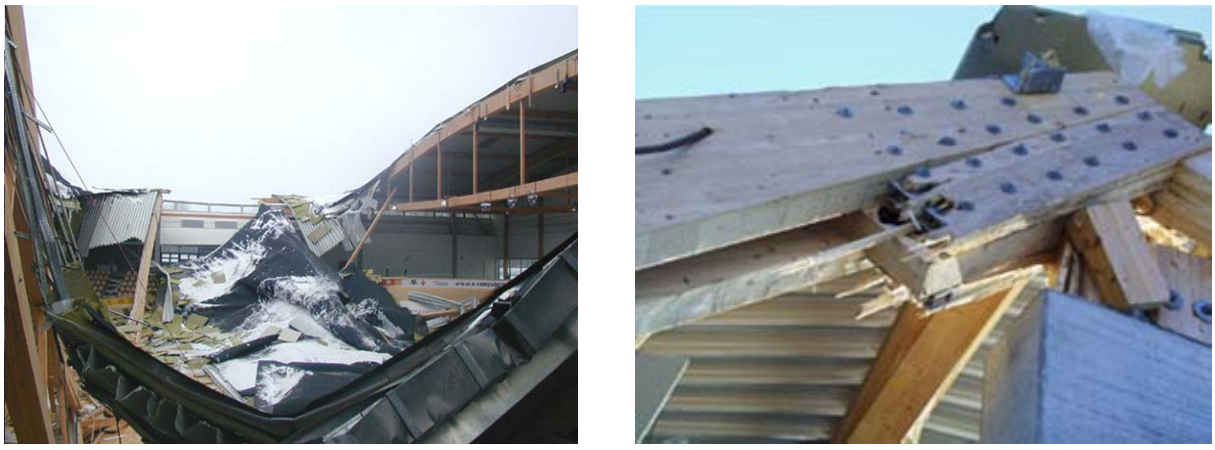

**Figure 1-1:** Siemens Arena in Denmark with free spans of 73 m collapsed in 2003 (Skaug 2004)

The joint stiffness influences on the moment, shear and normal force distributions in statically indeterminate frame structures, and thus the stress situation beyond the actual connection areas. A good joint model can therefore be important for a realistic load distribution in the global system, although this is often treated in a very simplified way (Thelandersson and Larsen 2003).

Timber joints are often less effective than joints in steel structures due to low embedding strengths, especially perpendicular to grain. As a consequence, relatively large spacing and end distances are required to avoid splitting. Load transfer volumes and areas in wooden structures can therefore be relatively large, and may be the critical factor defining the sizes of adjacent members. Joints can be based on direct compressive transfer, adhesives, glued-in rods, nail plates or dowel-type fasteners. The latter constitute the most common type, including nails, staples, drift pins, screws and (threaded) bolts. Slotted-in steel plates with dowel fasteners are shown in Figure 1-2. An excellent description of the various types is given in Thelandersson and Larsen (2003) and will not be repeated here.

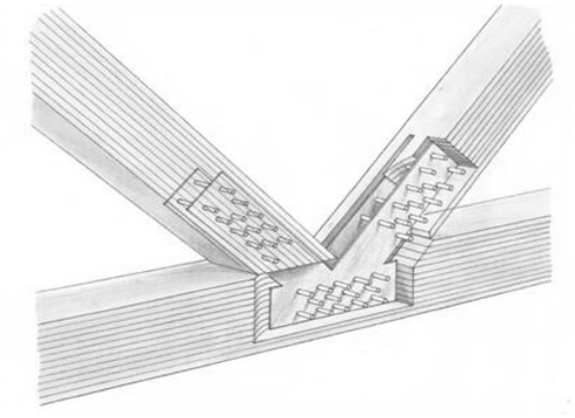

**Figure 1-2:** Typical dowel joint with slotted in plates used at the Olympic arenas at Lillehammer (1994)

## 1.3. Design of joints

Design of joints is normally done by hand-calculation procedures based partly on empirical data, and, for the case of dowel type connections, on the Johansen (1949) theory, which considers the dowel as a beam embedded in the wood. Plastic hinges and embedding zones are assumed to occur, and the theory is therefore not valid for brittle failure caused by wood splitting. The risk of splitting is ensured by minimum distances to ends, edges and other fasteners. However, sufficient ductility capabilities can be difficult to obtain, especially for large scale joints (Sjödin 2008). The Johansen theory has proved to be robust and efficient, but can, in cases where the configuration deviates from the empirical basis, give erroneous results. Important issues are bolt group effects, slender dowel effects, eccentricities and axial withdrawal and ductility capacities. Nonlinearity, material behaviour perpendicular to grain and possible reinforcement of wood based on self-tapping screws are therefore important research fields (Larsen 2003, Nielsen 2003). Stress and strain fields caused by fluctuating moisture are also relevant.

In numerical models of timber structures, for instance of trusses, the members are typically modelled by beam elements with system lines coinciding with the centre of gravity, whereas the joints normally are modelled as hinges. In more refined models, eccentricities between system lines are included by small auxiliary elements at each joint. Since many joints are capable of transferring bending moment, fictitious elements may be introduced to mimic real behaviour. The moment capacity and its distribution between the adjacent members are thus directly dependent upon the localization and stiffness of the fictitious elements relative to the hinge, see Figure 1-3.

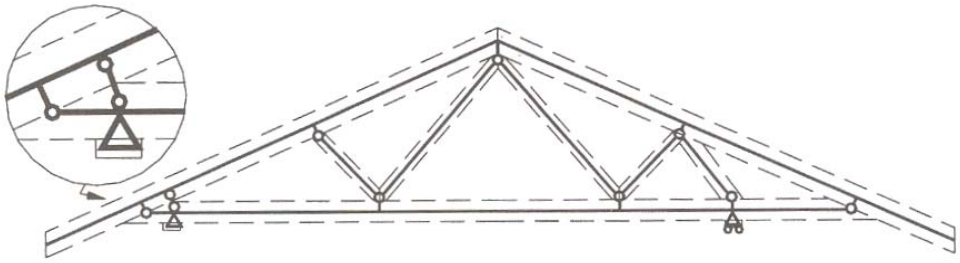

**Figure 1-3:** Truss model with a fictitious element in the joint region (Nielsen 2003)

Many of today's software programs are based on this approach, although the strategy to determine a reasonable stiffness of the fictitious elements, and thus the forces acting on each joint, is somewhat obscure. Since the force and stress distributions of the joint are not determined, a correct joint deformation can hardly be accounted for in the overall deflection. This may partly be alleviated by introducing rotational spring elements, where joint slip and plasticity can be included by nonlinear element features. However, reasonable spring stiffness can be hard to determine. Furthermore, possible splitting of the wood is not taken into account (Nielsen 2003).

By using three-dimensional models in advanced finite element method (FEM) codes, and dividing even small regions into a large number of elements, very detailed models can be obtained. The modelling capabilities offered by commercial FEM codes such as ABAQUS and ANSYS are overwhelming, and a great challenge lies in user-knowledge and modelling in order to obtain a sufficiently realistic model. In principle, any geometry and load configuration can be analysed. Figure 1-4 shows the three-dimensional FEM-model of a tensile specimen of spruce subjected to bolt loading, representing a simple joint. Models of structural joints may comprise three-dimensional effects from torsion and out-of-plane bending moments, in addition to eccentricities, nonlinearities and contact and friction forces on a detailed level. A direct consequence of model refinement is the need for more sophisticated material models on the macro scale level, taking into account direction dependency, material nonlinearity and failure criteria. Whereas an isotropic assumption is often used for global analysis, a transversal isotropic or orthotropic material law should thus be assumed.

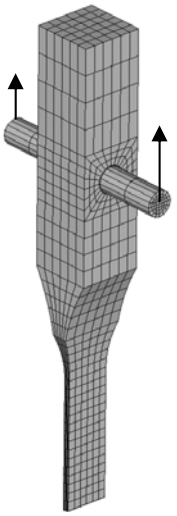

**Figure 1-4:** Finite element model of a clear wood tensile specimen loaded by a steel dowel

## 1.4. Objective

The objective of the thesis is to explore and document the mechanical behaviour of clear wood from spruce softwood. This comprises the three-dimensional direction dependency, normally referred to as orthotropy, and includes shear and normal stress components in compression and tension over the complete loading range up to ultimate capacities. The aim is to quantify the behaviour by a set of linear, nonlinear and failure parameters. Moreover, statistical quantification of parameters is emphasized. The inherent theory is described in Ch. 3–6.

## 1.5. Limitations

Wooden beams from timber normally span 5–7 m, whereas structural timber trusses often are used for larger spans. For large structures, engineered wood products are required, of which glue laminated timber (glulam) is a competitive product. Norway spruce is often preferred in glulam due to its glue-technical properties. With a focus on larger structures, spruce is therefore chosen in this study. Additional limitations are summarized below:

- Effects from location in trunk and provenance are not treated.
- Effects from fluctuating moisture and temperature are not studied.
- Loading rates and elapsed time until ultimate capacity are held steady at levels given by the various test standards. Consequently, only short-term static tests with constant deformation rates are used, and no effects from creep (viscosity), load cycling (fatigue) or load duration are included.
- Size effects and material inhomogeneities are not covered.
- The focus is basically on a quantitative characterization of the mechanical behaviour, and anatomical and phenomenological effects governing the mechanical performance are not included.
- Only clear wood properties are studied, see Ch. 2.2. and 2.7.

## 1.6. Outline of the thesis

The thesis contains eight separate papers on clear wood properties. An introductory part consisting of 6 chapters is included as a motivation and theoretical background. Experimental assessments and a summary of the publications with conclusions and suggestions for future research are found in Ch. 7–9.

# 2. Softwood material

## 2.1. Norway spruce

Norway spruce (*Picea Abies*) is classified as a softwood (gymnospermae), which differs from the hardwoods (angiospermae) in that softwoods produce seeds that lack a covering layer. Both types are included in the botanical division spermatophytes. The softwoods have needle-like leaves; they are often known as evergreens, of which many bear cones. The softwoods are therefore referred to as conifers, and include spruce (*Picea*) as one of the main groups. Around 500 different softwoods are registered (Haygreen and Bowyer 1996). About 35 of these are of commercial importance, of which Norway spruce constitutes an important subspecies and is the most dominating in Norway today. Its name origins from the Englishmen who imported large quantities from Norway after the city fire in London in 1666. It has been used extensively in Norway for housing, boats and crafts, and has furthermore been essential for the sawmill industry. It is also well suited for pulpwood utilization due to its long cells. The tree can grow 35–50 m tall with a trunk diameter of more than a meter.

The geographical distribution of *Picea Abies Karst.* is shown in Figure 2-1, covering large parts of northern Europe, but also mountain areas in central Europe like the Alps and the Carpathians. The northern limit in Norway is just north of 70˚N, whereas the eastern limit is given by the Ural Mountains. Norway spruce is one of the most widely planted spruces, also outside its native range, and can for example be found in North America.

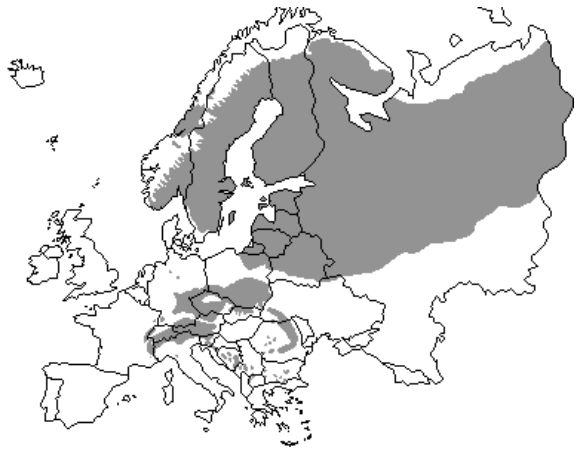

**Figure 2-1:** Distribution of *Picea Abies Karst.*

In addition to glulam, it should be noted that spruce can be used for engineered wood products (EWPs) such as Laminated Veneer Lumber (LVL) and I-joists. EWPs possess several advantageous features as they can be produced in very large sizes adapted market requirements, with better dimensional stability and tolerances, and less defects and variation. EWPs are consequently attractive for structural purposes. It can be noted that orthotropic properties documented for clear wood are relevant for many EWPs, which in principle are manufactured from clear wood. The orthotropic properties may, in fact, be more salient in an EWP than in ordinary timber, where a cylindrical coordinate system and more irregularities are present.

## 2.2. Anatomical scales

Material properties are generally dependent upon the material scale they are determined from, and can consequently be observed and systematized on different levels. Since wood is quite inhomogeneous, material parameters ought to be determined on a scale which corresponds with the structural level of the problem which is to be analysed. The features of wood are often separated into four: massive; macro; meso and micro scale (Smith et al. 2003), as illustrated in Figure 2-2. The massive scale comprises the global or structural level of a structure, whereas the micro scale constitutes the cell level. The term wood refers herein to clear wood corresponding with the macro level, whereas timber describes material on the massive scale. The different anatomical levels are naturally dependent on each other, and properties at one level govern the other. The division is consequently motivated by pragmatic reasons in experimental testing and numerical analyses.

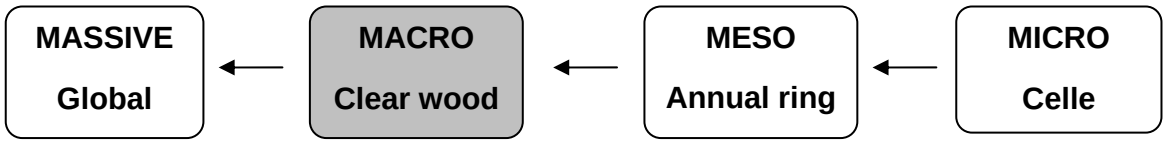


**Figure 2-2:** Scale differentiation for wood

The main focus herein is given to the macro scale level. Only the timber stem is regarded, i.e. roots, bark and crown system (branches) are not included in the consideration. Moreover, the nano scale (microfibrils) and the molecular level fall beyond the scope.

## 2.3. Massive scale

Massive wood comprises solid wood members produced by sawing or gluing, typically with cross-section dimensions over 100 mm. Structural timber on the massive (global) scale represents wood at its most inhomogeneous, where various defects such as knots, fibre inclination, cracks, reaction wood and resin pockets are present. The massive scale properties can therefore not be related directly to the clear wood properties, and separate testing on structural timber is consequently required. Structural size tests are standardized by i.a. ASTM D198 (1999) and ASTM D3500 (1990), whereas for instance NS-EN 408 (2003) treats both massive and clear wood bending moduli. Global stiffness and strength values are typically given on element level rather than on material level, although results are presented in stress units assuming elastic theory. The influence of apparent defects is thus implicitly included in structural analyses, and reduction factors on clear wood properties are superfluous. This is also the background for different capacities for different loading modes, where for example the ultimate bending stress deviates from pure tensile and compressive capacities (Thelandersson and Larsen 2003). Due to imperfections, the massive scale has typically lower strengths than the macro. Failure in structural wood is often governed by localised processes, which makes knowledge of wood behaviour on the lower scales essential (Smith et al. 2003).

Visual or machine grading is used to quantify and control timber properties. Both types are non-destructive, and result in grading classes stated by for instance NS-EN 338 (2003). Machine grading is based on expected correlation between a measured indicative property and strength and stiffness values. The measurements are typically based on radiation techniques, stress wave speeds or flatwise short-span bending. The correlations between the elastic modulus and bending or tensile

strengths are proved to be high ($r^2$ = 0.50–0.70), partly because the measurements are capable of picking up disturbing effects from abnormalities such as knots and spiral grain (Thelandersson and Larsen 2003).

In spite of grading routines, the general uncertainty in stiffness and strength of wood is high. The interrelations between various clear wood parameters are relatively obscure, as are the dependency to grading class for many of the orthotropic properties. Furthermore, the relations between clear wood and timber properties are absolutely not definite. It can be noted that Foslie and Moen (1968) found 31% higher longitudinal elastic modulus with structural size than clear wood bending specimens from Norway spruce, and a relatively high correlation of 0.78.

## 2.4. Macro scale

Features of wood detectable without microscope are referred to as macroscopic characteristics. By observing from the outside, as illustrated in Figure 2-3, a layer of outer bark is followed by an inner layer (phloem) surrounding the wood (xylem). The cambium is found between, where the growth of phloem and xylem occurs, creating a new layer of annual rings. Water and nutrients move up in the outer part of the xylem (sapwood), whereas sugar, as sap, moves down in the phloem. Sap required for building xylem travels horizontally from the phloem through radially oriented rays. Due to the rays, the radial stiffness is higher than the tangential and the radial drying shrinkage smaller.

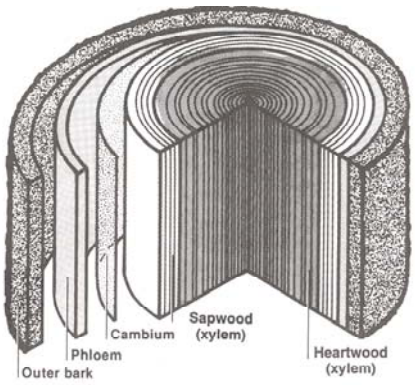


**Figure 2-3:** Parts of mature stem (Haygreen and Bowyer 1996)

The inner part (50–80%) of the xylem is referred to as heartwood, which continuously starts transforming from sapwood when the tree has reached an age of 14–18 years. The heartwood cells are dead in the sense that they have lost the ability to carry on metabolic processes, and can no longer subdivide. Instead they form thickened and lignified cell walls wherein various extractives (polyphenols) evolve. Heartwood is often darker with higher density, lower water content and more decay-resistance than sapwood (Haygreen and Bowyer 1996).

The annual rings occurring with certain regularity are salient on the macro level, indicating where a piece is cut in the trunk. Similarly they define the principal orientations and planes, designated by the directions longitudinally ($L$) along the fibres, radially ($R$) toward the annual rings and tangentially ($T$) along the annual rings, see Figure 2-4. The macro scale level (0.1–1.0 m) is normally assumed for two and three-dimensional stress analyses of engineered wood components (Smith et al. 2003). The relations presented under linear and nonlinear orthotropic behaviour in Ch.

3 and 4 assume wood on a macro scale level. In massive scale analyses, the radial and tangential directions may be treated as a combined principal direction (perpendicular *P*), see Ch. 3.3.

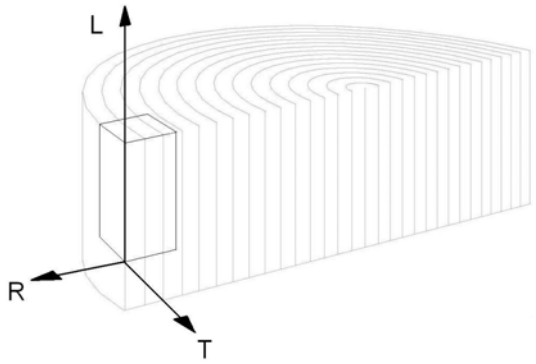


**Figure 2-4:** Orthogonal material axis system *LRT* in wood block (PAPER I - Dahl and Malo 2009f)

The longitudinal stiffness is 10–15 times higher than the radial, and 20–30 times higher than the tangential. Due to the thin walls of early wood cells in the radial direction, the shear stiffness in the radial-tangential plane is very low for most softwood species, often in the range of 5% of the radial stiffness. The ratios between strengths are relatively similar, which is the primary cause of the frequently reported failures perpendicular to grain in timber structures.

The arrangement of vertically aligned cells is referred to as grain or fibres. Their length direction are normally oriented parallel to the length axis of the stem, although it is not uncommon that fibres are arranged at a slight angle, see Figure 2-5. The deviation is often in the range of 4 degrees (Dinwoodie 2000). The phenomenon is also known as spiral graining or fibre inclination, and may actually be the rule rather than the exception. It affects wood properties significantly through reduced strength and stiffness of sawn lumber. Reversed spiral (interlocked) grain can be found between different annual layers in certain species, and can be highly valued for its visual qualities (Haygreen and Bowyer 1996).

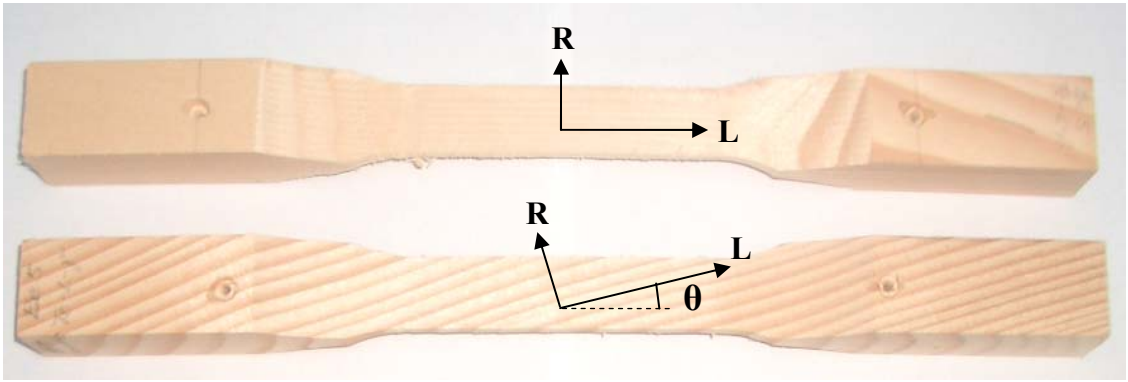


**Figure 2-5:** Two tensile specimens of which the lower shows fibre inclination in the LR-plane (rejected)

Natural macro level variation includes inhomogeneity due to different properties over the distance from pith to bark, and variation caused by the annual ring structure. Other sources are compression/tension wood, fibre inclination, cracks and resin pockets, damages from frost and harvesting, biological attacks and knots. Incorporation of living branches into the stem gives knots that constitute an integrated part of the wood, so-called intergrown or tight knots, and do not

become loose upon drying, although the grain direction in the vicinity is highly distorted. Knots resulting from dead branches, on the contrary, result in loose knots. In both cases, knots represent deviation from regular anatomy with direct implications on the mechanical properties of the material, and are undoubtedly the most common and serious defect. Whereas tension capacities normally are reduced by irregularities, the shear strength will be enhanced by the presence of knots. Another peculiar feature is growth stresses, although they normally disappear after felling.

## 2.5. Meso scale

The meso scale refers to the annual rings being present where wood growth is seasonal. The growth occurs by division of the cambium, which during winter is dormant. During spring, the cells subdivide radially by primary walls into new cells, which will partly develop into bark and partly into wood. Growth proceeds rapidly during spring and slows down in the summer before it ceases in the fall, which can be seen as relatively regular and distinct bands of light earlywood and darker latewood with transition wood between. Rapidly grown earlywood consists of relatively large diameter cells with thin walls, whereas latewood visa versa is stronger and stiffer with small lumens and radial diameters. Earlywood holds densities of 300 kg/m$^3$ whilst latewood can reach as high as 1000 kg/m$^3$, often with a combined average of approximately 400 kg/m$^3$.

## 2.6. Micro scale

Softwood is composed of axially oriented slender cells called tracheids, occupying 90–95% of the timber volume. Their cross sections are relatively rectangular with hollow centres (lumen). Earlywood tracheids are relatively large with thin walls, facilitating transport of water and nutrients, and visa versa for latewood which contributes to material strength and stiffness. Numerous pits are located on the radial cell walls for tracheids-to-tracheids linkages. The diameter is 20–40 μm and the length is 2–4 mm. The cell wall consists of cellulose, hemicelluloses and lignin which forms and glues the so-called micro-fibrils together. Due to varying portion of chemical content and different micro-fibril angles (MFA), the cell wall can be divided into four separate layers, as illustrated in Figure 2-6. Out of these, the S2-layer is the thickest and has therefore the greatest effect on the mechanical properties, including anisotropy and failure properties. A phenomenon like compression wood is also very dependent on the S2-layer.

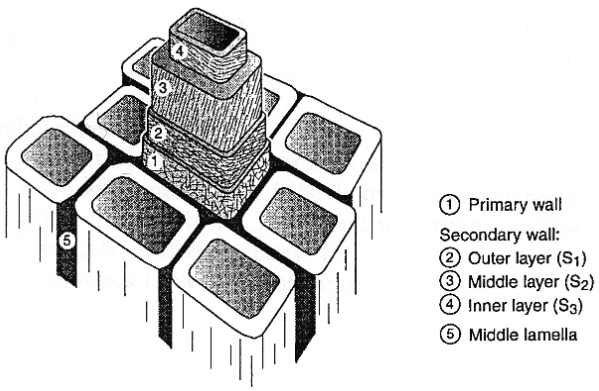


**Figure 2-6:** Schematic drawing of wood cell wall (Ormarsson 1999)

Cells for energy storage and fluid conduction are known as parenchyma cells, and are the last to remain functional prior to heartwood transition. They form thin secondary walls, are mainly

oriented radially and contribute little to the overall mechanical stiffness. Special parenchyma cells can form intercellular resin canals in pine and spruce species. Such resin-secreting cells are known as epithelium cells, and are believed to have a function in healing damaged material and to resist insect invasions. Rays running radially are either composed by ray parenchyma or ray tracheids. They often consist of several cells in height but only one in width, where pitting on the ray sidewalls secures connection to longitudinal cells. Rays containing a resin canal are known as a fusiform ray. In softwoods, longitudinal tracheids and ray parenchyma constitute the substantial part of the structure (Smith et al. 2003).

## 2.7. Clear wood

Clear wood refers to macro scale material without apparent defects and irregularities such as knots, cracks, decay, resin pockets, juvenile and reaction wood. The specimen size is limited (0.01–0.1 m) and represents bulk behaviour averaged over relatively few growth rings. It is normally recognized between the principal directions $L$, $R$ and $T$, and the property determination is based on the assumption that clear wood is homogeneous and continuous, i.e. a smeared annual ring structure (Thelandersson and Larsen 2003, Smith et al. 2003). The homogenization is an idealization, but is quite adequate for clear wood as long as the considered material is large compared to the cells and growth rings. Moreover, it can be reasoned by the Saint Venant's principle, stating that the effect on stresses caused by an irregularity evens out some distance away.

Values derived from clear wood specimens are pertinent for analyses of joints and details in timber structures. Their size provide representative volume elements (RVE) corresponding well with adequate element sizes in finite element models with reasonable discretization. Moreover, small sized pieces collected some distance from the stem pith are required if orthotropic properties are to be related to a Cartesian axis system. Small clear wood specimens were originally used for the derivation of wood properties, but were during the 1970's partly superseded by structural size timber. Today, the small clear wood material still remains valid for material characterization and for comparison between various species and qualities (Dinwoodie 2000). Massive scale specimens (structural timber) seem less adequate for detailed analyses, as potential deviation in property values may be introduced due to size effects. Moreover, the use of large pieces is more costly.

# 3. Linear elastic behaviour

Wood can be assumed to behave linearly elastic up to moderate stress levels for short term loading (< 0.1 hours) (Smith et al. 2003). For the macro scale, or clear wood level, the material can be considered anisotropic with Cartesian or cylindrical material axes depending on where the material is cut in the trunk. If a piece is cut at a sufficient distance from the pith, so that the growth ring curvature can be neglected, a Cartesian system can be assumed. The anisotropy implies that the mechanical properties depend upon direction. The characteristic directions are defined by three mutually perpendicular planes of material symmetry. Thus, wood can be classified as orthotropic, referring to the three orthogonal directions *L*, *R* and *T* defining these planes, as described in Ch. 2.4. The ratio between the elastic moduli in the *L* and *T* direction is approximately 25, which actually makes wood the most highly orthotropic material known (Bodig and Jayne 1993). If the *R* and *T* properties are assumed equal, which is required in many design situations, the material classifies as transverse isotropic.

## 3.1. Anisotropy

The stress at a point in a general continuum can be represented by nine stress components $\sigma_{qr}$ where $\{q, r\} = \{1, 2, 3\}$. The components act on the surface planes of a three dimensional element whose planes are defined by the orthogonal reference coordinate system *1, 2, 3* represented by the coordinates $x_i$ and the base vectors $\mathbf{e}_i$, $\{i\} = \{1, 2, 3\}$. The strain is similarly represented by nine strain components $\varepsilon_{qr}$. The stress and strain is related by Hooke's law, which in indicial notation can be stated as

$$\begin{aligned} \varepsilon_{qr} &= S_{qrst}\sigma_{st} \\ \sigma_{qr} &= C_{qrst}\varepsilon_{st} \end{aligned} \qquad \{q, r, s, t\} = \{1, 2, 3\} \tag{3.1}$$

where $S_{qrst}$ designate the compliance components and $C_{qrst}$ the stiffness components. The fourth order tensors **C** and **S** contain $3^4$ components each. A total number of 81 elastic constants would thus be required to characterize a material completely. However, from basic mechanics it is known that mutual shear components are equal in magnitude, implying (minor) symmetry:

$$\sigma_{qr} = \sigma_{rq} \qquad \varepsilon_{qr} = \varepsilon_{rq} \tag{3.2}$$

which reduces the number of elastic constants to 36, i.e.

$$C_{qrst} = C_{rqst} = C_{qrts} \tag{3.3}$$

The general strain energy function *w* for any linear elastic material is for a volume unit defined by

$$w = \int \sigma_{qr} d\varepsilon_{qr} = \int C_{qrst}\varepsilon_{st} d\varepsilon_{qr} = \frac{1}{2} C_{qrst}\varepsilon_{qr}\varepsilon_{st} \geq 0 \tag{3.4}$$

It is assumed that the *w* is sufficiently smooth, and it follows that

$$\frac{\partial^2 w}{\partial \varepsilon_{qr} \partial \varepsilon_{st}} = C_{qrst} = \frac{\partial^2 w}{\partial \varepsilon_{st} \partial \varepsilon_{qr}} = C_{stqr} \tag{3.5}$$

implying (major) symmetry. Combination of major and minor symmetry gives

$$C_{qrst} = C_{rqst} = C_{qrts} = C_{stqr} \tag{3.6}$$

Consequently, the number of independent elastic constants in an anisotropic material is being reduced to 21. In a similar way it can be shown that the major and minor symmetry also holds for $S_{qrst}$ (Daniel and Ishai 2006), which on Voigt matrix form with tensor indices reads

$$\begin{bmatrix} \varepsilon_{11} \\ \varepsilon_{22} \\ \varepsilon_{33} \\ \gamma_{23} \\ \gamma_{13} \\ \gamma_{12} \end{bmatrix} = \begin{bmatrix} S_{1111} & S_{1122} & S_{1133} & S_{1123} & S_{1113} & S_{1112} \\ & S_{2222} & S_{2233} & S_{2223} & S_{2213} & S_{2212} \\ & & S_{3333} & S_{3323} & S_{3313} & S_{3312} \\ & & & S_{2323} & S_{2313} & S_{2312} \\ & sym & & & S_{1313} & S_{1312} \\ & & & & & S_{1212} \end{bmatrix} \begin{bmatrix} \sigma_{11} \\ \sigma_{22} \\ \sigma_{33} \\ \sigma_{23} \\ \sigma_{13} \\ \sigma_{12} \end{bmatrix} \tag{3.7}$$

## 3.2. Orthotropy

A material plane of symmetry implies that the elastic components must remain unchanged (invariant) if the axis is reflected through the symmetry plane. An orthotropic material has three mutually perpendicular planes of material symmetry, as illustrated for wood in Figure 3-1.

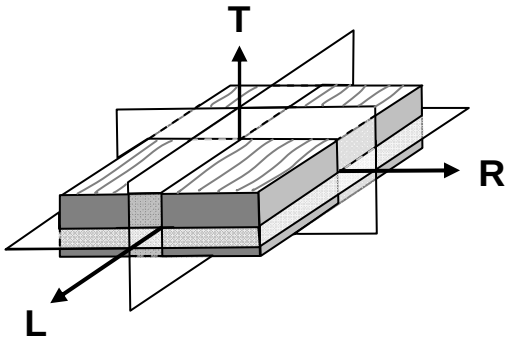


**Figure 3-1:** Principal directions and symmetry planes in clear wood (after Bodig and Jayne 1993)

Hence, there exist three transformations which leave the constitutive equations invariant. The transformation can be defined by three sets of base vectors $\mathbf{e}_q$ and $\bar{\mathbf{e}}_i$ with components $e_{qj}$ and $\bar{e}_{ij}$ related through

$$\begin{aligned} \bar{e}_{ij} &= M_{iq} e_{qj} & \bar{\mathbf{e}}_i &= M_{iq} \mathbf{e}_q \\ e_{ij} &= M_{qi} \bar{e}_{qj} & \mathbf{e}_i &= M_{qi} \bar{\mathbf{e}}_q \end{aligned} \tag{3.8}$$

$M_{iq}$ are here components in a transformation matrix, and do not represent a tensor. Coordinates are analogously transformed by

$$\begin{aligned} \bar{x}_i &= M_{iq} x_q & \bar{\mathbf{x}} &= \mathbf{M}\mathbf{x} \\ x_i &= M_{qi} \bar{x}_q & \bar{\mathbf{x}} &= \mathbf{M}^{\mathrm{T}}\mathbf{x} \end{aligned} \tag{3.9}$$

where the orthotropic transformation matrices are defined by

$$\mathbf{M}^1 = \begin{bmatrix} -1 & 0 & 0 \\ 0 & 1 & 0 \\ 0 & 0 & 1 \end{bmatrix}, \quad \mathbf{M}^2 = \begin{bmatrix} 1 & 0 & 0 \\ 0 & -1 & 0 \\ 0 & 0 & 1 \end{bmatrix}, \quad \mathbf{M}^3 = \begin{bmatrix} 1 & 0 & 0 \\ 0 & 1 & 0 \\ 0 & 0 & -1 \end{bmatrix} \tag{3.10}$$

The stress and strain matrices are correspondingly transformed by

$$\bar{\sigma}_{ij} = M_{iq} M_{jr} \sigma_{qr} \qquad \bar{\boldsymbol{\sigma}} = \mathbf{M}\boldsymbol{\sigma}\mathbf{M}^{\mathrm{T}} \tag{3.11}$$

$$\bar{\varepsilon}_{ij} = M_{iq} M_{jr} \varepsilon_{qr} \qquad \bar{\boldsymbol{\varepsilon}} = \mathbf{M}\boldsymbol{\varepsilon}\mathbf{M}^{\mathrm{T}} \tag{3.12}$$

$$\varepsilon_{qr} = M_{iq} M_{jr} \bar{\varepsilon}_{ij} \qquad \boldsymbol{\varepsilon} = \mathbf{M}^{\mathrm{T}}\bar{\boldsymbol{\varepsilon}}\,\mathbf{M} \tag{3.13}$$

The strain energy potential given by Eq. (3.4) is invariant to transformations, and it follows that

$$w = \frac{1}{2} C_{qrst} \varepsilon_{qr} \varepsilon_{st} = \frac{1}{2} \bar{C}_{ijkl} \bar{\varepsilon}_{ij} \bar{\varepsilon}_{kl} = \frac{1}{2} C_{qrst} M_{iq} M_{jr} M_{ks} M_{lt} \bar{\varepsilon}_{ij} \bar{\varepsilon}_{kl} \tag{3.14}$$

where *qrst* and *ijkl* are referring to the different sets of base vectors. Hence

$$\bar{C}_{ijkl} = M_{iq} M_{jr} M_{ks} M_{lt} C_{qrst} \tag{3.15}$$

Transformations **M** within the symmetry group of the material imply $\bar{C}_{ijkl} = C_{ijkl}$. The constitutive equations will thus be unchanged. For e.g. component $\bar{C}_{1111}$ and the transformation $\mathbf{M}^1$, the condition is fulfilled since the following equality holds:

$$\bar{C}_{1111} = M_{1q} M_{1r} M_{1s} M_{1t} C_{qrst} = -1 \cdot -1 \cdot -1 \cdot -1 \cdot C_{1111} + 0 = C_{1111} \tag{3.16}$$

While for e.g. component $C_{1123}$ and transformation $\mathbf{M}^2$,

$$\bar{C}_{1123} = M_{1q} M_{1r} M_{2s} M_{3t} C_{qrst} = 1 \cdot 1 \cdot -1 \cdot 1 \cdot C_{1123} + 0 = -C_{1123} \tag{3.17}$$

which consequently proves that the equality is satisfied for $C_{1123} = 0$ only. Corresponding considerations for each of the components and the $\mathbf{M}^i$ matrices result in Eq. (3.18), which is presented in Voigt matrix form:

$$\begin{bmatrix}\sigma_{11}\\ \sigma_{22}\\ \sigma_{33}\\ \sigma_{23}\\ \sigma_{13}\\ \sigma_{12}\end{bmatrix} = \begin{bmatrix} C_{1111} & C_{1122} & C_{1133} & 0 & 0 & 0 \\ & C_{2222} & C_{2233} & 0 & 0 & 0 \\ & & C_{3333} & 0 & 0 & 0 \\ & & & C_{2323} & 0 & 0 \\ & sym & & & C_{1313} & 0 \\ & & & & & C_{1212} \end{bmatrix} \begin{bmatrix}\varepsilon_{11}\\ \varepsilon_{22}\\ \varepsilon_{33}\\ \gamma_{23}\\ \gamma_{13}\\ \gamma_{12}\end{bmatrix} \tag{3.18}$$

As long as **C** satisfies transformation by two of the three $\mathbf{M}^i$ matrices, transformation by the third will also be satisfied. The same can be shown for the compliance tensor **S**, writing

$$\begin{bmatrix}\varepsilon_{11}\\ \varepsilon_{22}\\ \varepsilon_{33}\\ \gamma_{23}\\ \gamma_{13}\\ \gamma_{12}\end{bmatrix} \equiv \begin{bmatrix}\varepsilon_{11}\\ \varepsilon_{22}\\ \varepsilon_{33}\\ \varepsilon_{23}+\varepsilon_{32}\\ \varepsilon_{13}+\varepsilon_{31}\\ \varepsilon_{12}+\varepsilon_{21}\end{bmatrix} = \begin{bmatrix} S_{1111} & S_{1122} & S_{1133} & 0 & 0 & 0 \\ & S_{2222} & S_{2233} & 0 & 0 & 0 \\ & & S_{3333} & 0 & 0 & 0 \\ & & & S_{2323} & 0 & 0 \\ & sym & & & S_{1313} & 0 \\ & & & & & S_{1212} \end{bmatrix} \begin{bmatrix}\sigma_{11}\\ \sigma_{22}\\ \sigma_{33}\\ \sigma_{23}\\ \sigma_{13}\\ \sigma_{12}\end{bmatrix} \tag{3.19}$$

where it should be noted that the shear strain $\gamma_{qr}$ equals the sum of $\varepsilon_{qr}$ and $\varepsilon_{rq}$, which by definition are equal. In distinction to Eq. (3.7), it can be seen that no coupling exists between normal and shear components. This implies that application of normal stresses do not produce shear strains and visa versa in orthotropic materials when material and reference axes coincide (Hopperstad 2003).

Each of the compliance coefficients $S_{ijkl}$ in Eq. (3.19) can be related to a set of engineering material parameters comprising three moduli of elasticity $E_{ii}$, three shear moduli $G_{ij}$ and six Poisson's ratios $v_{ij}$ (Daniel and Ishai 2006). If the relations are set up with the *LRT* nomenclature normally used for clear wood, as illustrated in Figure 3-2 and denoted as

$$\begin{aligned} 1 &= L \\ 2 &= R \\ 3 &= T \end{aligned} \tag{3.20}$$

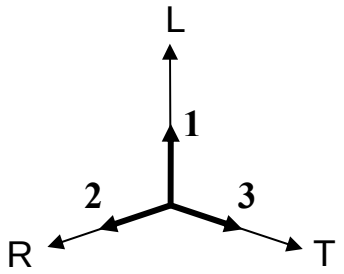


**Figure 3-2:** Reference coordinate system *123* relative to principal material system *LRT*

the compliance $S_{ijkl}$ $\{i, j, k, l\} = \{L, R, T\}$ can be stated as

$$\left[S_{ijkl}\right]=\begin{bmatrix} \frac{1}{E_{LL}} & -\frac{\nu_{LR}}{E_{LL}} & -\frac{\nu_{LT}}{E_{LL}} & 0 & 0 & 0 \\ -\frac{\nu_{RL}}{E_{RR}} & \frac{1}{E_{RR}} & -\frac{\nu_{RT}}{E_{RR}} & 0 & 0 & 0 \\ -\frac{\nu_{TL}}{E_{TT}} & -\frac{\nu_{TR}}{E_{TT}} & \frac{1}{E_{TT}} & 0 & 0 & 0 \\ 0 & 0 & 0 & \frac{1}{G_{RT}} & 0 & 0 \\ 0 & 0 & 0 & 0 & \frac{1}{G_{LT}} & 0 \\ 0 & 0 & 0 & 0 & 0 & \frac{1}{G_{LR}} \end{bmatrix}=\begin{bmatrix} \frac{1}{E_{LL}} & -\frac{\nu_{LR}}{E_{LL}} & -\frac{\nu_{LT}}{E_{LL}} & 0 & 0 & 0 \\ & \frac{1}{E_{RR}} & -\frac{\nu_{RT}}{E_{RR}} & 0 & 0 & 0 \\ & & \frac{1}{E_{TT}} & 0 & 0 & 0 \\ & & & \frac{1}{G_{RT}} & 0 & 0 \\ & sym & & & \frac{1}{G_{LT}} & 0 \\ & & & & & \frac{1}{G_{LR}} \end{bmatrix} \tag{3.21}$$

It can be seen that the major symmetry enforces the equality

$$S_{iijj}=\frac{\nu_{ij}}{E_{ii}}=\frac{\nu_{ji}}{E_{jj}}=S_{jjii} \qquad (i\neq j) \tag{3.22}$$

Consequently, only three of the totally six Poisson's ratios are independent. Hence, an orthotropic material is governed by 9 independent elastic constants out of totally 12. Given that the linear range prevails, the engineering parameters can be determined experimentally by observation of strain and stress increments, writing

$$E_{ii}=\frac{d\sigma_{ii}}{d\varepsilon_{ii}} \qquad G_{ij}=\frac{d\sigma_{ij}}{d\gamma_{ij}} \qquad \nu_{ij}=-\frac{d\varepsilon_{jj}}{d\varepsilon_{ii}} \qquad (i\neq j) \tag{3.23}$$

Due to the minor symmetry properties of **C** and **S**, it can be noted that

$$d\sigma_{ij}=d\sigma_{ji} \qquad d\gamma_{ij}=d\varepsilon_{ij}+d\varepsilon_{ji}=d\gamma_{ji} \quad \Rightarrow \quad G_{ij}=G_{ji} \qquad (i\neq j) \tag{3.24}$$

Figure 3-3 shows measurements from the *LR* material plane of clear spruce wood loaded longitudinally in compression. The active strain (black) and the passive strain (grey) yield $E_{LL}$ and $\nu_{LR}$ estimates, respectively, both visualized with white lines.

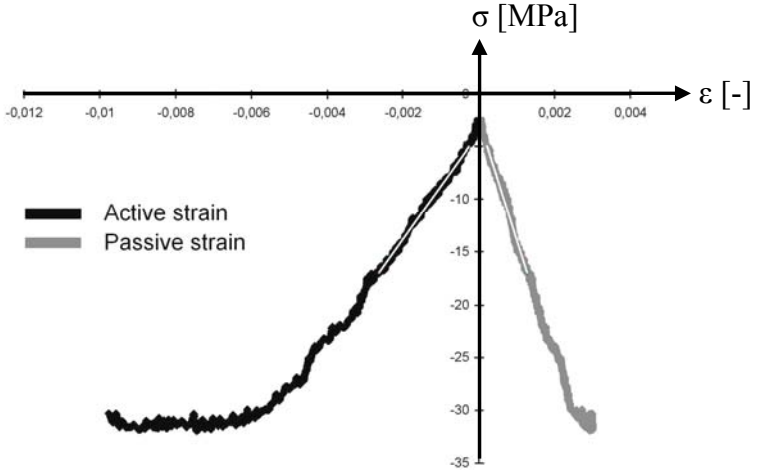


**Figure 3-3:** Determination of linear elastic parameters of spruce

Transformation of the compliance tensor $S_{ijkl}$ into the inverse elastic modulus tensor $C_{ijkl}$ gives (Daniel and Ishai 2006, Bodig and Jayne 1993):

$$C_{ijkl} = \begin{bmatrix} \frac{1-\nu_{RT}\nu_{TR}}{E_{RR}E_{TT}|S|} & \frac{\nu_{RL}-\nu_{RT}\nu_{TL}}{E_{RR}E_{TT}|S|} & \frac{\nu_{TL}-\nu_{RL}\nu_{TR}}{E_{RR}E_{TT}|S|} & 0 & 0 & 0 \\ & \frac{1-\nu_{TL}\nu_{LT}}{E_{LL}E_{TT}|S|} & \frac{\nu_{RT}-\nu_{RL}\nu_{LT}}{E_{LL}E_{RR}|S|} & 0 & 0 & 0 \\ & & \frac{1-\nu_{RL}\nu_{LR}}{E_{LL}E_{RR}|S|} & 0 & 0 & 0 \\ & & & G_{RT} & 0 & 0 \\ & sym & & & G_{LT} & 0 \\ & & & & & G_{LR} \end{bmatrix} \tag{3.25}$$

$$|S| = \frac{1}{E_{LL}\cdot E_{RR}\cdot E_{TT}}\cdot\left(1-2\nu_{RL}\nu_{TR}\nu_{LT}-\nu_{LT}\nu_{TL}-\nu_{RT}\nu_{TR}-\nu_{LR}\nu_{RL}\right) \tag{3.26}$$

## 3.3. Transverse isotropy

A material is transversely isotropic if there exist a plane such that every plane perpendicular to it is a material symmetry plane. If the characteristic plane is defined by the $\mathbf{e}_2\,\mathbf{e}_3$ base vectors, the material is restricted by the reflective $\mathbf{M}^2$ and $\mathbf{M}^3$ matrices stated for orthotropic materials in Eq. (3.10) and the rotation $\mathbf{M}^{1\text{-rot}}$ about the $e_1$ axis defined as

$$\mathbf{M}^{1-rot} = \begin{bmatrix} 1 & 0 & 0 \\ 0 & \cos\theta & \sin\theta \\ 0 & -\sin\theta & \cos\theta \end{bmatrix} \tag{3.27}$$

Similarly as described in Ch. 3.2, it can be shown that this results in the stiffness matrix

$$\left[C_{ijkl}\right] = \begin{bmatrix} C_{1111} & C_{1122} & C_{1122} & 0 & 0 & 0 \\ & C_{2222} & C_{2233} & 0 & 0 & 0 \\ & & C_{2222} & 0 & 0 & 0 \\ & & & \left(\frac{C_{2222}-C_{2233}}{2}\right) & 0 & 0 \\ & sym & & & C_{1212} & 0 \\ & & & & & C_{1212} \end{bmatrix} \tag{3.28}$$

The transversely isotropic material is thus characterized by 5 independent elastic constants (Daniel and Ishai 2006), which appears from the compliance matrix

$$\left[S_{ijkl}\right]=\begin{bmatrix} \frac{1}{E_{LL}} & -\frac{\nu_{LP}}{E_{LL}} & -\frac{\nu_{LP}}{E_{LL}} & 0 & 0 & 0 \\ & \frac{1}{E_{PP}} & -\frac{\nu_{PP}}{E_{PP}} & 0 & 0 & 0 \\ & & \frac{1}{E_{PP}} & 0 & 0 & 0 \\ & & & \frac{1+\nu_{PP}}{2\cdot E_{PP}} & 0 & 0 \\ & sym & & & \frac{1}{G_{LP}} & 0 \\ & & & & & \frac{1}{G_{LP}} \end{bmatrix} \tag{3.29}$$

where the following nomenclature is used

$$\begin{aligned} 1 &= L \\ 2 = 3 &= P \qquad \text{(transverse / perpendicular to grain)} \end{aligned} \tag{3.30}$$

$E_{LL}$ and $E_{PP}$ are the elastic moduli in the $L$ and $P$ directions, respectively. $G_{LP}$ and $\nu_{LP}$ are the in-plane shear modulus and Poisson's ratio, respectively, and $\nu_{PP}$ is the out-of-plane Poisson's ratio corresponding to the $RT$-plane in wood. Note that a transversely isotropic material also is orthotropic. The assumption of transversely isotropic materials is used in timber engineering, whereas it is normally separated between the radial and tangential directions in testing of clear wood (Gustafsson 2003, Smith et al. 2003). Although it can be argued that the radial and tangential properties are different, this variation is often lower than variation along the stem and from pith to bark.

## 3.4. Polar orthotropy

If the timber stem is considered, or a piece is cut relatively near the pith so that the annual ring curvature is obvious, a polar/cylindrical coordinate system can be plausible. This is a three-dimensional system where each point is given by three coordinates, two polar ($r$, $\varphi$) and one axial ($x$). For wood, the two polar coordinates describe the position in the $RT$-plane and $x$ the plane's position along the stem, with the axis running through the centre (pith) of the perpendicular $RT$-plane, see Figure 3-4.

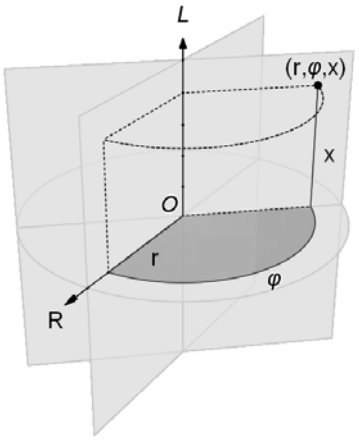


**Figure 3-4:** Polar coordinate system

A polar system is naturally not capable of comprising local perturbations such as knots or growth ring irregularities, but offers a more detailed representation than the transversely isotropic model, as it distinguishes between the two perpendicular directions *R* and *T*. According to Shipsha and Berglund (2007), the clear wood behaviour can be strongly dependent on elastic properties and the orientation of annual rings to the load. Despite simple uniaxial loading, shear coupling due to off-axis effects can cause an inhomogeneous and complex state of stresses. Hence, the assumption of polar orthotropy can be important for prediction of stresses in wood. This has also been proved by Aicher et al. (2001), who found good correspondence between experimental and numerical results in the *RT*-plane by assuming polar orthotropy.

It should be noted that experimental determination of linear elastic orthotropic parameters from polar systems seems complicated, as an inhomogeneous strain field may occur just because of orthotropy. Nevertheless, orthotropic parameters obtained in Cartesian systems may be applied in numerical analyses based on polar coordinate systems.

## 3.5. Linear orthotropic parameters

While the ultimate bending and compressive capacities and the corresponding modulus of elasticity are relatively well documented for wood longitudinally, the scarcity of characterization of other properties is noteworthy. Standardized tests do not separate between the radial and tangential directions, and seem in many cases less suited for an accurate characterization of the transverse properties. Tension tests have, partly due to practical problems, received limited use, and comparisons between tensile, compressive and bending stiffness properties are rare. Accurate shear testing also seems to be a challenge. It is furthermore interesting to note that standardized tests do not exist for the Poisson's ratios and the transverse elasticities, and that most comprehensive studies on the 12 linear elastic orthotropic parameters are relatively old, and based on a variety of test methods. As regards spruce, these parameters have been investigated in 8–10 independent studies on nearly as many subspecies. They are presented in comprehensive publications like Hearmon (1948), Kollmann and Côté (1968), Bodig and Jayne (1993), FPL (1999) and Dinwoodie (2000), although it should be noted that most of these values are based on earlier studies. The original references for spruce are tentatively summarized in Table 1. Except for NS 3470 (1999), it seems like the subspecies Norway spruce was investigated by Carrington (1923) only. Statistical analyses of the values in Table 1 give relatively high linear correlations with the density $\rho$ (kg/m$^3$) for $E_{LL}$ ($r^2$ = 0.74) and $E_{TT}$ ($r^2$ = 0.46), and low for the other. However, it should be noted that the values constitute averages, and that they consequently are not representative for the true variation in experimental data.

**Table 1:** Linear elastic orthotropic parameter values for various spruce species from literature ($E_{ii}$ and $G_{ij}$ in MPa)

| Type | Ref. | ρ | $E_{LL}$ | $E_{RR}$ | $E_{TT}$ | $\nu_{LR}$ | $\nu_{LT}$ | $\nu_{RL}$ | $\nu_{RT}$ | $\nu_{TL}$ | $\nu_{TR}$ | $G_{LR}$ | $G_{LT}$ | $G_{RT}$ |
|---|---|---|---|---|---|---|---|---|---|---|---|---|---|---|
| C14 | 1 | 350 | 7000 | 230 | 230 | - | - | - | - | - | - | 440 | 440 | - |
| C18 | " | 380 | 9000 | 300 | 300 | - | - | - | - | - | - | 560 | 560 | - |
| C24 | " | 420 | 11000 | 370 | 370 | - | - | - | - | - | - | 690 | 690 | - |
| C30 | " | 460 | 12000 | 400 | 400 | - | - | - | - | - | - | 750 | 750 | - |
| C40 | " | 500 | 14000 | 470 | 470 | - | - | - | - | - | - | 880 | 880 | - |
| Engelm. | 2 | - | 10300 | 690 | 410 | 0.76 | - | 0.08 | 0.49 | - | 0.25 | 620 | 620 | 50 |
| " | 3 | 314 | 6887 | 762 | 374 | 0.37 | 0.34 | - | 0.42 | - | 0.36 | 645 | 625 | 54 |
| " | " | 319 | 6322 | 780 | 361 | 0.47 | 0.49 | 0.07 | 0.47 | 0.04 | 0.20 | 854 | 788 | 71 |
| " | " | 330 | 6046 | 1301 | 350 | 0.49 | 0.48 | 0.11 | 0.88 | 0.04 | 0.20 | 962 | 873 | 76 |
| " | " | 318 | 5605 | 351 | 378 | 0.35 | 0.54 | 0.07 | 0.35 | 0.09 | 0.27 | 618 | 705 | 55 |
| " | 4 | 350 | 9790 | 1253 | 578 | 0.42 | 0.46 | 0.08 | 0.53 | 0.06 | 0.26 | 1213 | 1175 | 98 |
| " | 3 | 320 | 10438 | 700 | 386 | - | - | - | - | - | - | 610 | 590 | 51 |
| Black | " | 380 | 11527 | 830 | 494 | - | - | - | - | - | - | 699 | 663 | 66 |
| Red | " | 380 | 11506 | 830 | 494 | - | - | - | - | - | - | 699 | 663 | 66 |
| Sitka | " | 380 | 11823 | 830 | 494 | - | - | - | - | - | - | 699 | 663 | 66 |
| " | 5 | 390 | 11600 | 900 | 500 | 0.37* | 0.47* | 0.03* | 0.43* | 0.02* | 0.25* | 750 | 720 | 39 |
| " | 4 | 350 | 10890 | 849 | 468 | 0.37 | 0.47 | 0.04 | 0.44 | 0.03 | 0.25 | 697 | 664 | 33 |
| " | 3 | 362 | 10748 | 649 | 348 | 0.34 | 0.40 |  | 0.42 | - | 0.38 | 533 | 438 | 41 |
| White | " | 380 | 10162 | 830 | 494 | - | - | - | - | - | - | 699 | 663 | 66 |
| Spruce | 6 | 440 | 15919 | 686 | 392 | 0.43* | 0.54* | 0.02* | 0.42* | 0.01* | 0.24* | 617 | 760 | 36 |
| " | " | 500 | 16706 | 810 | 633 | 0.37* | 0.56* | 0.02* | 0.43* | 0.02* | 0.33* | 624 | 853 | 35 |
| " | 7 | 500 | 16600 | 850 | 690 | 0.36 | 0.52 | 0.02 | 0.43 | 0.02 | 0.33 | 630 | 840 | 37 |
| " | " | 370 | 9900 | 730 | 410 | 0.44 | 0.56 | 0.03 | 0.57 | 0.01 | 0.29 | 496 | 607 | 21 |
| " | " | 390 | 10700 | 710 | 430 | 0.38 | 0.51 | 0.03 | 0.51 | 0.03 | 0.31 | 500 | 620 | 23 |
| Norway | " | 390 | 10900 | 640 | 420 | 0.39 | 0.49 | 0.03 | 0.64 | 0.02 | 0.32 | 580 | 590 | 26 |
| Silver | 8 | 430 | 13500 | 890 | 480 | 0.45 | 0.54 | - | 0.56 | - | 0.30 | 717 | 496 | 34 |
| Spruce | 9 | 440 | 15900 | 690 | 390 | 0.44 | 0.38 | 0.03 | 0.47 | 0.01 | 0.25 | 620 | 770 | 36 |
| Average |  | 390 | 10991 | 716 | 435 | 0.42 | 0.48 | 0.05 | 0.50 | 0.03 | 0.28 | 682 | 693 | 49 |

*) Poisson's ratios are probably reconciliated by Eq. (3.22).

1. NS 3470 (1999)
2. Goodman and Bodig (1970)
3. Bodig and Goodman (1973)
4. FPL (1999)
5. Doyle et al. (1945)
6. Kollmann and Côté (1968)
7. Carrington (1923)
8. Jenkin (1920)
9. Stamer (1935)

# 4. Nonlinear behaviour

It is broadly recognized that wood shows relatively linear elastic behaviour in tension, followed by brittle failure, whereas nonlinearity can be observed in compression, and to some extent in shear. This applies to a varying degree to each of the three principal material directions and planes of the cellular and porous material, permitting substantial compaction in compression and shear. The nonlinearity is in the longitudinal direction caused by local cell wall buckling and separation of fibres until a defined ultimate load is reached, whereas the mechanisms of the two transverse directions are more obscure, with indistinct compressive capacities. Either case results in non-recoverable (inelastic) strain causing permanent change of shape after removal of the load. On a macroscopic level, the deformation occurs relatively homogeneously, whereas it on microscopic levels appears localized in single rows of cells. So-called densification can occur for very high compressive strains (>30–50%). The behaviour of the various principal directions and planes are indicated in Figure 4-1.

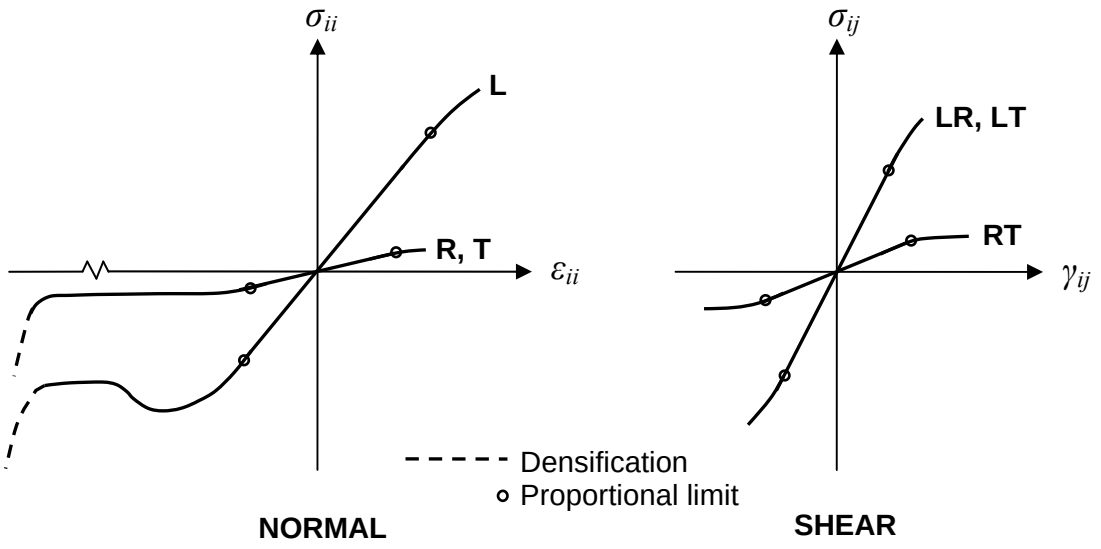


**Figure 4-1:** Stress-strain curves of clear wood in each material direction *i* and plane *ij*

Nonlinearity in wood resembles metallic plasticity, although the basic mechanisms in many ways are different. For simplicity, and for the lack of more appropriate concepts, the nonlinearity is in the following described with terms and theory referring to metallic plasticity. Therein, inelasticity due to external loading translates into changes in the inter-atomic spacing. If the post-yield stress-strain relation shows a positive slope, the behaviour is defined as elasto-plastic with strain hardening. If the slope on the other hand is zero, it is defined as elasto-ideal-plastic. The magnitude of plastic deformations before failure defines whether a material can be characterized as brittle or ductile.

The nonlinear zone is generally avoided in design of timber structures. However, in order to model highly stressed regions such as the connection points of a structure accurately, macro scale nonlinearity should be accounted for. The wood crushing, or plastification, around dowel bolts can be of importance for the global behaviour of systems including ductility, redundancy and post failure characteristics. If a linear elastic model is assumed, stresses may in certain areas be highly overestimated, whereas stress redistribution is not accounted for. An elasto-ideal-plastic model can

partly remedy the latter, but is vulnerable to predict too low stresses where hardening in reality is present. Some kind of an orthotropic elasto-plastic model may therefore be appropriate for modelling nonlinearity on the macro scale of wood (Moses and Prion 1999). A short survey of general plasticity theory, as a framework for quantification of nonlinearity in wood, is given in the following.

## 4.1. Theory of plasticity

A basic assumption in the general theory of plasticity is the existence of a yield surface defined by a function $f(\boldsymbol{\sigma}, \mathbf{q})$, dependent on the 6 stress components in $\boldsymbol{\sigma}$ and a set of internal variables $\mathbf{q}$ governing the surface evolution. If the material is assumed elasto-ideal-plastic, the yield function is independent of $\mathbf{q}$ and the relation reduces to $f(\boldsymbol{\sigma})$. A material is defined to be in an elastic state when $f < 0$, and in a plastic state when $f = 0$. That is, if the stresses exceed a critical value, the material will undergo plastic or irreversible deformation, also referred to as yielding. Further deformation is restricted by stresses to remain on the yield surface, although the surface itself may change shape and size during yielding. The function $f$ depends on material, and can be given by well-known criteria like the von Mises or Tresca, or by more advanced variants such as the modified anisotropic Hill criterion (ANSYS 2005c) described in PAPER IV (Dahl and Malo 2009e).

The theory is based on an incremental formulation, where the stress increment is related to strain increments separated into elastic and plastic parts, writing

$$d\varepsilon_{qr} = d\varepsilon_{qr}^{e} + d\varepsilon_{qr}^{p} \tag{4.1}$$

The elastic increment can be expressed by Eq. (3.19), whereas the plastic is defined by a flow rule, writing

$$d\varepsilon_{qr}^{e} = S_{qrst} d\sigma_{st} \tag{4.2}$$

$$d\varepsilon_{qr}^{p} = d\lambda\, r_{qr} = d\lambda \frac{\delta g}{\delta \sigma_{qr}} \tag{4.3}$$

where $d\lambda$ (plastic multiplier) denotes the magnitude of the incremental plastic strain, and $r_{qr}$ denotes the yield-gradient. The flow rule is referred to as associative if $g = f$. For materials with strain hardening (not ideal-plastic), material parameters constituting $\mathbf{q}$ can be determined by experiments as described in PAPER III and VIII (Dahl and Malo 2009d, h). Moreover, the assumption of plastic incompressibility is important for the evolution of the plastic strains. It falls beyond the scope of this thesis to evaluate this any further.

## 4.2. Nonlinear parameters

Experimental data for the nonlinear range of wood are hard to find in the literature. Moreover, it does not seem like any general constitutive law comprising nonlinearity exists for wood. Comprehensive publications like Kollmann and Côté (1968), Bodig and Jayne (1993), Dinwoodie (2000) and Smith et al. (2003) all state that wood behaves nonlinearly in the upper stress range, but

quantifications of the behaviour are scarce. Nonlinear behaviour in compression and shear was presented by tri-linear stress-strain relationships by Patton-Mallory et al. (1997), although coupling between the principal directions was ignored. Constitutive laws for continuous materials were hence not obeyed (Kharouf 2001, Smith et al. 2003). Elasto-plastic models based on the modified Hill criterion (Hill 1956, Shih and Lee 1978), in conjunction with bilinearity or trilinearity, has been used by Moses (2000), Kharouf (2001), Clouston and Lam (2001) and Hong and Barrett (2006, 2008) to estimate three-dimensional stress states in wood and wooden composites. These models are originally developed for anisotropic metals, and allow different yield stresses and tangent moduli for each stress component in tension and compression. However, it seems like simplifications have been necessary in several cases for the lack of parametric data. Moreover, experimentally based parameters for spruce violate the inherent plastic incompressibility assumption (ANSYS 2005c), and thereby a set of consistency equations, making it less suited for a general representation of nonlinear wood behaviour (PAPER IV - Dahl and Malo 2009e).

Several studies have been focusing on nonlinear uniaxial compression. Thelandersson and Larsen (2003) refer to an empirically based power law for the longitudinal direction, although species is not assigned. Likewise, Ramberg and Osgood (1943) and O´Halloran (1973) fitted continuous power functions for spruce in compression, presumably in the longitudinal direction. Yoshihara and Ohta (1992, 1994, 1997) found power and exponential functions for uniaxial compressive behaviour of specimens with varying fibre inclination angles in the *LR*-plane, including the longitudinal and radial directions. Tabiei and Wu (2000) used these power functions, together with similar shear results, to obtain correspondence between numerical and experimental nonlinear data for shear and compression in the *LR*-plane. Dumail and Salmén (1997) investigated water saturated Norway spruce loaded perpendicularly in compression. A rather distinct proportional limit was found, followed by relatively low strain hardening up to 30% strain, from where a rise in the hardening was observed. The latter was probably caused by cell voids reaching a minimum, and is referred to as densification. Mackenzie-Helnwein et al. (2003) included both strength degradation (strain softening) and subsequent densification (strain hardening) for compression in the longitudinal direction of spruce by exponential and a power functions, respectively. No degradation could be substantiated radially, and strain hardening followed by densification (increased strain hardening) was modelled in the radial direction. Parameters originating from different studies were used (Faessel et al. 1999, Lucena-Simon et al. 2000, Eberhardsteiner 2002, Adalian and Morlier 2002).

As regards tension and shear, nonlinear shear behaviour was documented by means of torsion tests by Yoshihara and Ohta (1995a, c, 1996), Yoshihara et al. (1997) and Yamasaki and Sasaki (2003, 2004). Similar results were found by means of the Iosipescu shear test by Yoshihara et al. (1999, 2001) and Yoshihara and Matsumoto (2005). Ukyo and Masuda (2006) used the ASTM D143 (1984) shear block test to document nonlinearity. It does not seem like any of the aforementioned studies have focused on nonlinearity in tension. Moreover, tangentially oriented compression, as well as rolling shear seem to be neglected. It may consequently be concluded that the experimental basis is not sufficient for a general nonlinear description of spruce. This is also due to the fact that many studies are focusing on other species, and that quite different experimental tests and adaption models have been used in the various studies. As stated by many of the aforementioned references, it is thus a need for a more thorough description of the nonlinear range of wood, including development of a generalized constitutive model.

# 5. Failure prediction

Wood is characterized by quite different strengths in tension and compression in the three material directions, and for the case of shear, between the three material planes. A major concern in timber engineering is the low tensile capacities in the two transverse directions. In real structures, more failures have probably occurred due to stresses perpendicular to grain than parallel, although the latter is the principal direction of stresses in most structural members, except in joint regions. Among several others, Gustafsson (2003) states the basis for engineering strength analyses in timber constructions to be somewhat crude, both with respect to failure theory and strength parameters. Because of direction dependency, traditional criteria like von-Mises and Tresca will not provide useful predictions. A short survey of more appropriate strength theories for wood is summarized in the following.

## 5.1. Failure theory

A stress-based failure criterion may generally be written as

$$F\left(\sigma_{ij}, \lambda\right) = 1 \tag{5.1}$$

where $F < 1$ predicts sufficient capacity, whereas $F \geq 1$ predicts an instable condition of failure, wherein $\lambda$ is a set of material parameters typically comprising the uniaxial strength(s). Hence, the criterion is phenomenological in the sense that the structural component is assumed to fail as soon as the state of stresses in some point of the geometry fulfils the criterion, although it does not distinguish between brittle and ductile failures. It should be noted that $F$ can be formulated on a strain basis instead of stresses. It is also important to recognize that $F$ is empirically based, assuming a homogeneous and continuous material. Hence, it will not work properly in regions with steep stress gradients or where irregularities are present. Moreover, the criteria are incapable of representing stress redistribution occurring on meso and micro levels (Smith et al. 2003).

Eq. (5.1) describes a single failure surface in stress space. It should be noted that Mackenzie-Helnwein et al. (2003) made use of a multi-surface model with four surfaces for the two-dimensional *LR* case. This was mainly motivated by the need of distinguishing the failure mode with respect to subsequent softening or hardening rules, see Ch. 4.2. Eberhardsteiner (2002) found that a single surface model based on the Tsai-Wu criterion fitted the same experimental failure data well (Mackenzie-Helnwein et al. 2003).

## 5.2. Ultimate stress criterion

The ultimate (or maximum) stress criterion $F^{MAX}$ is probably the most intuitive failure criterion, as normal and shear stresses in each principal direction and plane, respectively, are limited to the corresponding strength values, writing (not sum over indices)

$$F^{MAX} = \max\left\{\frac{\sigma_{ii}}{\sigma_{+ii}^{ult}}, \frac{\sigma_{ii}}{-\sigma_{-ii}^{ult}}, \frac{\left|\sigma_{ij}\right|}{\sigma_{ij}^{ult}}\right\} \qquad \{i,j\} = \{L, R, T\},\ i \neq j \tag{5.2}$$

Here, $\sigma_{\pm ii}^{ult}$ denotes the orthotropic strengths in tension (+) and compression (–) and $\sigma_{ij}^{ult}$ correspondingly in shear. Totally 3 shear capacities and 6 normal capacities are thus required to comprise the compressive and tensile sides of an orthotropic material ($\sigma_{-ii}^{ult}$ handled positive). All can be determined experimentally, although the shear and particularly transverse strengths can be somewhat cumbersome to obtain for wood. Any effect from interaction between the stresses is not included, which in certain cases may lead to non-conservative design.

## 5.3. Hankinson formula

The first formula for the compressive strength of wood at an arbitrary angle $\psi$ to the grain was proposed by Hankinson (1921) for a two-dimensional case:

$$\sigma_{-\psi}^{ult} = \frac{\sigma_{-LL}^{ult} \cdot \sigma_{-PP}^{ult}}{\sigma_{-LL}^{ult} \cdot \sin^2 \psi + \sigma_{-PP}^{ult} \cdot \cos^2 \psi} \tag{5.3}$$

Later, Kollmann and Côté (1968) found that the relation, in a modified form, also is suitable for evaluating the tensile strength:

$$\sigma_{+\psi}^{ult} = \frac{\sigma_{+LL}^{ult} \cdot \sigma_{+PP}^{ult}}{\sigma_{+LL}^{ult} \cdot \sin^n \psi + \sigma_{+PP}^{ult} \cdot \cos^n \psi} \tag{5.4}$$

where $\sigma_{\pm LL}^{ult}$ and $\sigma_{\pm PP}^{ult}$ denote the normal strengths in the longitudinal (*L*) and perpendicular (*P*) to grain directions, respectively, analogously to the indices in Ch. 3.3 for transverse isotropy. Values of *n* from 1.5–2.0 were found to give satisfactory agreement with experimental data. The Hankinson formulas, although strictly empirical, have according to Liu (1984) proved to fit experimental data for wood reasonably well in several studies. However, Thelandersson and Larsen (2003) state that the criterion (with $n = 2$) is generally on the unsafe side, especially for small angles $\psi$.

## 5.4. Norris criterion

Norris (1962) developed a strength theory for orthotropic materials based on the Henky-von-Mises isotropic theory, assuming a plane state of stresses and no distinction between radial and tangential properties:

$$F^N = \sqrt{\left(\frac{\sigma_{LL}}{\sigma_{\pm LL}^{ult}}\right)^2 + \left(\frac{\sigma_{PP}}{\sigma_{\pm PP}^{ult}}\right)^2 + \left(\frac{\sigma_{PL}}{\sigma_{\pm PL}^{ult}}\right)^2} \tag{5.5}$$

where the strength denotation is as described in Ch. 5.3, and $\sigma_{PL}^{ult}$ is the shear strength in the *PL* plane. Gustafsson (2003) states a tripartite variant including an extra term, comprising each combination of the three orthotropic directions. The criterion has been verified for wood by off-axis compressive and tensile tests. It is an obvious drawback that the criterion does not separate between tensile and compressive capacities, and consequently must be applied in a piecewise manner (Smith

et al. 2003). Nevertheless, Liu (1984) states that the Norris criterion and the Hankinson formula have enjoyed more popularity in the wood industry than any other criteria.

## 5.5. Tsai-Wu criterion

The failure criterion suggested by Tsai and Wu (1971) seems particularly suited for wood, as it includes both orthotropy and interaction effects, and moreover allows different tensile and compressive capacities, writing

$$F^{TW} = F_{ii}\sigma_{ii} + F_{ijkl}\sigma_{ij}\sigma_{kl} \qquad \{i, j, k, l\} = \{L, R, T\} \tag{5.6}$$

where $F_{ii}$ and $F_{ijkl}$ are strength tensors of 2nd and 4th order, respectively. Higher order terms ($F_{ijklmn}$ $\sigma_{ij}\,\sigma_{kl}\,\sigma_{mn}$) are ignored, since the number of components in a 6th order tensor would run into the hundreds, and the failure surface then would become open-ended in stress space (Tsai and Wu 1971). Given that the axis system is unidirected with the principal material orientations *LRT*, components $F_{iikl}$ ($k \neq l$) vanish, i.e. no coupling exists between normal and shear stress components. With the indices given in Eq. (3.20), Eq. (5.6) reads (in Voigt matrix form)

$$F^{TW} = \begin{bmatrix} \sigma_{LL} \\ \sigma_{RR} \\ \sigma_{TT} \\ \sigma_{RT} \\ \sigma_{LT} \\ \sigma_{LR} \end{bmatrix}^T \begin{bmatrix} F_{LL} \\ F_{RR} \\ F_{TT} \\ 0 \\ 0 \\ 0 \end{bmatrix} + \begin{bmatrix} \sigma_{LL} \\ \sigma_{RR} \\ \sigma_{TT} \\ \sigma_{RT} \\ \sigma_{LT} \\ \sigma_{LR} \end{bmatrix}^T \begin{bmatrix} F_{LLLL} & F_{LLRR} & F_{LLTT} & 0 & 0 & 0 \\ & F_{RRRR} & F_{RRTT} & 0 & 0 & 0 \\ & & F_{TTTT} & 0 & 0 & 0 \\ & & & F_{RTRT} & 0 & 0 \\ & sym & & & F_{LTLT} & 0 \\ & & & & & F_{LRLR} \end{bmatrix} \begin{bmatrix} \sigma_{LL} \\ \sigma_{RR} \\ \sigma_{TT} \\ \sigma_{RT} \\ \sigma_{LT} \\ \sigma_{LR} \end{bmatrix} \tag{5.7}$$

Due to symmetry, the function involves twelve non-zero parameters. Nine can be related directly to the respective failure stresses by (not sum over indices)

$$F_{ii} = \frac{1}{\sigma_{+ii}^{ult}} - \frac{1}{\sigma_{-ii}^{ult}} \qquad F_{iiii} = \frac{1}{\left(\sigma_{+ii}^{ult} \cdot \sigma_{-ii}^{ult}\right)} \qquad F_{ijij} = \frac{1}{\left(\sigma_{ij}^{ult}\right)^2} \quad (i \neq j) \tag{5.8}$$

wherein compressive strengths $\sigma_{-ii}^{ult}$ are handled as positive numbers. $F_{ii}$ accounts for differences in compressive and tensile strengths, which distinguishes the criterion from the criterion by Hill (1956). The three remaining components $F_{iijj}$ ($i \neq j$) are so-called coupling or strength interaction coefficients between normal stress components, which must be determined experimentally by biaxial or off-axis uniaxial tests (Tsai and Wu 1971). However, in order to define an elliptic (closed, not hyperboloid) surface in the plane of normal stress components, they must satisfy

$$F_{iiii}F_{jjjj} - F_{iijj}^2 \geq 0 \qquad (i \neq j) \tag{5.9}$$

Geometrically, this insures that the failure surface will intercept each stress axis. By using the default value stated in Eq. (5.10), it can be shown that the Tsai-Wu criterion is a generalization of the von-Mises criterion (Tsai and Hahn 1980), writing (not sum over indices)

$$F_{iijj} = F_{jjii} = -\frac{1}{2}\sqrt{F_{iiii}F_{jjjj}} = -\frac{1}{2}\left(\sigma_{+ii}^{ult}\cdot\sigma_{-ii}^{ult}\cdot\sigma_{+jj}^{ult}\cdot\sigma_{-jj}^{ult}\right)^{-\frac{1}{2}} \qquad (i \neq j) \qquad (5.10)$$

For wood in a biaxial state, Cowin (1979) used a strength interaction coefficient of

$$F_{iijj} = \sqrt{F_{iiii}F_{jjjj}} - \frac{1}{2}F_{ijij} \qquad (i \neq j) \qquad (5.11)$$

Eberhardsteiner (2002) documented the *LR* interaction coefficient ($F_{LLRR}$) of spruce by means of biaxial tests, whereas Clouston et al. (1998) used off-axis tests to document one of the interaction coefficients in laminated veneer from Douglas fir.

## 5.6. Strength parameters

Except for the Tsai-Wu interaction coefficients, all criteria in Eq. (5.2)–(5.6) can be fully described by means of the orthotropic failure stresses, where it is distinguished between tension and compression. There are numerous studies reporting the longitudinal compressive and tensile strengths of wood, although the tensile references are fewer. Strength values of the two transverse directions are scarce, and seem to be vulnerable to distorted values in standardized testing, see PAPER VI (Dahl and Malo 2009b). Moreover, it is seldom distinguished between the radial and tangential directions. Shear strengths also seem to be vulnerable to test configuration effects, as outlined in PAPER III and V (Dahl and Malo 2009d, g), and especially rolling shear is neglected in experimental testing. Other aspects of pertinent interest are possible size effects, especially for brittle failure modes. Out of studies focusing on orthotropic strength parameters, relatively few refer to Norway spruce, and particularly to the subspecies *Picea Abies* L. Karst. Hence, no known study exists that comprise all orthotropic strength values of Norway spruce.

It is beyond the scope of this thesis to summarize strength values for spruce from the various studies, and only some references pertaining to *Picea Abies* L. Karst. from Norway will be referenced: Okstad and Kårstad (1985) tested clear wood specimens from Northern Norway and found an average longitudinal compression strength of 40.5 N/mm$^2$ and a tangential compression strength of 4.65 N/mm$^2$, although the latter presumably was tested laterally with strengths referring to the proportional limit stress (NTI 1966), and thus not necessarily reflects real properties. Similarly, Foslie (1971) found a longitudinal compressive strength of 41.7 N/mm$^2$. NS 3470 (1999) states lower 5–percentils for compression from 16–27 N/mm$^2$ longitudinally and 4.3–5.7 N/mm$^2$ transversely for grading class C14–C30. For tension, the corresponding values range from 8–18 N/mm$^2$ and 0.3–0.4 N/mm$^2$. The shear strengths lie between 1.7–3.0 N/mm$^2$ for ordinary shear, whereas it is stated that rolling shear hold 50% of these values. Some values in NS-EN 338 (2003) vary somewhat from NS 3470 (1999); this might be caused by other provenances.

# 6. Probabilistic properties

As wood is an inhomogeneous material with highly variable properties, even over moderate sizes, it is pertinent to document the probabilistic properties on massive and macro scale levels. This is underpinned by the fact that wood often fails in a brittle mode, with little or no redundant capacity from ductility such as steel exhibits. Distributional parameters can be applied directly in probabilistic analyses in modern FEM packages in conjunction with orthotropy, nonlinearity and failure prediction (ANSYS 2005a, b). This is a fascinating approach which allows more thorough analyses comprising sensitivity studies between input and output, serviceability, overall structural redundancy and general reliability assessments. Especially effects from uncertainties in material parameters may be quantified with a higher degree of accuracy. However, the scarcity of statistical input is to some extent hampering probabilistic analyses in timber engineering, particularly in macro scale analyses where more material parameters definitively are required. The lack of statistical data for proper quantification of variability in wood is among others discussed by Isaksson (2003). Köhler et al. (2007) state that it is of utmost importance to develop consistent probabilistic models for solid wood and wood based materials, with a particular focus on timber connections in order to improve competitiveness to other building materials. In this sense, probabilistic methods may facilitate innovations in application and manufacture of wood and wood-based products for structural use (Foschi 2003).

Many factors may influence property variation in clear wood, such as moisture content, temperature, specimen size and loading time. These factors are due to the scope not studied herein. Moreover, it is assumed that that the probabilistic properties are constant within the macro scale specimens, which hence can be regarded as the representative volume elements (RVE).

In addition to distributional characteristics, investigation of parametric interrelationships (correlation) is aspired. Correlations can be utilized in probabilistic analyses to narrow output variability, and may hence be important for a highly variable material like wood. Moreover, as timber is a graded material with certain indicative material properties documented, such as density and longitudinal (bending) modulus, interrelationships can be used to estimate undocumented orthotropic parameters.

## 6.1. Probabilistic analyses

Among the most efficient methods to calculate probabilities in structural problems are approximate methods referred to as FORM and SORM (First/Second Order Reliability Methods). These are based on the calculation of a reliability index, which can be understood by a geometrical approach excellently described by Foschi (2003).

A more straightforward variant is Monte Carlo analyses. By repeating a calculation $N$ times, for which stochastic input values $x_i$ are drawn from statistical distributions, a set of deterministic output values are generated. If $N$ is sufficiently large and $N_f$ designates the number of non-performance events, the probability of failure $P_f$ will simply be $N_f / N$. Hence, the method is relatively intuitive from an engineering viewpoint, and can easily be undertaken by means of sequential FEM simulations in commercial software, see PAPER VII (Dahl and Malo 2009c). It should be noted that in cases where $P_f$ in reality is small, a very large number of simulations must be undertaken to attain

a reasonable approximation. This can consequently cause time-consuming analyses for complex and nonlinear problems. To remedy this, adaptive sampling methods can be used, mainly drawing $x_i$ values from regions of importance. For very efficient analyses required for instance in dynamic problems, response surfaces may be produced, based on a sufficient set of distinct points with mathematical fitting between (Foschi 2003).

## 6.2. Statistical distributions

Based on assignments for timber by JCSS (2006), the normal, lognormal and Weibull distributions were assessed as most pertinent for characterization of the clear wood properties. The distributions can be found in any introductory book to statistics, but are briefly presented in the following for consistency and symbol definition.

**The normal distribution**

The normal probability density function for $x$ is given by

$$f(x,\sigma,\mu) = \frac{1}{\sigma\sqrt{2\pi}} \cdot e^{\left(-\frac{(x-\mu)^2}{2\sigma^2}\right)} \tag{6.1}$$

where $\mu$ is the mean and $\sigma$ is the standard deviation. The function is symmetrical about $\mu$. If experimental data gives a distribution with left dominance, its skewness $g$ is said to be positive, and visa versa for right dominated data, and may indicate that another distribution is more appropriate. The normal (Gaussian) distribution comprises both positive and negative values of $x$, which may give erroneous results in probabilistic analyses where stiffness and strength cannot attain negative values, particularly for low $\mu$ and relatively high $\sigma$ values.

**Lognormal distribution**

A continuous random variable $x$ is lognormal distributed if ln($x$) follows a normal (Gaussian) distribution. The lognormal probability density function for $x$ is given by

$$\begin{aligned} f(x,\xi,\delta) &= \frac{1}{x\cdot\delta\cdot\sqrt{2\pi}} \cdot e^{\left(-\frac{(\ln(x)-\xi)^2}{2\delta^2}\right)} && \text{for } x \geq 0 \\ f(x,\xi,\delta) &= 0 && \text{for } x < 0 \end{aligned} \tag{6.2}$$

where $\xi$ is the logarithmic mean value equal to the mean value of ln($x$), and $\delta$ is the logarithmic deviation equal to the standard deviation of ln($x$). A lognormal distribution is specified either by $\xi$ and $\delta$, or the mean value and the standard deviation of the random input variable $x$ (Walpole 2002, ANSYS 2005a, b). The parameters are related to the mean E($x$) and the variance Var($x$) by

$$E(x) = e^{\left(\xi+\delta^2/2\right)} \qquad Var(x) = \left(e^{\delta^2}-1\right)e^{\left(2\xi+\delta^2\right)} \tag{6.3}$$

The fact that $f = 0$ for negative $x$-values makes the lognormal distribution well suited for representing strength and stiffness parameters. A three-parameter lognormal distribution is defined by replacing $x$ by $(x–x_0)$ in Eq. (6.2), where $x_0$ is denoted the location (threshold) parameter, defining the lower limit of $x$ (Minitab 2006). A negative $x_0$ value is unphysical for strength and stiffness values, although a positive value also can be hard to substantiate, which all in all makes the two-parametric variant more pertinent for this purpose.

**Weibull distribution**
The Weibull probability density function for $x$ is given by

$$f\left(x,k,m,x_0\right) = \frac{k}{m}\cdot\left(\frac{x-x_0}{m}\right)^{k-1}\cdot e^{\left(-\left(\frac{x-x_0}{m}\right)^{k}\right)} \qquad \text{for } x \geq 0$$
$$f\left(x,k,m,x_0\right) = 0 \qquad \text{for } x < 0 \tag{6.4}$$

where $k$ (> 0) is the so-called shape parameter, $m$ (> 0) is the scale parameter and $x_0$ is the location (threshold) parameter defining the lower limit of $x$. When $x_0 = 0$ it reduces to a two-parameter Weibull distribution, which may be more physical meaningful, analogous to the lognormal distribution. It can be shown that the Weibull is an asymptotic representation of the distribution corresponding to the minimum value among a large number of samples of the variable $x$. This makes the Weibull distribution suited for representing strengths, especially for brittle materials such as wood loaded in shear and tension (Foschi 2003).

## 6.3. Probabilistic parameters

The Wood Handbook by FPL (1999) states coefficients of variation (CV) for the basic strength parameters of wood between 0.14–0.28, with highest variation transversely. Similarly, the probabilistic model code by JCSS (2006) states CVs of European solid softwoods between 0.1–0.3 for strength and stiffness parameters used in timber engineering (massive scale). It is moreover given correlation coefficients between 0.2–0.8, inter-parametric relationships (linear or power functions) and statistical distribution types for the various properties. Orthotropic clear wood properties are not treated, although it should be noted that some can be related to the stated values. Köhler and Faber (2006) assert that more experimental data should be culled and assessed in order to develop the JCSS (2006) code for timber further.

Okstad and Kårstad (1985) found relatively normal distributed longitudinal modulus ($E_{LL}$) with $\mu$ = 9700 N/mm$^2$, CV = 0.18 and $g$ = 0.58 by means of bending tests of small clear specimens from Norway spruce. Similarly, the compressive strength longitudinally ($\sigma^{ult}_{-LL}$) resulted in $\mu$ = 40.5 N/mm$^2$, CV = 0.14 and $g$ = 0.31, whereas the tangential strength ($\sigma^{lin}_{-TT}$) gave $\mu$ = 4.65 N/mm$^2$, CV = 0.20 and $g$ = 0.75, all with left dominance. Foslie (1971) found $E_{LL}$ with $\mu$ = 9 807 N/mm$^2$ and CV = 0.16, and $\sigma^{ult}_{-LL}$ with $\mu$ = 41.7 N/mm$^2$ and CV = 0.21, both normal distributed with left dominances ($g$ not given).

# 7. Experimental assessments

As stated in Ch. 3.5 and 5.6, many standardized tests seem less appropriate for determination of representative material properties, and are apparently historically based in several cases. Moreover, many macro scale parameters lack standardized experimental procedures. The tests used herein are therefore based on so-called exploratory methods, where the following is emphasized:

- Specimens are tentatively designed to yield a uniform and pure state of stresses in the measured and critical parts. Stress and strain gradients are consequently sought minimized.

- Configurations effects are sought reduced to a minimum. For example, tensile specimens are loaded by means of bolts instead of clamping to avoid introduction of bending moments.

- Although specimens are designed to yield realistic material data, it is generally recognized that experimental data can hardly yield the true material characteristics due to inevitable configuration and measurement effects. Numerical analyses of experimental results are therefore emphasized for possible parameter modification.

- Specimens are given a size which corresponds with finite elements pertinent for meso scale problems (0.01–0.1 m).

- In order to obtain consistency between the various parameters, the tests are organized so that the linear, nonlinear and failure parameters governing the behaviour of a stress component can be determined from the same specimen. Moreover, the same specimen type and size is tentatively used for all principal material directions and planes, although some compromises are necessary in tension and shear due to very different strengths. Hence, configuration and size effects ought to be relatively congruent.

- Material inhomogeneity is minimized by the use of clear wood, partly from graded material, and partly from logs taken directly from the forest, see Figure 7-1.

- Specimens are tentatively produced with a Cartesian coordinate system instead of a polar system, as discussed in Ch. 3.4, so as to facilitate plane strain measurements with reference to material axes. It should be noted that this requires specimens to be taken predominantly from the outer part of the wooden stems, implying that sapwood is overrepresented, and heartwood visa versa. According to Sunde (2005), this may cause the longitudinal elastic modulus to be lower, although Bengtson (2000) and Dahlblom et al. (2000) contrarily reported increasing modulus from the pith and outwards in spruce. Foslie (1971) found that material from the top has generally better quality than from the lower end in Norway spruce.

- The three in-plane strain components are measured in all experiments, allowing investigation of both elastic moduli and Poisson's ratios in tensile and compressive testing, and shear moduli in shear testing. Moreover, the inclusion of shear strain may provide useful information also in compressive and tensile tests, as it indicates fibre inclination in orthotropic materials; see PAPER VII (Dahl and Malo 2009c).

- A minimum of 30 tests are tentatively used for determination of each parametric value, in order to obtain estimates with an acceptably low spread. The number is stipulated by rearrangement of the 95% confidence interval formula, writing

$$\sqrt{n} = \frac{2 \cdot 1,96}{100 \cdot TOL} \cdot CV \qquad (7.1)$$

  With a tolerance (*TOL*) of 15%, limiting the confidence interval to ±15% of the average value, and an assumed coefficient of variation (CV) of 20% for the various parameters (FPL 1999), the number equals $n = 27$. A CV of 30% results in $n = 62$, whereas a TOL of 5% gives $n = 246$, which definitively is too many tests from a practical point of view. A minimum of 30 tests gives an estimated tolerance somewhat lower than ±15%, which is assessed acceptable for a highly variable material such as wood.

- The material is conditioned to a reference climate of 12% moisture and 20˚C in order to correspond with test standard specifications. Similarly, loading rates are chosen so as to comply with the various specifications. Determined values should consequently be comparable to similar studies.

**Figure 7-1:** Timber logs with large diameters (0.6–0.8 m) during conditioning

# 8. Summary of publications

## 8.1. Appended papers

PAPER I **PLANAR STRAIN MEASUREMENTS ON WOOD SPECIMENS**
K.B. Dahl, K.A. Malo
*Experimental Mechanic*s *(2009) 49 (4): 575–586 © Springer*
*DOI: 10.1007/s11340–008–9162–0*
Description of the experimental method used for measurement and calculation of the three in-plane strain components.

PAPER II **LINEAR SHEAR PROPERTIES OF SPRUCE SOFTWOOD**
K.B. Dahl, K.A. Malo
*Wood Science and Technology (2009) 43 (5): 499–525 © Springer*
*DOI: 10.1007/s00226–009–0246–5*
Experimental and numerical determination of the 3 orthotropic shear moduli tested by means of the Arcan shear test, including probabilistic properties.

PAPER III **NONLINEAR SHEAR PROPERTIES OF SPRUCE SOFTWOOD: EXPERIMENTAL RESULTS**
K.B. Dahl, K.A. Malo
*Wood Science and Technology (2009) 43 (7): 539-558 © Springer*
*DOI: 10.1007/s00226–009–0247–4*
Experimental characterization of apparent nonlinear shear properties and strengths in each orthotropic plane, tested by means of the Arcan shear test.

PAPER IV **NONLINEAR SHEAR PROPERTIES OF SPRUCE SOFTWOOD: NUMERICAL ANALYSES OF EXPERIMENTAL RESULTS**
K.B. Dahl, K.A. Malo
*Composites Science and Technology (2009) 69 (13): 2144–2151 © Elsevier*
*DOI: 10.1016/j.compscitech.2009.05.011*
Numerical analyses of nonlinear shear behaviour reported in PAPER III, based on the modified Hill criterion, bilinearity in shear and optimization procedures.

PAPER V **SHEAR STRENGTHS OF SPRUCE SOFTWOOD: NUMERICAL ANALYSES OF EXPERIMENTAL RESULTS**
K.B. Dahl, K.A. Malo
*To be submitted*
Numerical analyses of the 3 orthotropic shear strengths reported in PAPER III and PAPER IV based on the ultimate stress and the Tsai-Wu failure criteria.

PAPER VI **LINEAR TENSILE AND COMPRESSIVE PROPERTIES OF SPRUCE SOFTWOOD: EXPERIMENTAL RESULTS**
K.B. Dahl, K.A. Malo
*To be submitted*

Experimental characterization of the 3 linear elastic moduli and the 6 Poisson's ratios tested in tension and compression in each orthotropic direction and plane.

PAPER VII **LINEAR TENSILE AND COMPRESSIVE PROPERTIES OF SPRUCE SOFTWOOD: NUMERICAL ANALYSES OF EXPERIMENTAL RESULTS AND FIBRE INCLINATION EFFECTS**
K.B. Dahl, K.A. Malo
*To be submitted*
Numerical analyses comprising Monte-Carlo simulations, of configuration and fibre inclination effects on results presented in PAPER VI, including probabilistic data.

PAPER VIII **STRENGTHS AND NONLINEAR PROPERTIES OF SPRUCE SOFTWOOD TESTED IN TENSION AND COMPRESSION: EXPERIMENTAL RESULTS**
K.B. Dahl
*To be submitted*
Experimental characterization of strengths and small-strain nonlinear behaviour in tension and compression, in each orthotropic direction and plane.

K.B. Dahl planned and conducted most experimental tests, and evaluated the experimental data in conjunction with numerical analyses. The first versions of the papers were written by K.B. Dahl, whereupon modifications from K.A. Malo were added. The papers are appended as finally submitted to the journals.

## 8.2. Other publications

In addition to the appended papers, the following works have been prepared:

I **DESIGN AND MODELLING OF CONNECTIONS IN TIMBER STRUCTURES**
K.B. Dahl
Project completion of TRE|UND at Britannia, Trondheim, Norway, November 2005

II **EVALUATION OF STRESS LAMINATED BRIDGE DECKS BASED ON FULL SCALE TESTS**
K.B. Dahl, N.I. Bovim, K.A. Malo
9th World Conference on Timber Engineering, Portland, OR, USA, 2006

III **NUMERICAL MODELLING OF WOOD**
K.B. Dahl
Project meeting at the Norwegian Institute of Wood Technology (NTI), Oslo, Norway, 2008

IV **TESTING OF SHEAR PROPERTIES OF SPRUCE SOFTWOOD - REPORT R-14-08**
K.B. Dahl
Dept. of Structural Engineering, NTNU, Trondheim, Norway, 2008

V **SHEAR TESTING OF NORWAY SPRUCE – LINEAR – NONLINEAR - PROBABILISTIC PROPERTIES**
K.B. Dahl
COST E55 meeting at NTNU, Trondheim, Norway, March 2009

# 9. Conclusions and further work

## 9.1. Conclusions

The present study provides linear, nonlinear and failure parameters for each orthotropic material direction and plane of clear wood from Norway spruce. Moreover, statistical distributions and inter-parametric correlations are presented. Several quantities have hardly been documented for Norway spruce earlier, and are also scarcely documented for spruce softwood in general. The values enable a basis for deterministic and probabilistic three-dimensional numerical analyses of spruce softwood on the macro scale level, suited for studies of details and joints in timber structures. Norway spruce is extensively used in the glulam industry, and the results are thus pertinent also for larger glulam constructions, wherein less irregularities and defects are found than in sawn lumber. The stress-strain relations in the upper stress ranges are also emphasized, as accurate predictions of ultimate deformations and capacities are crucial in many analyses. The parameters are determined by experimental testing under constant climatic conditions and loading rates in accordance with standardized procedures. Non-standardized specimens and test configurations were applied in order to improve the accuracy and the applicability of the findings, suitable for input in numerical simulations. It is shown in PAPER VII (Dahl and Malo 2009c) that the influence from configuration and measurement effects in tensile and compressive specimens was small, as opposed to the Arcan shear test where modifications were found required. In order to remove distorting effects, numerical (FEM) analyses were utilized to modify parameter values, and numerical reproducibility of most experimental findings can thus be asserted.

It is in PAPER I (Dahl and Malo (2009f) concluded that the applied video extensometry technique provides reasonable parametric results. Moreover, the bidimensional and noncontacting measurements over relatively large areas were found advantageous for characterization of the inhomogeneous wood material over the complete loading ranges. The three in-plane strain estimates are furthermore suitable for investigation of orthotropic materials, where non-zero shear strain may indicate fibre inclination, i.e. deviation between material axis and the uniaxial loading axis. This was investigated in PAPER VII (Dahl and Malo 2009c), where the linear elastic moduli and the Poisson's ratios reported in PAPER VI (Dahl and Malo 2009b) from tensile and compressive tests were modified for unintentional fibre inclination. Although the effects turned out to be relatively low for a highly variable material like wood, this error source is worth recognizing, especially as more detailed measurement techniques are likely to yield shear strain in wood due to fluctuating material directions and inaccurate carpentry. It can be argued that such irregularities generally are present, and it may consequently be discussed whether the modified or unmodified data set is most representative. Nevertheless, such deviations may be interpreted as material perturbations, which deliberately can be included in numerical simulations.

The relatively high Poisson's ratios reported in PAPER VI can indicate that a noncontacting measurement technique is important for wood, as inherent stiffness in conventional strain gages may introduce significant errors in the passive and relatively soft orientations. This is also pointed out by Yoshihara and Ohta (1995b). It should be noted that the two minor Poisson's ratios ($v_{RL}$, $v_{TL}$) were generally difficult to measure, and that they apparently violate compliance symmetry. This may indicate that the material is not behaving purely orthotropic, or that the resolution of the

measured data is somewhat coarse. It is also interesting to note, that significant differences in Poisson's ratios emerge between positive and negative strain rates.

PAPER II – V (Dahl and Malo 2009a, d, e, g) report findings from the Arcan shear test, which in a somewhat modified form was found applicable for testing of the three orthotropic shear stresses, including rolling shear. However, numerical calculations proved that modifications of nominal stiffness and strength values were required. As opposed to the general assumption, nonlinearity was observed in the upper stress ranges, which was quantified by means of Voce and bilinear models, the latter comprising linear/proportional stress limits and tangent moduli. The linear limit stresses were found to lie between 35–55% of the corresponding shear strengths, whereas the tangent moduli were 50–70% of the initial moduli for the longitudinal planes, and around 30% for rolling shear. Compared to completely linearized (secant) models, the bilinearity improves the stress prediction accuracy by a factor of approximately two. Numerical analyses assuming the three-dimensional Tsai-Wu criterion showed that the nominal strengths were measured 15–25% too low. Moreover, some test configurations were found to be preferred in the determination of strengths due to differences in strain field homogeneity.

PAPER VIII (Dahl and Malo 2009h) treats nonlinear properties and strengths in tension and compression in each orthotropic direction. As normally assumed, it was found that clear wood behaves relatively linear and brittle in tension, although slight deflections could be found for many configuration types. Nonlinearity and ductility were observed in compressive tests, particularly transversely, which due to practical reasons were limited to small strains (<2% at maximum). The nonlinear ranges were adapted to bilinear models analogously as shear. Linear limit stresses were found to lie at 65–70% of tensile strengths, and at 63–80% of compressive. The tensile tangent moduli range from 58–74% of the initial moduli, whereas all compressive lie at approximately 30%. Compared to completely linearized models in tension, the bilinear models improve the stress prediction accuracies by 10–50%, with linearized (secant) moduli being 5–10% lower than the initial moduli. It is emphasized that a generalized constitutive law comprising the nonlinear behaviour is not included in the thesis.

In total, the determined parameters comprise 12 linear elastic orthotropic values, 9 linear elastic stress limits, 9 tangent moduli, 6 tangent Poisson's ratios and 9 ultimate stresses, i.e. a total number of 45 macro scale parameters. 3 of these are given by the other due to compliance symmetry. As the number of parameters is relatively high, simplifications may be necessary for practical design. If the radial and tangential properties are set equal, i.e. a transversely isotropic model is assumed, the number is reduced to 27. It will naturally be further reduced if the material is assumed linear elastic in tension and/or shear, and if symmetry in the bilinear tangent values can be assumed. By way of comparison, NS 3470 (1999) states 10 massive/global scale parameters. It can be noted that commercial FEM codes such as ANSYS 10.0 allows direct use of most parameters documented herein, including orthotropy, bilinearity and the Tsai-Wu failure criterion in addition to probabilistic values. However, it seems like models for the nonlinear range should still be improved.

Paper II, IV, V, VII and VIII (Dahl and Malo 2009a, c, e, g, h) report statistical distributions of the documented parameters. The lognormal distribution gave best fit both for the shear moduli and the elastic moduli, which corresponds to assignments given by JCSS (2006). The Poisson's values are in general sufficiently fit by normal distributions. Whereas the linear shear stress limits and shear strengths are well represented by normal distributions, the bilinear normal stress parameters and strengths were harder to adapt. Generally, the three-parametric Weibull distribution gave best

adaption for these values. JCSS (2006) states three different distribution types for the various massive scale strengths. In total, this may indicate that no general conclusion can be drawn regarding distribution type for normal strength parameters, although the assessments herein can be vulnerable to somewhat few observations. Nevertheless, averages and coefficients of variation are documented for all parametric values. Moreover, correlations to density and correlations between parameters determined from the same specimen type are given. It is interesting to note that the inter-parametric correlations in many cases are significant. Similar correlation coefficients are given by JCSS (2006) for massive scale properties. Such parametric interrelationships can be utilized in probabilistic analyses, and will consequently narrow output variability. All in all, the documented properties should give an improved basis for deterministic and probabilistic analyses of macro scale details in timber constructions of Norway spruce.

## 9.2. Future work

The topics assessed as most pertinent for future work are:

- Investigation of the effect from grading class on strength and stiffness values presented in PAPER VIII (Dahl and Malo 2009h).
- Increase the basis for statistical distributions presented herein by identical or similar tests, preferably from graded material so that effects from grading on distributions can be quantified and utilized in design. Moreover, the lower tails of distributions should be investigated, especially for strengths.
- Investigation of spatial correlation fields between parameters, by deliberate treatment of specimen location in the lumber
- Experimental tests with video extensometry measurements on two surfaces instead of one, enabling more correlation coefficients to be determined, and generally increasing the experimental parameter basis. Moreover, shear strains, and thus fibre inclination on the various planes, can be better controlled.
- Further studies on large strain nonlinearity in radial and tangential compression.
- Investigation of nonlinear properties under repeated loading, including whether the material behaves plastic or partly hyperelastic, and whether material damage may influence on the behaviour.
- Investigation of the three interaction coefficients in the Tsai-Wu strength criterion by means of off-axis or biaxial tests.
- Experimental testing of failures initiated by a combination of shear and normal stresses by means of off-axis Arcan shear tests, so as to investigate the applicability of various criteria.
- Investigation of size effects, especially on strength values, by experimental testing of various specimen sizes, where defects and irregularities may be included by a weakest link theory.
- Implementation of a generalized material model for clear wood from spruce softwood, taking into account nonlinearity, size effects, moisture and failure prediction.

# Bibliography


Adalian C., Morlier P. (2002) Wood Model for the dynamic behaviour of wood in multiaxial compression. Holz als Roh- und Werkstoff 60 (6): 433-439.

Aicher S., Dill-Langer G., Höfflin L. (2001) Effect of polar anisotropy of wood loaded perpendicular to grain. Journal of materials in civil engineering 13 (1): 2-9.

ANSYS (2005a). Documentation for ANSYS Release 10.0. Theory Reference. Probabilistic Modeling and Preprocessing Chapter 21.1 Canonsburg, PA: A, ANSYS Inc., Southpointe, 275 Technology Drive, Canonsburg, PA15317, U.S.A.

ANSYS (2005b). Documentation for ANSYS Release 10.0. Advanced Guide. Probabilistic Design Chapter 3.3 Employing Probabilistic Design. Canonsburg, PA, ANSYS Inc., Southpointe, 275 Technology Drive, Canonsburg, PA15317, U.S.A.

ANSYS (2005c). Documentation for ANSYS Release 10.0. Theory Reference. Structures with Material Nonlinearities Chapter 4.1.4 Generalized Hill Potential Theory. Canonsburg, PA, ANSYS Inc., Southpointe, 275 Technology Drive, Canonsburg, PA15317, U.S.A.

ASTM D143 (1984) Standard Methods of Testing Small Clear Specimens of Timber. American Society for Testing and Materials, p. 42.

ASTM D198 (1999) Standard Test Methods of Static Tests of Lumber in Structural Sizes. American Society for Testing and Materials, p. 78.

ASTM D3500 (1990) Standard Test Methods for Structural Panels in Tension. p. 467-471.

Bengtson C. (2000) Stiffness of spruce wood - Influence of moisture conditions. Holz als Roh- und Werkstoff (58): 344-352.

Bodig J., Goodman J. R. (1973) Prediction of elastic parameters for wood. Wood Science (5): 249-264.

Bodig J., Jayne B. A. (1993) Mechanics of Wood and Wood Composites (2nd ed.), Krieger Publishing Company, Florida, US, p. 712.

Carrington H. (1923) The Elastic Constants of Spruce. Phil. Mag., London (45 (269)): 1055-1057.

Clouston P., Lam F. (2001) Computational modeling of strand-based wood composites. Journal of Engineering Mechanics 127 (8): 844-851.

Clouston P., Lam F., Barett J. D. (1998) Interaction Term of Tsai-Wu Theory for Laminated Veneer. Journal of materials in civil engineering 10 (2): 112-116.

Cowin S. C. (1979) On the strength anisotropy of bone and wood. ASME Journal of Applied Mechanics 46 (4): 832-837.

CRFR (2008) "Carbon and Forests", Campbell River Forest Research Ltd., from http://www.crfr.ca

Dahl K. B., Malo K. A. (2009a) Linear Shear properties of Spruce Softwood. Wood Science and Technology 43: 499-525, DOI 10.1007/s00226-009-0246-5.

Dahl K. B., Malo K. A. (2009b) Linear Tensile and Compressive Properties of Spruce Softwood: Experimental Results. To be submitted.

Dahl K. B., Malo K. A. (2009c) Linear Tensile and Compressive Properties of Spruce Softwood: Numerical Analyses of Experimental Results and Fibre Inclination Effects. To be submitted.

Dahl K. B., Malo K. A. (2009d) Nonlinear Shear Properties of Spruce Softwood: Experimental Results. Wood Science and Technology (DOI 10.1007/s00226-009-0247-4).

Dahl K. B., Malo K. A. (2009e) Nonlinear Shear Properties of Spruce Softwood: Numerical Analyses of Experimental Results. Composites Science and Technology 69: 2144-2151, DOI 10.1016/j.compscitech.2009.05.011.

Dahl K. B., Malo K. A. (2009f) Planar strain measurements on wood specimens. Experimental mechanics 49: 575-586, DOI 10.1007/s11340-008-9162-0.

Dahl K. B., Malo K. A. (2009g) Shear strengths of Spruce Softwood: Numerical Analyses of Experimental Results. To be submitted.

Dahl K. B., Malo K. A. (2009h) Strengths and Nonlinear Properties of Spruce Softwood Tested in Tension and Compression: Experimental Results. To be submitted.

Dahlblom O., Petersson H., Ormarsson S. (2000) Stiffness and shape stability grading analysis of sawn timber based on experimentally found growth characteristics. World Conference on Timber Engineering, Whistler Resort, British Columbia, Canada.

Daniel I. M., Ishai O. (2006) Engineering mechanics of composite materials (2nd ed.), Oxford University Press, Inc., New York, p. 411.

Dinwoodie J. M. (2000) Timber. Its nature and behaviour (2nd ed.), E & FN SPON, London, p. 257.

Doyle D. V., Drow J. T., McBurney R. S. (1945) Elastic Properties of Wood. Report 1528 A+B, Report 1528, 1528-A, 1528-B, Forest Products Laboratory, Madison Wisconsin, p. 41+15+38.

Dumail J. F., Salmén L. (1997) Compression Behaviour of Saturated Wood Perpendicular to Grain under Large Deformations. Holzforschung (51): 296-302.
Eberhardsteiner J. (2002) Mechanisches Verhalten von Fichtenholz - Experimentelle Bestimmung der biaxialen Festigkeitseigenschaften, Springer, Vienna, p. 174.
Faessel C., Navi P., Jirasek M. (1999) 2D anisotropic damage model for wood in tension. In: Morlier P, Valentin G. COST Action E8 Workshop "Damage in Wood", Bordeaux: 21-37.
FOEN (2009) "The benefits of Wood", Swiss Federal Office of the Environment, from http://structura.wordpress.com/2009/01/14/the-benefits-of-wood/
Foschi R. O. (2003) Reliability of Structures with Timber and Wood-Based Products. Ch.11 in Timber Engineering ed. by Thelandersson, S., Larsen, H. Chichester West Sussex, Wiley**:** pp**.** 177-199.
Foslie M. (1971) Strength properties of Norwegian spruce (Picea Abies Karst.). Part 3: Strength properties of small, clear specimens, Report 42/317, Norwegian Institute of Wood Technology, Oslo, p. 12.
Foslie M., Moen K. (1968) Strength Properties of Norwegian Spruce (Picea Abies Karst.). Part 1: Bending strength, modulus of elasticity and tensile strength tested on the structural sizes 3"x8" and 2"x4", Report 33/285, Norwegian Institute of Wood Technology, Oslo, p. 40.
FPL (1999) Wood Handbook. Wood as an Engineering Material. Gen. Tech. Rep. FPL-GTR-113, United States Department of Agriculture, Forest Products Laboratory, p. 463.
Goodman J. R., Bodig J. (1970) Orthotropic Elastic Properties of Wood. Journal of the Structural Division, Proceedings of the American Society of Civil Engineering ASCE 1 (1): 2301-2319.
Gustafsson P. J. (2003) Fracture Perpendicular to Grain - Structural Applications. Ch.7 in Timber Engineering ed. by Thelandersson, S., Larsen, H. Chichester West Sussex, Wiley**:** pp**.** 103-130.
Hankinson R. L. (1921) Investigation of crushing strength of spruce at varying angles of grain. Air Service Information Circular III (259).
Haygreen J. G., Bowyer J. L. (1996) Forest Products and Wood Science (3rd ed.), Iowa State University Press, Ames, Iowa, p. 484.
Hearmon R. F. S. (1948) The Elasticity of Wood and Plywood, Report 7, Forest Products Research, Dept. of Scientific and Industrial Research, London, p. 83.
Hill R. (1956) The Mathematical Theory of Plasticity, Oxford University Press, New York, p. 355.
Hong J., Barrett J. D. (2006) Empirical wood material model for three dimensional finite element analysis of a nail joint. 9th World Conference on Timber Engineering, Portland, OR, USA.
Hong J., Barrett J. D. (2008) Wood material parameters of numerical model for bolted connections - Compression properties and embedment properties. 10th World Conference on Timber Engineering, Miyazak, Japan.
Hopperstad O. S. (2003). Lecture notes Nonlinear Finite Element methods. Basic Principles TKT 8207. Seminar 4: Linear Elasticity. Trondheim, Dept. of Structural Engineering, NTNU.
Isaksson T. (2003) Structural Timber - Variability and Statistical Modelling. Ch. 4 in Timber Engineering ed. by Thelandersson, S., Larsen, H. Chichester West Sussex, Wiley**:** pp**.** 45-66.
JCSS (2006) Probabilistic Model Code. Part III - Resistance Models. Ch. 3.5 Properties of Timber, Joint Committee on Structural Safety, p. 16.
Jenkin C. F. (1920) Report on Materials Used in the Construction of Aircraft and Aircraft Engines, Report H.M. Stationery Office, London, p. 95-131.
Johansen K. W. (1949) Theory of timber connections. International Association of Bridge and Structural Engineering (9): 249-262.
Kharouf N. (2001) Post-elastic behavior of bolted connections in wood (in English). Department of Civil Engineering and Applied Mechanics, McGill University. PhD thesis, p. 167.
Kollmann F. P., Côté W. A. (1968) Principles of Wood Science and Technology - Solid Wood (1st ed.), Springer Verlag, Berlin, p. 592.
Köhler J., Faber M. (2006) The JCSS Probabilistic Model Code for Timber - Examples and Discussion. 9th World Conference on Timber Engineering WCTE, Portland, OR, USA.
Köhler J., Sørensen J. D., Faber M. H. (2007) Probabilistic modeling of timber structures. Structural Safety 29: 255-267.
Larsen H. J. (2003) Fasteners, Joints and Composite Structures. Ch.16 in Timber Engineering ed. by Thelandersson, S., Larsen, H. Chichester West Sussex, Wiley**:** pp**.** 303-313.
Liu J. Y. (1984) Evaluation of the tensor polynomial strength theory of wood. Journal of Composite Materials 18: 216-226.
LMD (2008-2009) St.meld. nr 39: Klimautforingene - landbruket en del av løsningen. Landbruks og Matdepartementet, p. 27.
Lucena-Simon J., Kröplin B. H., Dill-Langer G., Aicher S. (2000) A fictitious crack approach for the anisotropic degradation of wood. Internation Conference on Wood and Wood Fiber Composites, Otto-Graf Institute, University of Stuttgart, Germany, COST Action E8: 229-240.

Mackenzie-Helnwein P., Eberhardsteiner J., Mang H. A. (2003) A multi-surface plasticity model for clear wood and its application to the finite element analysis of structural details. Computational Mechanics 31: 204-218.
Minitab (2006). Minitab v.15 Help, Minitab Inc. Statistical Software, State College, Pennsylvania.
Moses D. (2000) Constitutive and analytical models for structural composite lumber with applications to bolted connections (in English). Department of Civil Engineering, University of British Columbia. PhD thesis, p. 195.
Moses D. M., Prion H. G. L. (1999) Bolted connections in structural composite lumber: Anisotropic plasticity model. Pacific Timber Engineering Conference, Rotorua, Vol. 2: 92-99.
Nielsen J. (2003) Trusses and Joints with Punched Metal Plate Fasteners. Ch.19 in Timber Engineering ed. by Thelandersson, S., Larsen, H. Chichester West Sussex, Wiley**:** pp**.** 365-382.
Norris C. B. (1962) Strength of Orthotropic Materials subjected to Combined Stresses, Report 1816, U.S. Forest Products Lab., FPL, Madison, Wisconsin, p. 40.
NS-EN 338 (2003) Structural timber Strength Classes. European Committee for Standardization (2nd ed.), p. 7.
NS-EN 408 (2003) Timber Structures - Structural timber and glued laminated timber. Determination of some physical and mechanical properties. European Committee for Standardization (2nd ed.), p. 27.
NS 3470 (1999) Norsk Standard. Design of timber structures. Design rules. Part 1: Common rules. Norges Standardiseringsforbund (5th ed.), p. 82.
NTI 1966 Normer for prøving av små feilfri prøver av heltre (TRENORM 1-20). Norwegian Institute of Wood Technology.
O´Halloran M. R. (1973) A curvilinear stress-strain model for wood in compression (in English). Colorado State University. PhD thesis.
Okstad T., Kårstad H. (1985) The mechanical properties of spruce wood (Picea Abies L. Karst.) in Northern Norway, Report Norwegian Forest Research Institute, Ås, p. 47.
Ormarsson S. (1999) Numerical analysis of the moisture-related distortion in sawn timber (in English). Department of Structural Mechanics, Chalmers University of Technology. PhD thesis, p. 213.
Patton-Mallory M., Pellicane P. J., Smith I. W. (1997) Nonlinear material models for analysis of bolted wood connections. ASCE Journal of Structural Engineering 123 (8): 1063-1070.
Ramberg W., Osgood W. R. (1943) Description of the stress-strain curves by three parameters. Tech. Note No. 902, Report 902, National Advisory Committee for Aeronautics, Washington, DC, p.
Sasaki Y., Yamasaki M. (2004) Effect of pulsating tension-torsion combined loading on fatigue behavior in wood. Holzforschung 58: 666-672.
Shih C. F., Lee D. (1978) Further Developments in Anisotropic Plasticity. Journal of Engineering Materials and Technology 100: 294-302.
Shipsha A., Berglund L. A. (2007) Shear coupling effects on stress and strain distributions in wood subjected to transverse compression. Composites Science and Technology 67: 1362-1369.
Sjödin J. (2008) Strength and moisture aspects of steel-timber dowel joints in glulam structures - an experimental and numerical study (in English). School of Technology and Design, Växjö University. PhD thesis, p. 39.
Skaug E. (2004) Failures of modern timber structures in the Nordic countries (in Norwegian). Department of Structural Engineering, Norwegian University of Science and Technology. Master thesis, p. 96.
Smith I., Landis E., Gong M. (2003) Fracture and Fatigue in Wood, Wiley, Chichester, p. 234.
Stamer J. (1935) Elastizitätsuntersuchungen an Hölzern. Ingenieur-Archiv (6): 1-8.
Sunde F. F. (2005) Strength properties of small, clear wood specimens of Norway spruce (in Norwegian). Institutt for naturforvaltning, Norwegian University of Life Sciences. Master thesis, p. 53.
Tabiei A., Wu J. (2000) Three-dimensional nonlinear orthotropic finite element material model for wood. Composite Structures 50: 143-149.
Thelandersson S. (2003) Timber Engineering - General Introduction. Ch. 1 in Timber Engineering ed. by Thelandersson, S., Larsen, H. Chichester West Sussex, Wiley**:** pp**.** 103-130.
Thelandersson S., Larsen H. J. (2003) Timber Engineering (1st ed.), Wiley, Chichester West Sussex, p. 446.
Tsai S. W., Hahn H. T. (1980) Introduction to composite materials (1st ed.), Technomic Publishing Company, Inc., Lancaster, Pennsylvania U.S.A., p. 455.
Tsai S. W., Wu E. M. (1971) A General Theory of Strength for Anisotropic Materials. Journal of Composite Materials 5: 58-80.
Ukyo S., Masuda M. (2006) A new method for Measuring the True Shear Strength of Wood. 9th World Conference on Timber Engineering, Portland USA.
Walpole R. E., Myers, R. H., Myers, S. L., Ye, K. (2002) Probability & Statistics for Engineers & Scientists (7th ed.), Prentice Hall, New Jersey, p. 730.
Xavier J. C., Garrido N. M., Oliveira M., Morais J. L., Camanho P. P., Pierron F. (2004) A comparison between the Iosipescu and off-axis shear test methods for the characterization of Pinus Pinaster Ait. Composites: Part A 35: 827-840.
Yamasaki M., Sasaki Y. (2003) Elastic properties of wood with rectangular cross section under combined static axial force and torque. Journal of Materials Science 38: 603-612.

Yamasaki M., Sasaki Y. (2004) Yield Behavior of Wood Under Combined Static Axial Force and Torque. Experimental mechanics 44 (3): 221-227.
Yoshihara H., Matsumoto A. (2005) Measurement of the shearing properties of wood by in-plane shear test using a thin specimen. Wood Science and Technology 39: 141-153.
Yoshihara H., Ohsaki H., Kubojima Y., Ohta M. (1999) Applicability of the Iosipescu shear test on the measurement of the shear properties of wood. Journal of Wood Science 45: 24-29.
Yoshihara H., Ohsaki H., Kubojima Y., Ohta M. (2001) Comparisons of Shear Stress/Shear Strain Relations of Wood obtained by Iosipescu and Torsion Tests. Wood and Fiber Science 33 (2): 275-283.
Yoshihara H., Ohta M. (1992) Stress-Strain Relationship of Wood in the Plastic Region I. Mokuzai Gakkaishi 38 (8): 759-763.
Yoshihara H., Ohta M. (1994) Stress-Strain Relationship of Wood in the Plastic Region II. Mokuzai Gakkaishi 40 (3): 263-267.
Yoshihara H., Ohta M. (1995a) Determination of the Shear Stress-Shear Strain Relationship of Wood by Torsion Tests. Mokuzai Gakkaishi 41 (11): 988-993.
Yoshihara H., Ohta M. (1995b) Measurement of the In-Plane Elastic Constants of Wood by the Uniaxial Compression Test Using a Single Specimen. Mokuzai Gakkaishi 41 (2): 218-222.
Yoshihara H., Ohta M. (1995c) Shear Stress-Shear Strain Relationship of Wood in the Plastic Region. Mokuzai Gakkaishi 41 (6): 529-536.
Yoshihara H., Ohta M. (1996) Analysis of the Yield Behavior of Wood under Combined Shear Stresses in Torsion Tests. Mokuzai Gakkaishi 42 (6): 541-545.
Yoshihara H., Ohta M. (1997) Stress-Strain Relationship of Wood in the Plastic Region III. Mokuzai Gakkaishi 43 (6): 464-469.
Yoshihara H., Ohta M., Origuchi K. (1997) Yield Behavior of Wood under Compression-Shear Combined Stress Condition. J. Soc. Mat. Sci., Japan 46 (4): 385-389.

# PAPER I

## Planar strain measurements on wood specimens

**K. B. DAHL[1], K. A. MALO[2]**

*Experimental Mechanics (2009) 49:575-586*

**Abstract**
Wood specimens have been tested for compressive loading in the longitudinal direction. Planar deformation was recorded by means of video extensometry on the specimen surfaces. A post processing routine was developed to calculate stress and strain values from the sampled data. The routine made use of mathematical framework used in the finite element method. Material parameters were detected by means of an optimization algorithm, and the determined linear elastic parameters were in general found to be in good agreement with values given in literature. The utilized method offers simultaneous average values for active, passive and shear strains from the measured area. Moduli of elasticity, Poisson's ratios and shear deformation can thus be evaluated. In addition, the variation of the three strain components over the area is measured. The results can therefore be used for quantification of material inhomogeneity and are further suitable for direct comparison with numerically computed strains comprising nonuniform strain fields. Since video extensometry does not require any physical contact with the specimen, measurements can be undertaken until failure. The present method offers thus an efficient and relatively accurate way to measure and evaluate the material characteristics of anisotropic and inhomogeneous materials like wood.

**Keywords** – Wood, material characterization, video extensometry

[1] Ph.D-student, Dept. of Structural Engineering, Norwegian University of Science and Technology NTNU, M.Sc. Structural and Civil Engineer, Multiconsult AS, Boks 265 Skøyen, N-0213 Oslo, Norway.
[2] Professor, Dept. of Structural Engineering, Norwegian University of Science and Technology NTNU

## Introduction

Wood is an anisotropic material, i.e. its mechanical properties differ in the various spatial directions. The number of different directions is confined by the assumption of three mutually perpendicular planes of elastic symmetry. Wood may thus be regarded orthotropic, referring to the three orthogonal directions defining these planes. The directions are the longitudinal direction ($L$) along the fibres, the radial direction ($R$) toward annual rings, and the tangential direction ($T$) directed along the annual rings.

Despite of extensive use in many structural applications, numeric and analytic modelling of wood as well as general understanding of the mechanical behaviour remains insufficient. There are in general palpable few studies focusing on the behaviour of this widely used material. Studies are typically limited to the initial elastic behaviour without taking any nonlinearity into consideration, and are often focusing on specific structural details. There is thus a need for more accurate and generalized mechanical models for wood.

In order to characterize the mechanical properties, knowledge of the stress-strain relationships in the different directions is required. A reasonable way to obtain such information is mechanical experiments, although natural variability and inhomogeneity of wood complicate the testing considerably. The fact that the experience and routines within this field still is rather limited is also a challenge. In addition, the direction dependency requires much more tests to be undertaken compared to isotropic materials.

Strain measurement on wood and other materials has traditionally been performed with either electrical strain gages or mechanical extensometers. A typical challenge related to such measurements is the potential development of fracture causing abrupt change in the configuration. Furthermore, the unit cost and installation work makes strain gages a rather expensive alternative. Other test methods typically comprise the Moiré method and laser speckle interferometry, of which both has been used to some extent [1]. The drawback with these methods is however that they require treatment of the surface, which also can interfere with the mechanical behaviour of the material during testing.

Measurement by means of optical devices and computerized photogrammetry is a relatively new method, which to some extent has been used for strain measurement on wood earlier. The fast data acquisition and the capability of measuring large deformations make such equipment advantageous. Another advantage is that no testing apparatus is physically attached to the test specimen, and mechanical influence from the equipment is thus avoided. The fact that it can be used beyond component failure is also beneficial. The cost per specimen is moreover low since little labour effort is required and no test equipment is expended during testing. A great advantage is the bi-dimensionality which allows simultaneous strain measurement in the axial and the transverse direction over a moderate sized area. Since direction-dependant material behaviour does not affect the method's capability, the method is well suited for testing orthotropic and inhomogeneous materials like wood. Care must however be taken when interpreting results from video extensometry. Since the measuring system is fixed while the material is free to move, rigid body movement can result in spurious strains. Compared to observations from strain gages following the material deformation and thereby avoiding spurious strain contributions, a more comprehensive processing of data can be crucial.

Choi et al. [1] (1991) used a digital image correlation technique for in-plane strain measurements on wood and paper for determination of normal, shear and Poisson's ratio properties. Pine wood was loaded longitudinally in compression with observations in the longitudinal – tangential plane (*LT*) by means of 54 dots in a regular array system. In-plane engineering strain components were calculated with basis in dot displacement assuming small strains. They found that the method provided accurate observations which also allowed study of strain profiles and local strain concentrations with good correspondence to FEM results and independent strain measurements.

Reiterer et al. [2] (2001) made use of video extensometry to determine two-dimensional strain in compression tests on clear spruce wood marked with a grid of target dots. Specimens with five different orientations in the longitudinal – radial plane (*LR*) were tested in the study. Linear elastic orthotropic theory was used to assess stiffness values while failure capacities were compared to the so-called Tsai-Hill criterion [2]. Behaviour in the elastic as well as the large-strain area was observed. Good correspondence with hand calculated values in literature were found for the moduli of elasticity as well as the ultimate compressive loads for the different grain angles tested. The observed Poisson's numbers varied however somewhat from theoretical values.

Ukyo and Masuda [3,4] (2006) used a digital image correlation technique to measure shear strain on shear block specimens of birch and spruce loaded parallel to grain in the *LR* and *LT* planes. Two cameras simultaneously measuring the two planes were used. By means of an iteration scheme redistributing the load, a nonlinear stress-strain relationship for shear followed by strain softening was documented. Important in this work was the system's ability to measure nonuniform distribution of shear and normal strain components.

Sinha et al. [5] (2006) made use of digital image correlation in destructive testing of wood frame shear walls under monotonic and cyclic loading to describe behaviour during seismic loading. Two cameras, both in an angle to the specimen surface, provided stereoscopic images. The system allowed full field 3D displacement and strain data beyond the elastic limit of the system. Failure initiation and post failure strain could thereby be observed.

Franke et al. [6] (2007) also made use of video extensometry on wood components for observation of general deformation and for determination of fracture mechanics parameters. The tests comprised three and four point bending of specimens with notches and were performed on i.a. spruce with strain measurements over the whole cross section. Experimental observations were transferred to a finite element method (FEM) program and held together with results from numerical simulations.

## Experimental apparatus

In the present study, specimens made of softwood were tested for compressive loading in the longitudinal direction (*L*) with measurements on the *LR* and *LT* planes. The data acquisition was performed by means of a video extensometer (ME–46 Full Image Video extensometer) manufactured by Messphysik GmbH. The extensometer works by continuously measuring the in-plane coordinates $x$ and $y$ of marked target dots on the surface of the test specimen subjected to loading. The change in decomposed length $\Delta x$ and $\Delta y$ between two points expresses the deformation. Strain in, say the x-direction, can then in principle be calculated as

$$\varepsilon_x = \frac{\Delta x}{X_0} \tag{1}$$

where $X_0$ is the initial x-projected length between the two points.

The software assigns a gray scale value ranging from 0 to 255 to each pixel in the digitized picture. The data is stored in a so-called frame buffer and contrast diagrams for each scanned pixel line and column is subsequently processed. A rapid change in values indicates a distinct contrast peak. The peak pattern is interpreted by the software as targets whose coordinates are observed. In order to save processing cost, a measuring zone around each detected target is defined in the frame buffer. The algorithm will subsequently search and process data within these zones.

The camera scans the marked specimen with a certain frequency followed by the measurement process. The time between each sampling cycle depends on the hardware speed and on the amount of data to be processed. According to the instructions a maximum frequency of 25 Hz can be achieved. In this study a scanning rate of approximately 8 Hz was used.

A typical experimental setup using optical measurements is visualized in Figure 1, while a close-up of an actual test showing specimen and camera is shown in Figure 2.

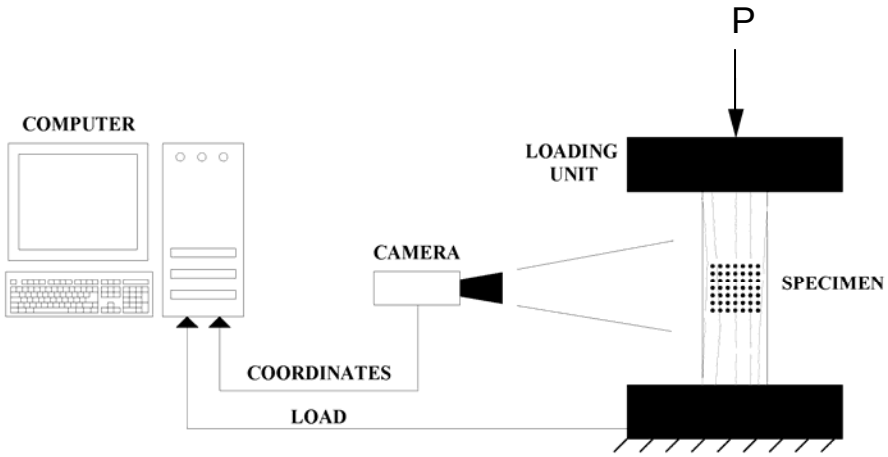


**Figure 1:** Testing apparatus used in the study consisting of computer, camera and loading unit.

Characteristics of the acquisition equipment used are:

- A monochrome video camera fitted with a high precision Charge Coupled Device (CCD) chip with photosensitive cells arranged in a grid system.
- High precision focal lenses which can be adjusted to a wide range of specimen sizes.
- An interface card connected to the camera with cables, converting the video signal into 8 Bit digital format whilst simultaneously generating 768 × 576 pixel images on the PC monitor. The grey scale level of each pixel is resolved in 256 shades.
- Special video-extensometer software which automatically detects the targets and follow them during testing.

Hence, the system offers a maximum theoretical displacement resolution of 1:196 608 and 1:147 456 in the two orthogonal directions. The measurement area is in practise smaller than the entire field of view, and the utilized resolution will consequently be somewhat lower.

## Experimental procedure

The specimen was fixed in a universal loading frame with the camera mounted on a rigid tripod localized approximately 2 m away. The distance between the camera and the specimen was thereby kept constant, which was crucial since any change in normal distance would affect the measured dot coordinate values. A predetermined length between two target dots was assigned prior to the tests in order to calibrate the coordinate system values in the camera setup. The camera was intentionally aligned at the centre of the specimen and positioned horizontally by means of a tripod bull eye since any deviation between camera axes and specimen geometry axes would result in measurement errors.

The measurement algorithm used by the video extensometer evaluates the grey contrast transition between targets and specimen surface. To secure adequate contrast on the yellowish wood, equally sized circular target dots with an approximate diameter of 0.5 mm were applied to the specimen surface with a black felt pen. The dots proved to give sufficient grey contrast for target detection and no inverse painting of the specimen was needed. A light source with evenly distributed halogen light was used to provide sufficient illumination conditions and to reduce the effect of backlight.

A total number of 49 dots were applied in an approximately quadratic 7 × 7 grid system by means of metal stencils with holes. The vertical and horizontal distances between the dots varied between 3 and 5 mm depending on the specimen size. There was no need of precisely equal distances between the dots since the system measured length relative to the preset calibration value.

**Figure 2:** Camera and compression specimen in the loading unit

## Post processing of data

The log files from the experiments contain the load level $P$ and discrete deformation data as target dot coordinates for each timestep. The resemblance between the sampled coordinate data and node displacement data in finite element analysis (FEA) is apparent. This motivated the development of an algorithm for post processing experimental data similar to the formulation used in FEA. This was advantageous from two perspectives. Firstly, the mathematical framework of FEA could be exploited; secondly it enabled a direct and fairly detailed comparison basis to results from numerical models.

Since the deformation data was measured in two dimensions, a plane element type formulation was chosen. Four adjacent target dots were interpreted as a four noded quadrilateral element. The 49 target dots gave thus 36 elements, confer Figure 3, and covered a nearly quadratic area with side lengths between 18 and 30 mm depending on specimen size.

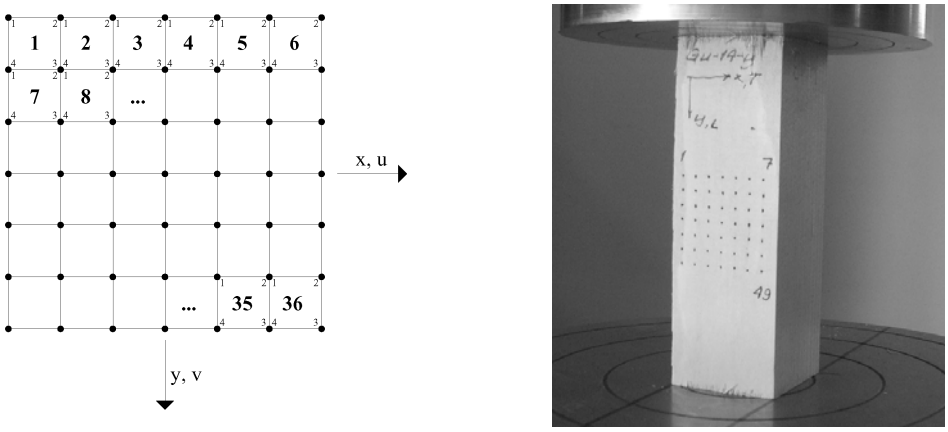


**Figure 3:** Grid of target dots on specimen surface, interpreted as 36 elements with four nodes each

The dot locations did in general not fulfil an exact geometrical pattern with rectangular elements between. An isoparametric formulation accommodating nonrectangular element shapes was thus convenient to use, confer Figure 4. This corresponds to the so-called bilinear quadrilateral element (Q4) formulation with a dimensionless natural coordinate system $\xi\eta$. Lagrangian interpolation functions were applied for the element geometry given by the nodal coordinates $x$ and $y$, and for $u$ and $v$ displacement fields in the $x$ and $y$-direction, respectively.

$$\begin{bmatrix} x \\ y \end{bmatrix} = \begin{bmatrix} \mathbf{N_g} & \mathbf{0} \\ \mathbf{0} & \mathbf{N_g} \end{bmatrix} \begin{bmatrix} \mathbf{x} \\ \mathbf{y} \end{bmatrix} \qquad \begin{bmatrix} u \\ v \end{bmatrix} = \begin{bmatrix} \mathbf{N_u} & \mathbf{0} \\ \mathbf{0} & \mathbf{N_u} \end{bmatrix} \begin{bmatrix} \mathbf{u} \\ \mathbf{v} \end{bmatrix} \tag{2}$$

Using the isoparametric formulation, shape functions $\mathbf{N_g}$ for geometry mapping and $\mathbf{N_u}$ for displacement field were set equal, reading

$$\begin{aligned} \mathbf{N_u} = \mathbf{N_g} = \mathbf{N}(\xi,\eta) &= \begin{bmatrix} N_1, & N_2, & N_3, & N_4 \end{bmatrix} \\ &= \tfrac{1}{4}\begin{bmatrix} (\xi-1)(\eta-1), & -(\xi+1)(\eta-1), & (\xi+1)(\eta+1), & -(\xi-1)(\eta+1) \end{bmatrix} \end{aligned} \tag{3}$$

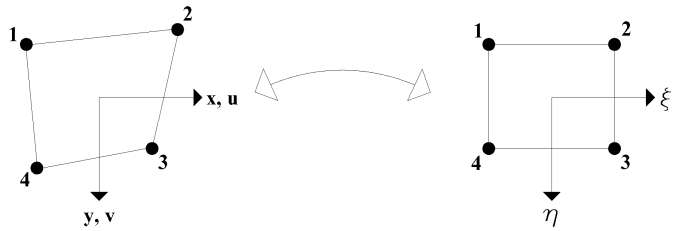


**Figure 4:** Mapping between physical coordinates and the natural coordinate system

Since the strain fields are first derivatives of the deformation *u* and *v*, the formulation gives constant normal and shear strain values within each element. This was however assumed sufficient due to relatively high resolution of target dots on the specimen surface.

Coordinate values (*x, y*) and displacements (*u, v*) at each of the four nodes defining an element are then

$$\mathbf{x}=\begin{bmatrix}x_1\\x_2\\x_3\\x_4\end{bmatrix}\quad \mathbf{y}=\begin{bmatrix}y_1\\y_2\\y_3\\y_4\end{bmatrix}\quad \mathbf{X}=\begin{bmatrix}X_1\\X_2\\X_3\\X_4\end{bmatrix}\quad \mathbf{Y}=\begin{bmatrix}Y_1\\Y_2\\Y_3\\Y_4\end{bmatrix}\quad \mathbf{u}=\mathbf{x}-\mathbf{X}=\begin{bmatrix}u_1\\u_2\\u_3\\u_4\end{bmatrix}\quad \mathbf{v}=\mathbf{y}-\mathbf{Y}=\begin{bmatrix}v_1\\v_2\\v_3\\v_4\end{bmatrix} \tag{4}$$

$X_j$ and $Y_j$ are here the initial coordinates of node $j$ at time $t = 0$, while the other variables are defined at an arbitrary timestep $t$. In order to calculate the strain, the derivates $u_{,x}$ , $u_{,y}$ , $v_{,x}$ and $v_{,y}$ of the displacement fields must be computed. These expressions are not available directly, but may be derived using the natural coordinates and the chain rule:

$$\begin{bmatrix}\frac{\partial}{\partial\xi}\\ \frac{\partial}{\partial\eta}\end{bmatrix}=\begin{bmatrix}\frac{\partial x}{\partial\xi} & \frac{\partial y}{\partial\xi}\\ \frac{\partial x}{\partial\eta} & \frac{\partial y}{\partial\eta}\end{bmatrix}\begin{bmatrix}\frac{\partial}{\partial x}\\ \frac{\partial}{\partial y}\end{bmatrix}=\begin{bmatrix}\left(\mathbf{N}_{,\xi}\mathbf{x}\right) & \left(\mathbf{N}_{,\xi}\mathbf{y}\right)\\ \left(\mathbf{N}_{,\eta}\mathbf{x}\right) & \left(\mathbf{N}_{,\eta}\mathbf{y}\right)\end{bmatrix}\begin{bmatrix}\frac{\partial}{\partial x}\\ \frac{\partial}{\partial y}\end{bmatrix}=\mathbf{J}\begin{bmatrix}\frac{\partial}{\partial x}\\ \frac{\partial}{\partial y}\end{bmatrix} \tag{5}$$

where **J** assigns the Jacobian matrix. The inverse expression can be written

$$\begin{bmatrix}\frac{\partial}{\partial x}\\ \frac{\partial}{\partial y}\end{bmatrix}=\frac{1}{J}\begin{bmatrix}\frac{\partial y}{\partial\eta} & -\frac{\partial y}{\partial\xi}\\ -\frac{\partial x}{\partial\eta} & \frac{\partial x}{\partial\xi}\end{bmatrix}\begin{bmatrix}\frac{\partial}{\partial\xi}\\ \frac{\partial}{\partial\eta}\end{bmatrix}=\frac{1}{J}\begin{bmatrix}\left(\mathbf{N}_{,\eta}\mathbf{y}\right) & -\left(\mathbf{N}_{,\xi}\mathbf{y}\right)\\ -\left(\mathbf{N}_{,\eta}\mathbf{x}\right) & \left(\mathbf{N}_{,\xi}\mathbf{x}\right)\end{bmatrix}\begin{bmatrix}\frac{\partial}{\partial\xi}\\ \frac{\partial}{\partial\eta}\end{bmatrix}=\left[\mathbf{J}\right]^{-1}\begin{bmatrix}\frac{\partial}{\partial\xi}\\ \frac{\partial}{\partial\eta}\end{bmatrix} \tag{6}$$

where $J$ assigns the determinant of the Jacobian matrix. A total Lagrangian formulation was chosen, implying that the Jacobian matrix is referring to the initial configuration. The Jacobi determinant for each of the quadrilateral elements could then be calculated as

$$J=\det\mathbf{J}=\mathbf{N}_{,\xi}\mathbf{X}\cdot\mathbf{N}_{,\eta}\mathbf{Y}-\mathbf{N}_{,\xi}\mathbf{Y}\cdot\mathbf{N}_{,\eta}\mathbf{X} \tag{7}$$

Thus, for the total Lagrangian formulation, $J$ was calculated for the initial element geometry and used for all time steps $t$. The derivates of the isoparametric functions are given below, with values calculated for the element midpoint $(\xi,\eta) = (0, 0)$:

$$\mathbf{N}_{,\xi} = \tfrac{1}{4}\left[(\eta-1),\ \ -(\eta-1),\ \ (\eta+1),\ \ -(\eta+1)\right] = \tfrac{1}{4}\left[(-1),\ \ 1,\ \ 1,\ \ (-1)\right] \tag{8}$$

$$\mathbf{N}_{,\eta} = \tfrac{1}{4}\left[(\xi-1),\ \ -(\xi+1),\ \ (\xi+1),\ \ -(\xi-1)\right] = \tfrac{1}{4}\left[(-1),\ \ (-1),\ \ 1,\ \ 1\right] \tag{9}$$

Thus,

$$\begin{aligned}
\mathbf{N}_{,\xi}\,\mathbf{X} &= \tfrac{1}{4}\left(-X_1 + X_2 + X_3 - X_4\right) & \mathbf{N}_{,\xi}\,\mathbf{u} &= \tfrac{1}{4}\left(-u_1 + u_2 + u_3 - u_4\right)\\
\mathbf{N}_{,\xi}\,\mathbf{Y} &= \tfrac{1}{4}\left(-Y_1 + Y_2 + Y_3 - Y_4\right) & \mathbf{N}_{,\xi}\,\mathbf{v} &= \tfrac{1}{4}\left(-v_1 + v_2 + v_3 - v_4\right)\\
\mathbf{N}_{,\eta}\,\mathbf{X} &= \tfrac{1}{4}\left(-X_1 - X_2 + X_3 + X_4\right) & \mathbf{N}_{,\eta}\,\mathbf{u} &= \tfrac{1}{4}\left(-u_1 - u_2 + u_3 + u_4\right)\\
\mathbf{N}_{,\eta}\,\mathbf{Y} &= \tfrac{1}{4}\left(-Y_1 - Y_2 + Y_3 + Y_4\right) & \mathbf{N}_{,\eta}\,\mathbf{v} &= \tfrac{1}{4}\left(-v_1 - v_2 + v_3 + v_4\right)
\end{aligned} \tag{10}$$

A set of expressions for the derivates of the displacements could then be established. These were calculated directly from the experimental data for each timestep and element $e$ as

$$\frac{du^e}{dx} = \frac{1}{J^e}\left[\frac{dy^e}{d\eta}\cdot\frac{du^e}{d\xi} - \frac{dy^e}{d\xi}\cdot\frac{du^e}{d\eta}\right] = \frac{1}{J^e}\left[\mathbf{N}_{,\eta}\mathbf{Y}^e\cdot\mathbf{N}_{,\xi}\mathbf{u}^e - \mathbf{N}_{,\xi}\mathbf{Y}^e\cdot\mathbf{N}_{,\eta}\mathbf{u}^e\right] \tag{11}$$

$$\frac{du^e}{dy} = \frac{1}{J^e}\left[-\frac{dx^e}{d\eta}\cdot\frac{du^e}{d\xi} + \frac{dx^e}{d\xi}\cdot\frac{du^e}{d\eta}\right] = \frac{1}{J^e}\left[-\mathbf{N}_{,\eta}\mathbf{X}^e\cdot\mathbf{N}_{,\xi}\mathbf{u}^e + \mathbf{N}_{,\xi}\mathbf{X}^e\cdot\mathbf{N}_{,\eta}\mathbf{u}^e\right] \tag{12}$$

$$\frac{dv^e}{dx} = \frac{1}{J^e}\left[\frac{dy^e}{d\eta}\cdot\frac{dv^e}{d\xi} - \frac{dy^e}{d\xi}\cdot\frac{dv^e}{d\eta}\right] = \frac{1}{J^e}\left[\mathbf{N}_{,\eta}\mathbf{Y}^e\cdot\mathbf{N}_{,\xi}\mathbf{v}^e - \mathbf{N}_{,\xi}\mathbf{Y}^e\cdot\mathbf{N}_{,\eta}\mathbf{v}^e\right] \tag{13}$$

$$\frac{dv^e}{dy} = \frac{1}{J^e}\left[-\frac{dx^e}{d\eta}\cdot\frac{dv^e}{d\xi} + \frac{dx^e}{d\xi}\cdot\frac{dv^e}{d\eta}\right] = \frac{1}{J^e}\left[-\mathbf{N}_{,\eta}\mathbf{X}^e\cdot\mathbf{N}_{,\xi}\mathbf{v}^e + \mathbf{N}_{,\xi}\mathbf{X}^e\cdot\mathbf{N}_{,\eta}\mathbf{v}^e\right] \tag{14}$$

Based on the derivates, the Green strain components were finally calculated for each timestep and element $e$ as

$$\boldsymbol{\varepsilon}^e = \begin{bmatrix}\varepsilon_{xx}^e\\ \varepsilon_{yy}^e\\ \gamma_{xy}^e\end{bmatrix} = \begin{bmatrix}\dfrac{du^e}{dx} + \dfrac{1}{2}\left(\dfrac{du^e}{dx}\right)^2 + \dfrac{1}{2}\left(\dfrac{dv^e}{dx}\right)^2\\ \dfrac{dv^e}{dy} + \dfrac{1}{2}\left(\dfrac{du^e}{dy}\right)^2 + \dfrac{1}{2}\left(\dfrac{dv^e}{dy}\right)^2\\ \dfrac{du^e}{dy} + \dfrac{dv^e}{dx} + \dfrac{du^e}{dx}\cdot\dfrac{du^e}{dy} + \dfrac{dv^e}{dx}\cdot\dfrac{dv^e}{dy}\end{bmatrix} \qquad e = \{1\ldots 36\} \tag{15}$$

where $\varepsilon_{xx}$ is strain in the passive direction, $\varepsilon_{yy}$ in the active (loading) direction and $\gamma_{xy}$ is shear strain in the plane defined by the active and passive directions.

The selection of Green strain instead of e.g. engineering strain was motivated from the fact that the video extensometer measures coordinates in a fixed system. Any rigid body rotation without corresponding transformations would thus generate spurious contributions to engineering strain. Such contributions are efficiently eliminated by use of Green strain.

Wood is an inhomogeneous material, and the strains may vary considerably from one location to another although the stress distribution is assumed to be nearly constant. In order to extract parameters useful for calculations, a homogenization over some representative volume element (RVE) must be performed. The size of the RVE may be discussed, but here the dimension of the measurement area containing the 7 × 7 dot system was chosen. Mean values for each strain component over all elements were thus calculated in the homogenization procedure. Since each of the measured elements was of unequal geometrical size, weighting of the individual element strain value contributions was pertinent. This was done by calculating mean length values $\Delta X^e$ and $\Delta Y^e$ and mean area $\Delta A^e$ for each element $e = \{1 \ldots 36\}$ at the initial configuration;

$$\begin{aligned} \Delta X^e &= \tfrac{1}{2}\left( X_2^e + X_3^e - X_1^e - X_4^e \right) \\ \Delta Y^e &= \tfrac{1}{2}\left( Y_3^e + Y_4^e - Y_1^e - Y_2^e \right) \\ \Delta A^e &= \Delta X^e \cdot \Delta Y^e \end{aligned} \tag{16}$$

The weighting factors for each element for passive, active and shear strain were then calculated as

$$W_x^e = \frac{\Delta X^e}{\sum_{g=1}^{36} \Delta X^g} \qquad W_y^e = \frac{\Delta Y^e}{\sum_{g=1}^{36} \Delta Y^g} \qquad W_{xy}^e = \frac{\Delta A^e}{\sum_{g=1}^{36} \Delta A^g} \tag{17}$$

The weighted mean strain values over the observed area (RVE surface) were finally calculated for each timestep as

$$\overline{\boldsymbol{\varepsilon}} = \begin{bmatrix} \overline{\varepsilon}_{xx} \\ \overline{\varepsilon}_{yy} \\ \overline{\gamma}_{xy} \end{bmatrix} = \begin{bmatrix} \sum_{e=1}^{36} \left( W_x^e \cdot \varepsilon_{xx}^e \right) \\ \sum_{e=1}^{36} \left( W_y^e \cdot \varepsilon_{yy}^e \right) \\ \sum_{e=1}^{36} \left( W_{xy}^e \cdot \gamma_{xy}^e \right) \end{bmatrix} \tag{18}$$

In order to quantify typical strain variation over the measured area, relative values for element strains to mean strains were calculated for each element. This was done for each of the $m$ timesteps with load levels between 30% and 70% of ultimate load $P_{ult}$, and covered typically between 500 and 3000 timesteps in the elastic domain. The selection was done to avoid inevitable disturbances caused by initial loading, material nonlinearity and failure. Average ratio values $\boldsymbol{r}_{\boldsymbol{\varepsilon}}^e$ over the timesteps were subsequently calculated for each element $e$.

$$\mathbf{r}_{\boldsymbol{\varepsilon}}^{e} = \begin{bmatrix} r_{\varepsilon-xx}^{\ e} \\ r_{\varepsilon-yy}^{\ e} \\ r_{\varepsilon-xy}^{\ e} \end{bmatrix} = \begin{bmatrix} \frac{1}{m}\sum_{t=1}^{m}\left(\frac{\varepsilon_{xx}^{\ e}}{\overline{\varepsilon}_{xx}}\right)_t \\ \frac{1}{m}\sum_{t=1}^{m}\left(\frac{\varepsilon_{yy}^{\ e}}{\overline{\varepsilon}_{yy}}\right)_t \\ \frac{1}{m}\sum_{t=1}^{m}\left(\frac{\gamma_{xy}^{\ e}}{\overline{\gamma}_{xy}}\right)_t \end{bmatrix} \qquad e = \{1\ldots 36\} \tag{19}$$

Strain ratio values for the defined range could thus be calculated and plotted for each element over the measured area. This enabled a quantification of the variation of the strain fields which can be visualized in plots and used in further evaluations.

The experimental nominal stress $\hat{\sigma}$ for each timestep $t$ was calculated as

$$\hat{\sigma} = \frac{P}{A_0} = \frac{P}{\left(l_2 \cdot l_3\right)} \tag{20}$$

where $l_2$ and $l_3$ are cross section dimensions at the initial configuration and $P$ is the load level at time $t$, confer Figure 5. Three different specimen sizes were tested, namely $l_2 = l_3 \approx 30$ mm, $l_2 = l_3 \approx 40$ mm and $l_2 = l_3 \approx 50$ mm. The height $l_1$ was consequently kept as three times the side lengths, i.e. 90 mm, 120 mm and 150 mm, respectively. The post-processing procedure resulted thus in experimental relationships between each of the average in-plane Green strain components $\overline{\varepsilon}_{xx}$, $\overline{\varepsilon}_{yy}$, $\overline{\gamma}_{xy}$ and the nominal stress $\hat{\sigma}$, typically comprising between 1000 and 5000 timesteps per test.

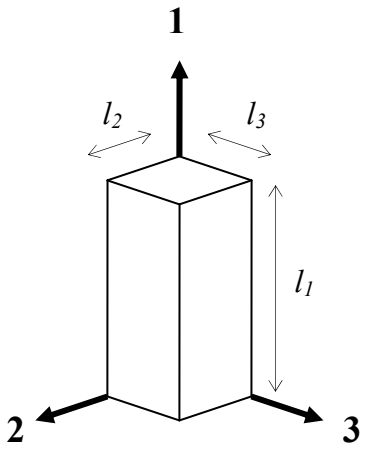


**Figure 5:** Compression specimen

## Experimental results

Specimens were made of clear wood from Norway spruce (*Picea Abies* (L.) Karst.*)* and were partly taken directly from forest, partly from graded lumber with strength classes C14, C18, C24 and C30 according to European Standard NS-EN 338 [7]. The material was conditioned for several months to approximately 12% moisture content and tested at a constant loading rate of 0.005 mm/s according to European Standard NS-EN 408 [8] part 16.2. Moisture content and density of each specimen were measured.

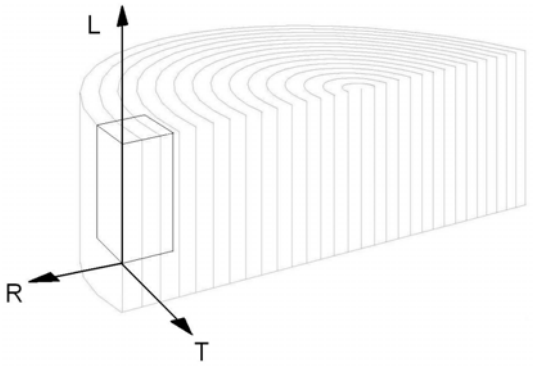


**Figure 6:** Orthogonal axis system in compression specimen of wood

The longitudinal direction (*L*) constituted the loading (active) direction, while the passive direction was oriented either radially (*R*) or tangentially (*T*), as depicted in Figure 6. A total number of 56 specimens were tested of each category *LR* and *LT*. Figure 7 shows active, passive and shear strain plotted against nominal stress $\hat{\sigma}$, resulting from a single compression test with the passive direction oriented radially. The strain component values are mean values over the measured area, i.e. the 36 elements according to equation (18). The graphs show that the active strain is larger than the passive, which corresponds to a Poisson's ratio less than 1.0. Moreover, the active strain demonstrates a nonlinear behaviour when approaching the ultimate stress level. The shear strain levels are relatively low, which is reasonable for on-axis loading of orthotropic materials. It can however be noted that the shear tends a little to the negative side, which may indicate some deviation between fibre and loading orientation in the assumed orthotropic system. The overall trend is quite representative for the typical behaviour of the tests, even if variation naturally occurs between the different specimens due to i.a. material inhomogeneity.

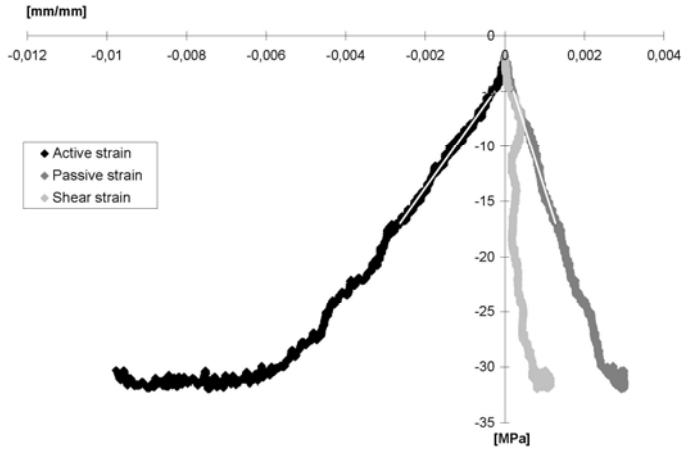


**Figure 7:** Stress and in-plane strains measured on *LR*-plane of longitudinally loaded wood in compression

An optimization algorithm was developed to fit material parameters to the observed stress-strain relationships. The algorithm was based on a Sum Square Error (SSE) strategy in which the difference between experimental stress and modelled stress for experimental strain values constitute the so-called error. Parameters were determined from the stress-strain path upward confined by approximately 40% of the ultimate stress observed. The determined values for the modulus of

elasticity and the Poisson's ratio are illustrated in Figure 7 as white lines with linear slopes $E_{LL}$ and $E_{LL}/v_{LR}$ for active and passive strain, respectively.

Modulus of elasticity values $E_{LL}$ measured on the two respective planes are plotted against density in Figure 8. The average of the *LT* sample is about 4% higher than the average *LR*, but not significantly different. The overall correlation with density is 0.33, which is relatively low compared to values given in e.g. Dinwoodie [9], who states a correlation of 0.88 for wood in general. It should however be noted that the range of density tested herein is rather narrow, making the sample more vulnerable to random variation and consequently lower correlation.

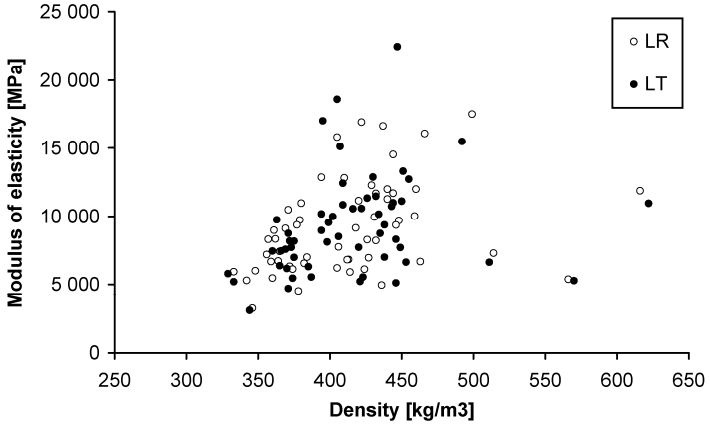


**Figure 8:** Modulus of elasticity $E_{LL}$ measured on *ij*-planes and plotted against density

The Poisson's ratios are in the following defined as

$$v_{ij} = -\frac{\varepsilon_{jj}}{\varepsilon_{ii}} \tag{21}$$

where $\varepsilon_{jj}$ is passive strain and $\varepsilon_{ii}$ is active strain. Modulus and Poisson average values are given in Table 1 together with corresponding literature values for Norway spruce (*Picea Abies*) published in Dinwoodie [9]. It should be noted that the literature values not necessarily are based on the same provenience and subspecies *Picea Abies* (L.) Karst., which naturally can affect deviation in sample values.

**Table 1:** Linear elastic material parameters for spruce from compression tests and literature

| Parameter | | Experimental | | | Literature | Unit |
|---|---|---|---|---|---|---|
| | | All | Sorted | 95% C.I. | | |
| $E_{LL}$ | Modulus of elasticity | 9 347 | 9 950 | [8 626 , 10 067] | 10 700 | MPa |
| $v_{LR}$ | Poisson's ratio | 0.468 | 0.451 | [0.431 , 0.506] | 0.38 | - |
| $v_{LT}$ | Poisson's ratio | 0.608 | 0.575 | [0.566 , 0.651] | 0.51 | - |

The experimental average modulus is somewhat lower and the Poisson's ratios somewhat higher than the literature values. This can be a result of slight fibre deviation affecting the measured values, as indicated by corresponding shear deformation being observed on many specimens, as illustrated in Figure 7. To investigate this effect, specimens with zero observed shear deformation were sorted out and averages for these specimens are given separately in the table. It can be seen that the modulus value is somewhat higher (6%) and the Poisson's ratios lower, and that the overall agreement to literature values is better than for values based on the whole sample. It is noteworthy that the sum of $v_{LT}$ and $v_{LR}$ is close to 1.0 for the sorted values, being more physically admissible. It can be noted that Reiterer et al. [2] (2001) also found relatively high $v_{LR}$ values for spruce by means of video extensometry, deviating from literature and orthotropic theory. Moreover, the mean moduli of elasticity assigned by the European Standard NS-EN 338 [7] for strength classes C18, C20 and C22 fall within the 95% confidence interval for $E_{LL}$, also substantiating the reasonability of the experimental results and the test method.

## Measurement accuracy

Any difference between a measured parameter and the actual parameter characterizing material behaviour constitutes a measurement error. Apparent error sources in the system used herein comprise insufficient optical and load accuracy, and incorrectly measured side lengths $l_2$ and $l_3$. The actual and measured modulus value determined from the tests can be given as

$$E_{ii} = \frac{P \cdot s_0}{l^2 \cdot (s_1 - s_0)} \tag{22}$$

$$E_{ii}^m = \frac{(P \pm \Delta P) \cdot (s_0 \pm \Delta s_0)}{(l \pm \Delta l)^2 \cdot (s_1 \pm \Delta s_1 - s_0 \pm \Delta s_0)} \tag{23}$$

where $\Delta$ denotes the various measurement errors, $s_0$ and $s_1$ denote the initial and final lengths between two measurement dots, and where the cross section dimensions $l_2$ and $l_3$ both are set equal $l$. By evaluating equation (23) and neglecting the 2nd order terms of the error variables $\Delta$, it can be shown that the extreme ratio between measured and actual modulus value equals

$$\frac{E_{ii}^m}{E_{ii}} = \frac{1 \pm \left(\frac{\Delta s_0}{s_0}\right) \pm \left(\frac{\Delta P}{P}\right)}{1 \mp \left(\frac{\Delta s_1 - \Delta s_0}{s_1 - s_0}\right) \mp 2\left(\frac{\Delta l}{l}\right)} \tag{24}$$

where

$$\left|\frac{\Delta s_1 - \Delta s_0}{s_1 - s_0}\right| \leq \left|\frac{2\Delta s_0}{\varepsilon \cdot s_0}\right| \tag{25}$$

and $\varepsilon$ typically equals 2‰ for the current test type. Equation (24) can then be interpreted as the upper and lower bounds for the relative error of the modulus of elasticity.

The resolution for optical coordinate measurements is given by the number of pixels and the number of grey tone levels as well as the utilized field of view. In general, the nearly quadratic measurement area comprised approximately 80% of the smaller dimension of the rectangular field. The resolution error relative to the measurement length for the total measurement area ($s_0$ = 18 mm) may then be estimated by

$$\frac{\Delta s_0}{s_0} = \frac{1}{0.8 \cdot 576 \cdot 256} = 0.0000085 \tag{26}$$

The corresponding resolution error for a separate element ($s_0$ = 3 mm) is 0.000051. In both cases, the smaller specimen size is conservatively assumed.

The measurements of the applied load was digitized by a 16 bits AD converter, resulting in a load resolution of 7.6 N for the load range of ±250 kN being used. However, this value will probably be exceeded by the repeatability and linearity properties of the load cell. In general, the load cell reading will give accuracy better than 0.2% of the measured values. Nevertheless, for small forces in the range around zero an accuracy of only 0.5% has been verified by accurate calibration. Consequently, the relative force error is bounded by

$$\frac{\Delta P}{P} = 0.005 \tag{27}$$

Manufacturing and measurement errors of the geometry dimensions has herein been estimated to less than $\Delta l = 0.1$ mm, leading to a relative error of

$$\frac{\Delta l}{l} = \frac{0.1}{30} = 0.0033 \tag{28}$$

which conservatively is based on the smallest specimen type with side lengths $l$ = 30 mm.

By introducing these error estimates into the procedures used for determination of the material parameters, the relative errors bounds for the modulus of elasticity are estimated to ±2% for the modulus value $E_{LL}$ determined from the total measurement area ($s_0$ = 18 mm). For a separate element ($s_0$ = 3 mm) within the measurement area, the corresponding estimate bounds are ±7%. Consequently, more variation must be expected in values from separate elements, even if these also should result in moderately accurate $E_{LL}$ values.

The Poisson value $v_{ij}$ constitutes according to equation (21) the ratio between passive and active strain. The measured passive strain can be assumed to be encumbered with optical resolution errors $\Delta s$, writing

$$\varepsilon_{jj}^{m} = \frac{\left(s_{j1} \pm \Delta s_{j1} - s_{j0} \pm \Delta s_{j0}\right)}{\left(s_{j0} \pm \Delta s_{j0}\right)} \tag{29}$$

where

$$s_{j1} - s_{j0} = \varepsilon_{jj} \cdot s_{j0} = v_{ij} \cdot \varepsilon_{ii} \cdot s_{j0} \tag{30}$$

The measured active strain $\varepsilon_{ii}^{m}$ can be expressed analogously to equation (29). The upper and lower bounds for the relative error of the Poisson's ratio $v_{ij}$ can by means of the calculated value in equation (26) then be estimated by

$$\frac{v_{ij}^{m}}{v_{ij}} = \frac{\varepsilon_{jj}^{m}}{\varepsilon_{ii}^{m} \cdot v_{ij}} \tag{31}$$

The bound values turn out to be strongly dependent on both the size of the measurement area and the actual value of $v_{ij}$ in equation (31). Using the values from the total measurement area ($s_0$ = 18 mm), the error estimate bounds read ±3% and ±18% for Poisson's ratios $v_{ij}$ of 0.5 and 0.05, respectively. Values based on separate elements ($s_0$ = 3 mm) are hardly useful since the error bounds in this case are estimated to ±16% and ±220%, respectively. The tested Poisson values in this study are according to Table 1 around 0.5, which then should give relatively accurate results of ±3% for values based on the total measurement area.

It is quite complicated to assess how the utilized sum square error strategy affects the accuracy of the determined parameters. The determined values should however be less vulnerable of single values possessed by errors since the sum includes hundreds of singular stress and strain points. One should therefore believe that the procedure should improve the accuracy instead of aggravating it, and that the aforementioned upper and lower bounds are conservative accuracy estimates.

## Specimen and loading

As in any material parameter test, it can be questioned to what extent the configuration and measurements are capable of procuring correct material characteristics. The specimen and test setup used herein is based on assignments from the Norwegian Dept. of Forestry [10] where a ratio between specimen length and width of 3:1 is prescribed. No lubricants or other efforts were used to reduce transverse friction forces between steel and wood at the specimen ends. While the friction forces on one hand can restrict the transverse deformation, the relatively short specimen can be vulnerable to develop a barrelled shape when compressed, resulting in higher Poisson values and lower moduli values than determined from other tests. A related aspect in this is the reasonability of comparing parameters resulting from different test setups and specimen types. Traditionally, the longitudinal modulus $E_{LL}$ of wood is measured by means of bending tests, assuming fulfilment of conventional linear elastic bending behaviour. Whether a direct comparison is plausible is not necessarily given.

It can also be commented that a relatively low $E_{LL}$ value can be expected from the tests since specimens partly were taken from ungraded material which probably would have been rejected by normal grading criteria. This effect is further amplified by the fact that ungraded material consequently was taken from the lower and outer section of the stems, holding significantly lower modulus than material from the inner part [11]. Whether this also affects the Poisson values is not reported.

The non-zero shear strain observed at the measurement plane is typically indicating in-plane or out-of plane deviation between material axis and load orientation in orthotropic materials. It should be recognized that such deviation in wood not necessarily is visible or measurable on the specimen surfaces, and consequently is hard to avoid during carpentry. Internal variation and micro effects in combination with inhomogeneity and possible non-orthogonal axes can furthermore encumber parameter evaluation based on orthotropic theory.

## Strain distribution

Strain ratio values $r_\varepsilon^e$ for active and passive strain were calculated according to equation (19) for each element and specimen. The variation between the 36 specimen specific element values can be understood as the sum of variation due to material inhomogeneity, measurement errors and strain profiles. Strain profiles comprise in this sense variation governed by the configuration, i.e. effects from geometry, boundary conditions and homogeneous material properties. The variation between corresponding element ratio values from different specimens of the same test type *ij* can on the other hand be interpreted as an expression of material inhomogeneity and measurements errors. Strain ratio values for a randomly chosen specimen are shown in Figure 9, which shows that the active strain field has considerably less variation than the passive.

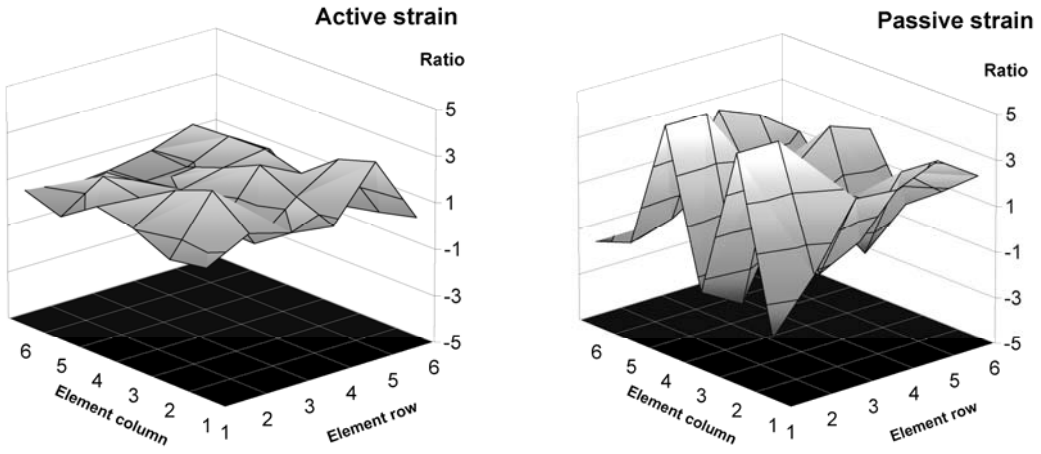


**Figure 9:** Experimental strain ratios on *LR* plane from a single compression specimen

In order to detect any strain profile tendencies, the corresponding ratio values were averaged between *ij* specimens to eliminate as much variation from errors and inhomogeneity as possible. Analysis of variance (ANOVA) of the 36 element ratio means were run in statistical software MINITAB [12] with the hypotheses

$$H_0: \mu_e = \mu_g \text{ (no detectable strain profiles)} \qquad H_1: \mu_e \neq \mu_g \text{ (strain profiles are detectable)}$$

where $\mu_e$ is the expected ratio value of element $e$, with $\{e, g\} = \{1\ldots36\}$ and $e \neq g$. ANOVA separates the total observed variance *SSTOT* into *SSTR* and *SSE*, where *SSTR* is variance which can be removed by the explanatory variables $\mu_e$. *SSE* is the remaining variance, which will be low if the observed data is well correlated with the explanatory variables. $H_0$ is consequently rejected if

$$F = \frac{\left(\frac{SSTR}{k-1}\right)}{\left(\frac{SSE}{n-k}\right)} \quad > \quad F_{\alpha,k-1,n-k} \tag{32}$$

where $F$ follows the Fisher distribution [13], $k = 36$ and $n$ is the number of observations within each group. That is, if the variance which can be removed by explanatory variables is low compared to the total variance in the data, the $H_0$ hypothesis can not be rejected, i.e. no difference between the $\mu_e$ can be asserted. $F$ is indirectly assigned through the corresponding $p$–value in MINITAB, i.e. the probability of incorrectly rejecting $H_0$. The one-way ANOVA was used since the specimen number should not play any role in this aspect. Normality and variance checks were run for some of the groups which proved that it is reasonable to assume normality and equal variances within each group $ij$, which is a requirement for the analysis. ANOVA results are presented in Table 2 with $p$–values and pooled standard deviations.

**Table 2:** ANOVA for experimental strain ratios for measurement plane *ij*

| | Active strain | | Passive strain | | |
|---|---|---|---|---|---|
| ij | *p*–value | StDev | *p*–value | StDev | n |
| LR | 0.604 | 1.057 | 0.953 | 4.439 | 56 |
| LT | 0.221 | 3.076 | 0.232 | 5.264 | 56 |

It can be seen that all groups are nonsignificant ($p > \alpha = 0.05$) and $H_0$ is thus confirmed with relatively high margin for both active and passive strain. That is, when specimens are observed as a whole, no significant strain profiles can be asserted to occur for any observations planes measured, and it is thus evident that the observed variation mainly stems from inhomogeneity and possible measurement errors. It can further be concluded that the *LT* plane demonstrates more variation than the *LR*, and that the passive strain in general varies more than the active.

## Size dependent inhomogeneity

Inhomogeneity can be quantified by the variation in corresponding element ratio values $r_\varepsilon^e$ between specimens of the same type $ij$. Since no strain profiles can be asserted to exist in the experimentally based ratios, this can be investigated by looking into the variation between all element ratio values for the same $ij$'s. This is advantageous since it alternatively would have resulted in quite comprehensive statistical testing. The calculated variance is thus the sum of variation governed by inhomogeneity, configuration and errors. Even if the magnitude of the variance itself is not too expressive, comparison of variance turns out to be a more interesting aspect since the effect of varying length $s_0$ between measurements dots can be analysed on a relative scale.

Bonferroni confidence intervals were used to test equal variances between the $m = 3$ different specimen sizes $l = 30$ mm, 40 mm and 50 mm with element side lengths $s_0 = 3$ mm, 4 mm and 5 mm, respectively. The intervals are supplied with $p$–values for the hypotheses

$H_0$: $S_e = S_g$ $\qquad$ $H_1$: $S_e \neq S_g$

Here, $S_e$ is the standard deviation of element group $e$, $e \neq g$ and $H_0$ is rejected if $p < \alpha = 0.05$, where $p$–values from Bartlett's test can be used since the data come from normal distributions [12]. Confidence intervals are shown in Figure 10 for measurements at the *LR* surface. The plots clearly indicate the effect of specimen size where the large specimen type holds very low variation in both active and passive strain fields compared to the smaller types. The zero $p$–values document that the standard deviations significantly differ between the specimen sizes. Measurements from the *LT* plane show a similar trend. It can thus be concluded that the variation in strain within the measurement area increases considerably with decreasing length $s_0$ between the measurement dots. Hence, the correspondence between the assumption of homogeneity and real behaviour is considerably improved by increasing the representative material volume (RVE) from say, 30 mm cubes to 50 mm.

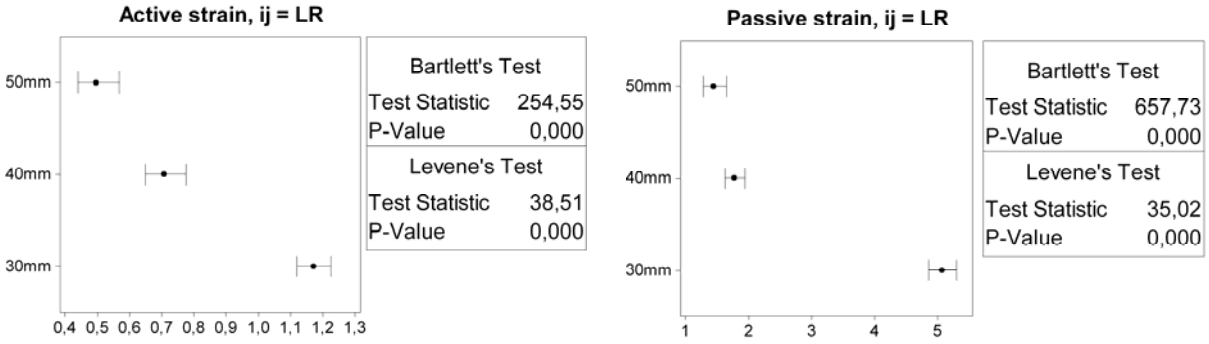


**Figure 10:** Confidence intervals for standard deviation $S_e$ of strain ratio $r_\varepsilon^e$ (hor.) against specimen size (vert.)

## Concluding remarks

Comparison of values for modulus of elasticity and Poisson's ratios demonstrates in general good agreement between experimentally based quantities and literature values. The method is therefore assessed to be applicable for mechanical testing of materials with a high degree of anisotropy and inhomogeneity like wood.

Deviation between material axis and load orientation produce a strain combination with non-zero shear strain in anisotropic materials. Since the test method efficiently returns the three simultaneous in-plane strain components, the method seems particularly advantageous for such materials. Compression and tension tests with intended or unintended deviation between material and loading axes can thus be evaluated more carefully. The method is moreover capable of returning appropriate characteristics for nonlinear material behaviour since the contact free measurements and the post processing procedure are independent of the material behaviour. Furthermore, the post processing formulation based on Green strain removes any effects from rigid body movement, and offers thus a practical and robust way to evaluate the strain fields.

Another advantage of the method is its capability to quantify inhomogeneity and nonuniform strain fields. While an ordinary strain gauge would measure strain as an average value over the gauge length, the method comprises separate strain component values for each of the measurement elements. Strain distribution and strain uniformity can thus be detected and assessed for active, passive and shear strain over the observed area, although plots showed strain fields with rather random variation in this study. The latter is probably due to inhomogeneity, and might also be

amplified by the relatively small measurement elements being used with side lengths between 3–5 mm depending on specimen size. This is approximately the same as the typical annual ring width for low density wood, which means that one element can contain a rather high amount of stiff latewood, while the neighbouring elements mainly consist of soft early wood. This will consequently cause the elements to return quite different strain magnitudes, resulting in highly varying strain fields. This can be the case even if the mean strain values returns reasonable results, since the total measurement area is more representative for the overall behaviour. The fact that variation in element strains within the measurement area decreased considerably by increasing the element side lengths, indicates that small measurement lengths and areas should be avoided. The size of wood specimen is therefore crucial in order to determine reasonable values for representative volume elements. Emphasis must also be put on the size of the measurement area in relation to the resolution and measurement accuracy and the parameters to be measured.

Finally, it can be mentioned that the method offers a good basis for development of constitutive relations for wood. The experimental results are collected and processed in a way that resembles the formulation of the finite element method. Results from numerical analysis with constitutive laws implemented can thus be compared more directly to experimentally based quantities. Furthermore, the method has a potential in describing statistical distributions for material properties and might thus be useful for more probabilistic approaches to material characterization. Altogether, this ought to be valuable for assessment of material parameters for wood applied in numerical codes.

## References


1. Choi D., Thorpe J. L., Hanna R. B. (1991) Image analysis to measure strain in wood and paper. Wood Science Technology (25): 251-262.
2. Reiterer A., Stanzl-Tschegg S. E. (2001) Compressive behaviour of softwood under uniaxial loading at different orientations to the grain. Mechanics of Materials 33: 705-715.
3. Ukyo S., Masuda M. (2004) Investigation of the True Stress-Strain Relation in Shear using the Digital Image Correlation Method. Journal of wood science - Official Journal of the Japan Wood Research Society 50 (3): 146-150.
4. Ukyo S., Masuda M. (2006) A new method for Measuring the True Shear Strength of Wood. 9th World Conference on Timber Engineering, Portland USA.
5. Sinha A., Gupta R., Muszyński L. (2006) Strain profile in wood frame shear walls – preliminary results. 9th World Conference on Timber Engineering, Portland USA.
6. Franke S., Franke B., Ratuenstrauch K. (2007) Strain analysis of wood components by close range photogrammetry. Materials and Structures (40): 37-46.
7. European Committee for Standardization NSF (2003) NS-EN 338 Structural timber Strength Classes (2nd ed.), p. 7.
8. European Committee for Standardization NSF (2003) NS-EN 408 Timber Structures - Structural timber and glued laminated timber. Determination of some physical and mechanical properties. (2nd ed.), p. 27.
9. Dinwoodie J. M. (2000) Timber. Its nature and behaviour (2nd ed.), E & FN SPON, London, p. 257.
10. SKOGFORSK (1992) Skandinaviske normer for testing av små feilfrie prøver av heltre, SKANORM, Dept. of Forestry, Agricultural University of Norway, p. 104.
11. Sunde F. F. (2005) Strength properties of small, clear wood specimens of Norway spruce (in Norwegian). Institutt for naturforvaltning, Norwegian University of Life Sciences. Master thesis, p. 53.
12. Minitab (2006). Minitab v.15 Help, Minitab Inc. Statistical Software, State College, Pennsylvania.
13. Larsen R. J., Marx, M. L. (1990) Statistics, Prentice-Hall Inc., New Jersey, p. 829.

# PAPER II

## Linear Shear Properties of Spruce Softwood

**K. B. DAHL[1], K. A. MALO[2]**

*Wood Science and Technology (2009) 43: 499-525*

**Abstract**
The shear test described by Arcan was used to investigate orthotropic shear properties of clear softwood from Norway spruce. The test was chosen on the basis of a thorough literature study, although the experimental setup was somewhat modified compared to the original. A total number of 85 specimens were tested for loading and unloading in 6 different configurations. Manufacturing and mounting of specimens as well as testing worked well. Video extensometry was used to measure strain in the critical specimen section, and the determined moduli were evaluated by means of FEM calculations. The average shear moduli were found to equal $G_{LR}$ = 640 MPa, $G_{LT}$ = 580 MPa and $G_{RT}$ = 30 MPa, which correspond well with values reported in literature for various spruce species. No significant differences in shear moduli could be found for configurations comprising the same material plane. Moduli determined from unloading generally showed higher values than those obtained in loading, but only the rolling shear *RT* demonstrated a significant difference. Each of the three shear moduli was found to be significantly different from each other, with $G_{LR}$ about 10% higher than $G_{LT}$, and approximately 20 times higher than $G_{RT}$. The coefficient of variation equalled 0.24, 0.37 and 0.28, respectively. The correlation with density was in general low. It was found that the 3-parameter Weibull distribution is most appropriate for a probabilistic description of the three orthotropic shear moduli of wood.

**Keywords** – Norway spruce, Orthotropy, Arcan shear test, Finite element analysis, Probabilistic methods

[1] Ph.D-student, Dept. of Structural Engineering, Norwegian University of Science and Technology NTNU, M.Sc. Structural and Civil Engineer, Multiconsult AS, Boks 265 Skøyen, N-0213 Oslo, Norway.
[2] Professor, Dept. of Structural Engineering, Norwegian University of Science and Technology NTNU

## Introduction

Determination of shear strength and stiffness of wood has long been impeded by difficulties in obtaining a state of pure and uniform shear in test specimens. In most specimen types, a combination of normal and shear stresses occur, which makes it difficult to interpret the pure shear behaviour. So far, the shear properties of wood have mainly been based on the notched shear block described by e.g. ASTM D143 (1984) and SKOGFORSK (1992). This is a longitudinally oriented cubical block with notches. The portion with the raised step is sheared off with a vertical load *P* applied to the top surface, while the other portion is resting on a fixed support, see Fig. 1.

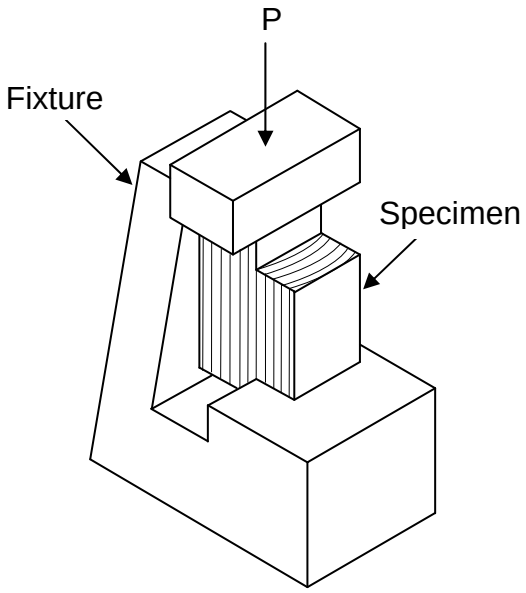


**Fig. 1** The notched shear block test for wood

Even if the method has been severely criticized by several authors (Liu 1984, Moses 2001), the ASTM test and modified versions have been extensively used, and are still the basis for determining the shear strength of wood and wood products. The specimen is not capable of producing a state of pure shear since a bending moment caused by the eccentric loading is inevitable, resulting in normal stresses perpendicular to the shear plane. The system stiffness and failure load is thus influenced by material properties perpendicular to grain, yielding incorrect results (Liu et al. 1999). The failure stress, in particular, is vulnerable since the low tensile capacity perpendicular to grain can govern the failure load. In addition, neither the normal stresses nor the shear stresses are uniform over the failure surface. According to Liu (1984), both photo-elastic analysis and measurements with strain gauges have shown rather unsymmetrical strain distribution, with strain concentrations in areas where pure shear is assumed to exist. A three-dimensional finite element model revealed a high stress concentration factor, resulting in underestimated shear strengths (Moses 2001). Moreover, it seems that the method has been confined to specimens oriented parallel to the grain, i.e. rolling shear has probably not been studied.

The plate twist test described in ASTM D3044 (1986) for determining shear moduli of plywood has also been used to some extent for wood, even if errors are easily introduced if grain is inclined to the plate geometry. Doyle et al. (1945) determined the three shear moduli by tests utilizing this

principle, and shear values presented in the Wood Handbook (FPL 1999) are based on this study. The results showed high variation for each of the shear moduli, and no correlations with densities or elastic moduli were found.

The European Standard NS-EN 384 (2004) states that the shear modulus can be calculated as 6.25% of the (longitudinal) modulus of elasticity, while NS-EN 408 (2003) assigns two bending test methods with sufficient accuracy for conventional structural design. The rolling shear is presumably not included in the methods. It is suggested to measure the shear strength in a fixture consisting of the wood specimen glued between two steel plates. By displacing one plate relative to the other, the wood will be subjected to shear forces. It is not known to what extent this setup has been used, and rolling shear does not seem to be covered by the method, although ASTM D2718 (1995) describes a similar method for testing of rolling shear in wood-based structural panels like plywood.

Shear tests by means of short beams have been proposed by e.g. Kollmann and Côté (1968), comprising beam specimens subjected to a uniformly distributed load over the midspan, with the ends either freely supported or clamped. It should be noted that normal stresses are inevitable due to the bending moment developing, resulting in an impure stress situation which can easily initiate fracture. This is visualized in Fig. 2, showing observations from preliminary tests of the present study.

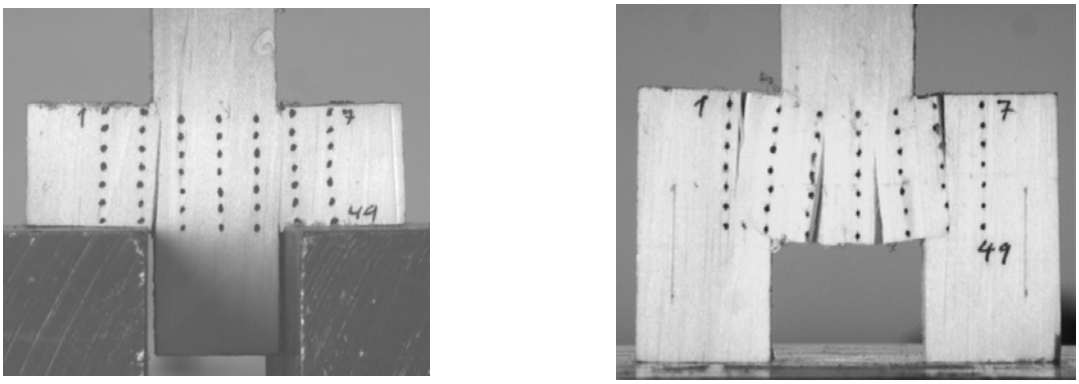


**Fig. 2** Short beams for testing of shear properties, marked with dots for video extensometry

Short beam shear tests have been investigated by Yoshihara and Kubojima (2002), Yoshihara and Furushima (2003) and Yoshihara and Ohhata (2003) for different configurations and wood species. For certain span widths, the asymmetric four-point bending proved to be applicable for testing of the shear modulus when combined with numerical analysis, although it was found that neither the three-point loading nor asymmetric four-point loading were suitable for determining shear strengths. A somewhat related method is the determination of the shear modulus by flexural vibration tests and Timoshenko's theory of bending. This method was used by Kubojima (1997), who, for certain beam depths and resonance mode numbers, found reasonable values for the moduli. However, the method is probably not suited for the determination of ultimate shear stresses.

Shear properties of composite materials are often determined by means of off-axis tension tests. Here the shear moduli are deduced from the shear strain developing from coupling between axial stress and shear strain in orthotropic materials loaded off-axis. The same principle can be used for wood, although nonuniform and impure strain fields make it difficult to assess the shear moduli, and particularly the ultimate shear stress capacities, with a high degree of accuracy. Off-axis testing

of wood comprises studies by Sliker and Yu (1993), Liu (2002), Yoshihara and Ohta (2000), Yoshihara and Satoh (2003) and Xavier et al. (2004).

Torsion tests have, to a limited extent, also been used, even if the underlying theory for obtaining the orthotropic shear characteristics is quite complex. Moreover, nonuniform strain fields and the presence of normal stress components complicate the assessment of shear moduli and ultimate shear stresses even further. Earlier studies undertaken by Carrington (1923) and Bodig and Goodman (1973) were based on torsion. Later studies comprise Yoshihara and Ohta (1995a, b, 1996) who investigated the elastoplastic shear behaviour of Sitka spruce in torsion around the *L* and *R* axes, and Yamasaki and Sasaki (2003) who studied the elastic properties of different wood species under combined axial force and torque around the *L* axis.

The so-called Iosipescu shear test consists of a beam with a 90˚ notch at the top and bottom of the central portion, as shown in Fig. 3. The loads are applied such that the bending moment is zero, whereas the shear is nonzero over the critical section. The failure can thus be regarded as purely shear induced. By orienting the specimen within the material, all shear types of an orthotropic material can in principle be investigated. Liu et al. (1999) and Liu (2000) found that the variant adopted in ASTM D5379 (1998) was unsatisfactory due to twisting and large transverse normal strains developing, although a slightly modified version gave reasonable values for wood. Other known studies of the Iosipescu test applied to wood are by Yoshihara et al. (1999, 2001), Dumail et al. (2000), Xavier et al. (2004) and Yoshihara and Matsumoto (2005). It can be noted that Xavier found about 20% higher shear modulus values with the Iosipescu test than the off-axis test. The overall conclusion is that the Iosipescu test gives adequate shear moduli, but that the shear failure stress can be somewhat corrupted by improper failure due to bending moment beside the crucial section. In particular, radially and tangentially oriented specimens are vulnerable to improper failure due to low tensile capacities in these directions.

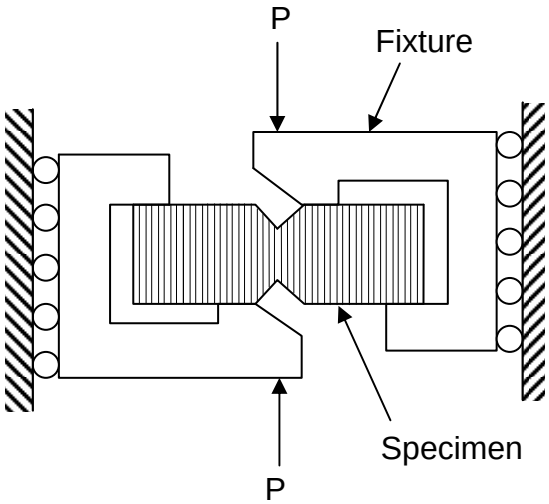


**Fig. 3** Iosipescu shear test

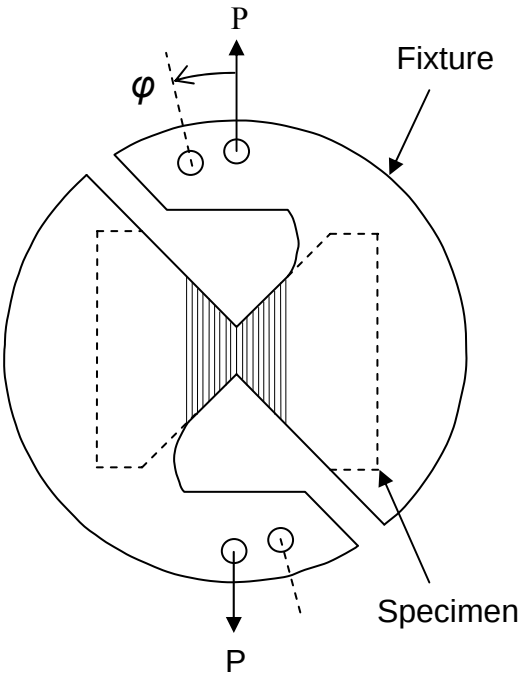


**Fig. 4** Arcan shear test

Arcan et al. (1978) developed a butterfly shaped specimen for shear testing of isotropic and orthotropic materials. The mechanical principle resembles the aforementioned Iosipescu test, but the fixture is somewhat simplified. The specimen is mounted in two separate stiff brackets which, during testing, are drawn apart so that the line of loading passes through the centreline of the butterfly, resulting in a plane and pure shear stress situation. Due to the butterfly shape, the failure will be located at the centre section of the specimen, enabling estimation of the pure shear strength. By altering the configuration with respect to the material axes, all three shear types in an orthotropic material can in principle be investigated. Furthermore, by varying the angle φ in Fig. 4, the material can be investigated for a combination of shear and normal stresses. By means of photo-elastic results, Arcan (1984) showed that the shear stress distribution is nearly uniform over the critical cross section, a fact that has been confirmed by subsequent finite element analyses (Liu and Floeter 1984). Liu (1984) and Liu and Floeter (1984) were the first to investigate shear properties of wood by means of the Arcan method. Specimens were glued with epoxy to aluminium plate brackets, and tested for pure shear and a combination of shear and normal stresses within the *LT* material plane, resulting in reasonable values. A modified variant, with bolts instead of glue, was used by Liu et al. (1996) on solid wood specimens of spruce species, with strain gauges mounted at the critical section. Somewhat lower shear strengths than those resulting from the ASTM D143 (1984) shear block test were found, while the shear modulus $G_{LT}$ agreed well. In later studies by Liu and Ross (1998) and Liu et al. (1999), shear tests were carried out for different angles in the *LR* plane, also showing good agreement with orthotropic theory. It was concluded that the Arcan test is the most reliable shear test for wood, but only shear strengths parallel to grain can be determined because of the low tension capacity perpendicular to grain. However, Oliveira (2004) tested shear strength and stiffness in each of the three orthotropic material planes of maritime pine wood by the Arcan method, and found reasonable results. Yoshihara and Matsumoto (2005) also tested shear by a slightly modified Arcan test formed as a tension test with notches, and found shear modulus values $G_{LT}$ that compared well with results from the Iosipescu test.

Based on the various references, it was concluded that the Arcan test seemed most appropriate for a general study of the shear properties of wood. The ability to produce a relatively uniform plane stress state seemed particularly desirable. Moreover, the test enables determination of parameters characterizing both linear and possible nonlinear behaviour, in addition to failure. The simplicity of both the setup and the estimation of parameters was also appealing. The fact that all material planes can easily be tested with the same configuration was also important, since it enables an equal assessment basis for all shear types.

## Experimental work

Arcan specimens were produced out of clear softwood from Norway spruce (*Picea Abies* (L.) Karst.). The tests were part of a more comprehensive test program which also involved on-axis and off-axis tension and compression tests in each of the three material planes. The material was taken directly from the forest at four different locations in southern Norway, comprising 8 different trees with a log length of approximately 0.5 m. The logs were chosen with diameters as large as possible in order to obtain material with a minimum of annual ring curvature. Confined by natural growth conditions, the log diameters ranged between 0.5 and 0.8 m. Since it is hard to obtain sawn and graded lumber without a high degree of curvature, such material was not included in the study. The material was conditioned in a climate room with 65% relative humidity and 20˚C for several

months to obtain approximately 12% moisture content. The densities ranged between 300 and 500 kg/m$^3$ with an average conditioned density of 398 kg/m$^3$ and a coefficient of variation of 9%.

## Specimens

Three plate types corresponding to each of the three material planes *LR*, *LT* and *RT* were produced. The plates were cut from the outer part of the stems to obtain specimens with Cartesian material axes coinciding with the specimen geometry axis, see Fig. 5. Fibre inclination to load orientation was thus minimized. Specimens were in general chosen so as to keep apparent inhomogeneities and macroscopic defects like knots at a minimum.

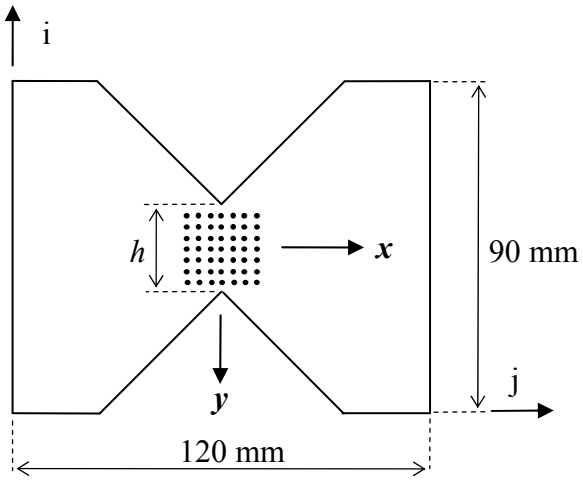


**Fig. 5** Specimen for testing of *ij* shear, with measurement dots and local axes *xy*

Specimens were made with the geometry shown in Fig. 5. Six different specimen types were produced, each designated by *ij*, where $\{i, j\} = \{L, R, T\}$ and $i \neq j$, as shown in Fig. 6. The first index *i* assigns the direction of the test load *P* relative to the material orientation, while the second index *j* denotes the normal vector of the loaded plane. Specimen type *ij* corresponded thus to testing of $\sigma_{ij}$ - $\gamma_{ij}$ shear. Six configurations were chosen instead of three in order to investigate if *i* or *j* oriented load could possibly affect the *ij* shear properties, a factor which according to orthotropic theory should not play any role.

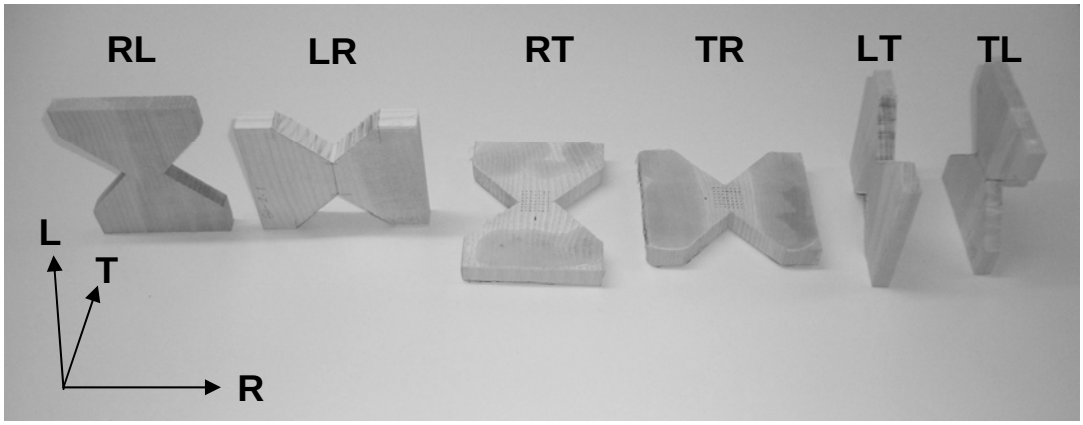


**Fig. 6** The six specimen types *ij* used for shear testing, oriented as taken out of the wood stem

Tentative testing revealed that the different specimen types should be given somewhat different geometry in order to obtain the desired failure. Specimen thicknesses $t$ and cross section heights $h$ for each type are specified in Table 1 with reference to Fig. 5. The tabulated values are approximate values used for carpentry, and a digital slide calliper was used to obtain accurate values of the critical geometry dimensions prior to testing. Between 20 and 30 specimens within each material plane were considered sufficient for reliable estimates of the parameters. A total number of 85 specimens were tested.

**Table 1** Specimen type geometries

| Type *ij* | Height *h* (mm) | Thickness *t* (mm) | Number of tests | Sum | Total |
|---|---|---|---|---|---|
| LR | 30 | 17 | 12 | 35 | 85 |
| RL | 25 | 12 | 23 | | |
| LT | 30 | 12 | 12 | 27 | |
| TL | 25 | 12 | 15 | | |
| RT | 25 | 17 | 11 | 23 | |
| TR | 25 | 17 | 12 | | |

## Fixture

The specimens were attached to the loading brackets by adhesives rather than bolts, partly because Liu et al. (1996) reported specimens to be vulnerable to fracture near the bolt groups instead of the critical section. Brackets were produced out of 5 mm aluminium plates with a hole for bolt loading in the loading jig, and glued onto the specimens by means of hot melt adhesives applied with an electrical glue pistol. In order to secure on-axis loading, the specimens were deliberately glued onto the plates so that the line of loading would pass exactly through the critical section. Clamps were used to strengthen the fixture. To ensure efficient testing and reduce the turnaround time, 15 sets of brackets, each consisting of 4 L-shaped aluminium plates, were produced. Test programs of 15 specimens per sequence could thus be undertaken before the brackets were cleaned and ready for reuse. This was important since the preparation of each specimen for testing was quite time-consuming, as the adhesives required several days of drying in order to attain full strength.

## Testing

The European Standard NS-EN 408 (2003) states that failure in shear tests shall be reached within 300 ± 120 s., whereas SKOGFORSK (1992) specifies 105 ± 15 s. ASTM D143 (1984) states that the notched shear block shall be loaded continuously at 0.6 mm/min. As a compromise between the various configurations *ij*, a rate of 0.3 mm/min was chosen for all tests, resulting in maximum capacities reached after 200 to 400 s. The specimen and fixture are shown in Fig. 7 and Fig. 8 before and after failure, respectively.

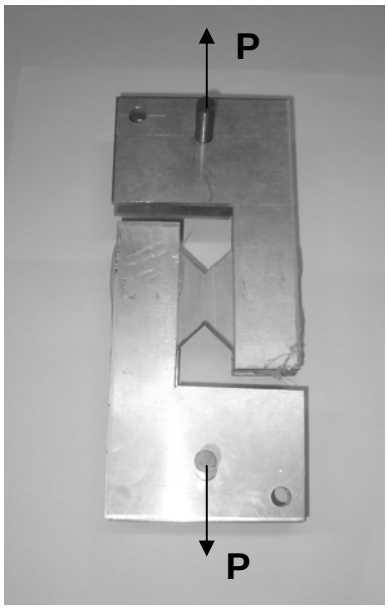


**Fig. 7** Shear test configuration for clear wood

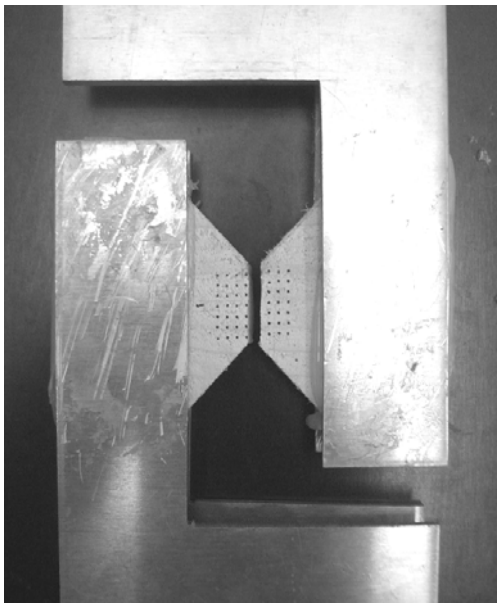

**Fig. 8** Specimen after failure (RT-configuration)

The tests were run in an acclimatized atmosphere of 20˚C and 65% relative humidity. Each specimen was exposed to a loading sequence as shown in Fig. 9. The first loading was up to approximately 40% of the assumed component capacity, followed by unloading and reloading until failure for investigation of ultimate capacities and possible elastoplastic behaviour. The linear behaviour is treated herein, while the nonlinear and ultimate stresses will be discussed in a later study.

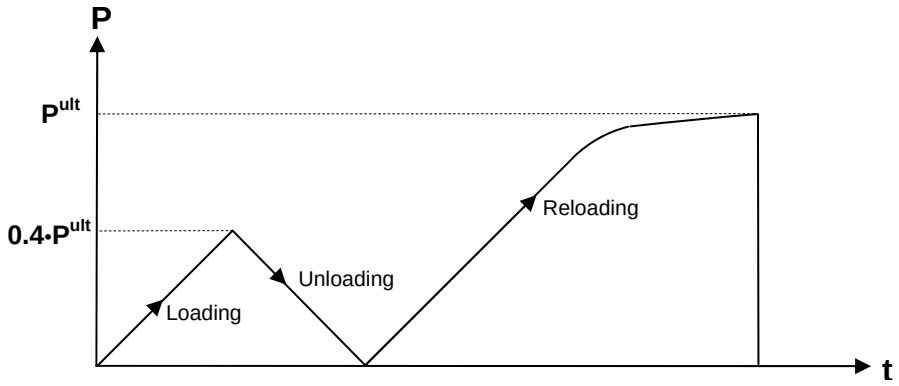


**Fig. 9** Loading sequence used for shear testing

After failure and dismounting, the glue was removed from the specimen and one of the pieces was weighed to determine the acclimatized mass $m_w$. The piece was subsequently submerged into water and the corresponding weight increase was measured. Archimedes law implies that the altered weight of the water tub can be related directly to the acclimatized volume $V_w$. The volumes of the irregular specimen pieces could thus be estimated. The pieces were subsequently dried at 105˚C for 2 days and then weighed a second time to determine dry substance mass $m_0$. Moisture content and density could finally be calculated for each specimen as:

$$w = \frac{m_w - m_0}{m_0} \cdot 100\% \qquad \rho_w = \frac{m_w}{V_w} \qquad \rho_{12} = \left[1 - 0.005\left(w - 0.12\right)\right] \cdot \rho_w \qquad (1)$$

where $w$ is moisture content (%)
$\rho_w$ is density at the observed moisture content $w$ (kg/m$^3$)
$\rho_{12}$ is density at 12% moisture content (kg/m$^3$)

The moisture content was in general found to equal approximately 12%, nevertheless the densities were modified by means of the empirically based formula for $\rho_{12}$, which is valid for $7\% < w < 17\%$, a requirement which was fulfilled by all specimens tested (SKOGFORSK 1992).

## Stress and strain observations

Deformation was measured by means of video extensometry described by Dahl and Malo (2009) and briefly summarized in the following. Prior to the test, a quadratic 18 mm × 18 mm grid of target dots was applied on the wood surfaces at the critical section as illustrated in Fig. 10.

**Fig. 10** Arcan specimen marked with an array of dots for deformation measurements

The in-plane $xy$ coordinates of the dots were continuously measured by the camera throughout loading. Based on the coordinate values, a post-processing routine calculated normal and shear strain over the measured area (Dahl and Malo 2009). Simultaneous estimates for the three in-plane strain components $\varepsilon_{ii}$, $\varepsilon_{jj}$ and $\gamma_{ij}$ could thus be held together with the nominal shear stress $\hat{\sigma}_{ij}$ for evaluation of the overall material behaviour, estimated for each timestep by

$$\hat{\sigma}_{ij} = \frac{P}{h \cdot t} \qquad (i \neq j) \qquad (2)$$

where $h$ and $t$ are the measured cross section dimensions at the initial configuration, and $P$ is the load level. It can be noted that the stress estimate is calculated analogously as for the Iosipescu shear test on wood described by e.g. Dumail et al. (2000) and Yoshihara et al. (1999).

Shear stress $\sigma_{ij}$ is plotted against the average shear strain $\overline{\gamma}_{ij}$ over the measurement area for each configuration *ij* in Fig. 11. It can be seen that the shear moduli as well as the nonlinear behaviour and ultimate shear stresses vary considerably between the three different shear types.

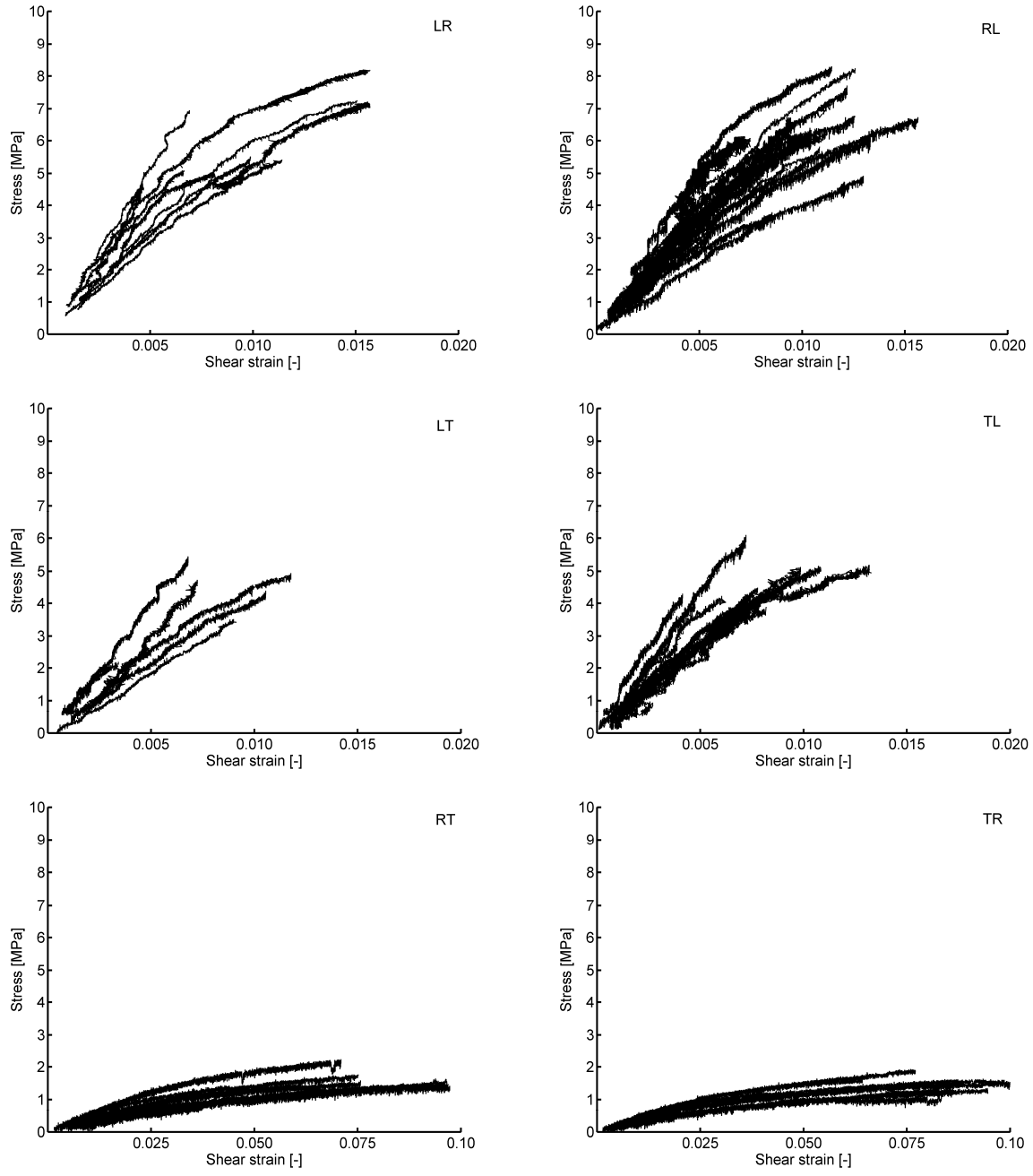


**Fig. 11** Experimental stress-strain curves for the various configuration types *ij*

## Experimental data analysis

The linear trend was obtained by extracting a set of $q$ timesteps from the experimental stress-strain relationship. The set was upward confined by the timestep corresponding to approximately 40% of the ultimate stress observed. Initial disturbances were deliberately removed in the lower part. Typically, the remaining linear set contained between 500 and 1000 timesteps.

A least sum square error (SSE) optimization algorithm was used to fit the linear elastic shear moduli estimate $\hat{G}_{ij}$ to the observed stress-strain relationships as indicated by Eq. (3).

$$SSE = \sum_{t=1}^{q}\left[\hat{\sigma}_{ij-t} - \sigma_{ij-t}^{\text{mod}}\right]^2 = \sum_{t=1}^{q}\left[\hat{\sigma}_{ij-t} - \left(A_g + \left(\hat{G}_{ij} \cdot \overline{\gamma}_{ij-t}\right)\right)\right]^2 \qquad \{i, j\} = \{L, R, T\}\ i \neq j \quad (3)$$

Hence, the mean shear strain $\overline{\gamma}_{ij}$ is used as explanatory variable, while $A_g$ is correcting for nonzero experimental stress for zero experimental strain. The parameterized relationship was automatically plotted together with the experimental data as a check of reasonability, see Fig. 12. It can be seen that the shear strain follows a nonlinear progress to ultimate stress, while the two normal strain components remain relatively steady at zero strain.

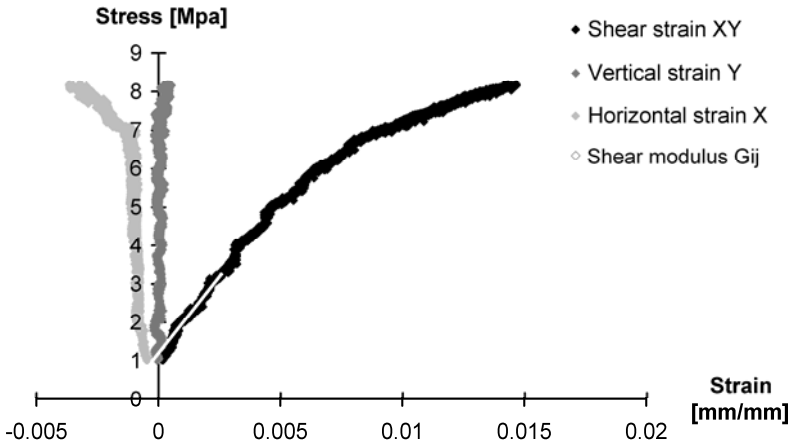


**Fig. 12** Experimental strain ($ij = LR$) plotted with the estimated shear modulus $\hat{G}_{ij}$

## Test results

Experimental mean values of the shear moduli estimates $\hat{G}_{ij}$ are given in Table 2 for each configuration type *ij*. Coefficients of variation CV are also tabulated; in addition to correlation *r* to density, and the number of tests *n* which enters into each of the estimates. It can be noted that *n* varies somewhat between the three loading sequences since some of the stress-strain paths not were adaptable. Results for each specimen are to be found in Dahl (2008).

**Table 2** Shear moduli estimates $\hat{G}_{ij}$ (MPa) for the various configuration types *ij*

| Type (*ij*) | | Density (kg/m³) | Loading | Unloading | Reloading | Average |
|---|---|---|---|---|---|---|
| *LR* | Mean | 388 | 650 | 669 | 754 | 702 |
| | CV | 0.05 | 0.15 | 0.17 | 0.30 | 0.24 |
| | r | - | 0.25 | -0.15 | 0.03 | 0.31 |
| | n | 12 | 7 | 8 | 12 | 12 |
| *RL* | Mean | 400 | 642 | 828 | 734 | 738 |
| | CV | 0.10 | 0.25 | 0.20 | 0.20 | 0.23 |
| | r | - | 0.02 | 0.10 | 0.37 | 0.28 |
| | n | 23 | 17 | 19 | 20 | 22 |
| *LT* | Mean | 409 | 597 | 701 | 586 | 631 |
| | CV | 0.06 | 0.55 | 0.50 | 0.27 | 0.45 |
| | r | - | -0.46 | -0.64 | 0.30 | -0.50 |
| | n | 12 | 7 | 8 | 7 | 9 |
| *TL* | Mean | 415 | 674 | 718 | 657 | 681 |
| | CV | 0.07 | 0.31 | 0.36 | 0.27 | 0.31 |
| | r | - | 0.15 | 0.05 | 0.17 | 0.13 |
| | n | 15 | 13 | 13 | 15 | 15 |
| *RT* | Mean | 381 | 30.5 | 37.7 | 32.0 | 33.4 |
| | CV | 0.10 | 0.30 | 0.24 | 0.31 | 0.29 |
| | r | - | 0.62 | 0.54 | 0.17 | 0.39 |
| | n | 10 | 9 | 9 | 10 | 10 |
| *TR* | Mean | 381 | 34.3 | 41.5 | 36.7 | 37.5 |
| | CV | 0.11 | 0.30 | 0.24 | 0.26 | 0.27 |
| | r | - | 0.13 | 0.25 | 0.16 | 0.18 |
| | n | 12 | 12 | 12 | 12 | 12 |

From the table, it can be seen that the $\hat{G}_{ij}$ values from *ij* and *ji* configurations clearly resemble each other, and thus substantiate the assumption of orthotropy. The highest deviation in average modulus between mutual configurations occurs for the rolling shear, i.e. $\hat{G}_{RT}$ and $\hat{G}_{TR}$, with a difference of 15%. This can be explained by configuration effects, as investigated below. The overall coefficients of variation CV lie between 0.23 and 0.45, which is relatively high. The correlations to density are correspondingly low.

## Configuration study

In order to study the mechanical behaviour of the shear specimens in more detail, finite element models of the test configurations were modelled with the commercial FEM code ANSYS 10.0. Each of the configurations *ij* was modelled with geometry given in Fig. 5 and Table 1. The average shear modulus estimate $\hat{G}_{ij}$ was used for the corresponding configuration *ij*, while values in Table 3 were used for the eight remaining orthotropic material parameters, where $E_{ii}$ denotes moduli of elasticity and $v_{ij}$ denotes Poisson's ratios. These parameters are based on values available in the literature for different spruce species, and are determined as average values from assignments in Jenkin (1920), Carrington (1923), Stamer (1935), Doyle et al. (1945), Kollmann and Côté (1968), Goodman and Bodig (1970), Bodig and Goodman (1973), FPL (1999) and NS 3470 (1999). It must be noted that none of the references specifically refer to Norway spruce (*Picea Abies* (L.) Karst).

**Table 3** Linear elastic parameters for spruce used in simulation. *E* and *G* are given in MPa

| $E_{LL}$ | $E_{RR}$ | $E_{TT}$ | $G_{LR}$ | $G_{LT}$ | $G_{RT}$ | $V_{LR}$ | $V_{LT}$ | $V_{RT}$ | ρ |
|---|---|---|---|---|---|---|---|---|---|
| 10 991 | 716 | 435 | 682 | 693 | 49 | 0.42 | 0.48 | 0.50 | 390 |

The aluminium brackets were modelled as isotropic with $E = 70\,000$ MPa, $v = 0.3$ and with a density $\rho$ of 2700 kg/m$^3$. The weight of the clamps was included in the model as point loads at appropriate locations with masses based on weighing. The bolted joints at each end of the fixture were modelled as hinged supports allowing rotation in the *xy*-plane. The lower support was restricted against translation in all directions, while the upper was subjected to the vertical test load *P* and hence free to move in the vertical (*y*) direction. The magnitude of *P* was set to correspond to approximately 50% of the assumed elastic limit stresses in the wood for the various configurations, in order to achieve a representative effect of the fixture weight on the total linear elastic behaviour. The adhesive between aluminium and wood was simulated by means of contact elements enforcing equal *x* and *y* displacement in adjacent nodes of the two materials in the glued areas. First-order eight noded hexahedral elements (SOLID45) with reduced integration were used for both materials providing constant stress and strain fields within the elements. Different meshes, ranging from 5000 to 80 000 elements, were used.

The analyses revealed that the shear stiffness measured by the experiments is typically higher than the real moduli characterizing the material. This must be due to the fact that the measurement area covers a quadratic area which is larger than the critical cross section. On each side of the critical section, the shear stress is distributed over a larger area because of the notched specimen form. The shear strain is thus decreasing with increasing horizontal distance from the critical section. Consequently, the average shear strain over the 18 mm × 18 mm area will be lower than for a case where only the critical section is considered. The system stiffness measured is therefore too stiff, resulting in an apparent shear modulus that is too high. This may indicate that the measurement area could have been reduced, although a larger area is preferred in order to avoid encumbered values due to inhomogeneity effects.

The experimental strain data were based on coordinates of quadratic arrays consisting of 49 dots applied as a 7 × 7 grid pattern on the central section of the wood surfaces, and post-processed as 36 constant strain "elements" as described in Dahl and Malo (2009). In order to enable a direct comparison basis between experimental and numerical data, the volume was meshed so that in-plane numerical shear strain values $\gamma_{ij}$ could be collected from the same location on the specimen.

The strain values were subsequently averaged over the field for direct comparison to experimentally based strain. Based on the average shear strain resulting from the load $P$ and the cross-section dimensions $h$ and $t$, a numerically based shear modulus was estimated. This estimate could then be directly compared to the $\hat{G}_{ij}$ value used for the simulation, and a modulus modification factor $a_{ij}$ was calculated as the ratio between them;

$$a_{ij} = \frac{\hat{G}_{ij} \cdot h \cdot t \cdot \overline{\gamma}_{ij}}{P} \tag{4}$$

Because of the form of the notched specimen, the shear strain typically showed nonuniform distributions over the measurement areas. As a consequence, the $a_{ij}$ factors showed some sensitivity to the element size used in the measurement region of the numerical analyses. In order to approach the real behaviour, a very large number of elements should ideally have been used. Restricted by model size and CPU limitations, it was decided to use a strategy by which $a_{ij}$ was determined from values obtained by models with different element sizes $e$ in the measurement region. Linear regression was used to obtain a best fit relation, which subsequently was used to estimate the value of $a_{ij}$ for $e \approx 0$ by extrapolation. The points and corresponding best fit lines for the various configurations are shown in Fig. 13, while modification factors $a_{ij}$ determined for $e \approx 0$ are given in Table 4.

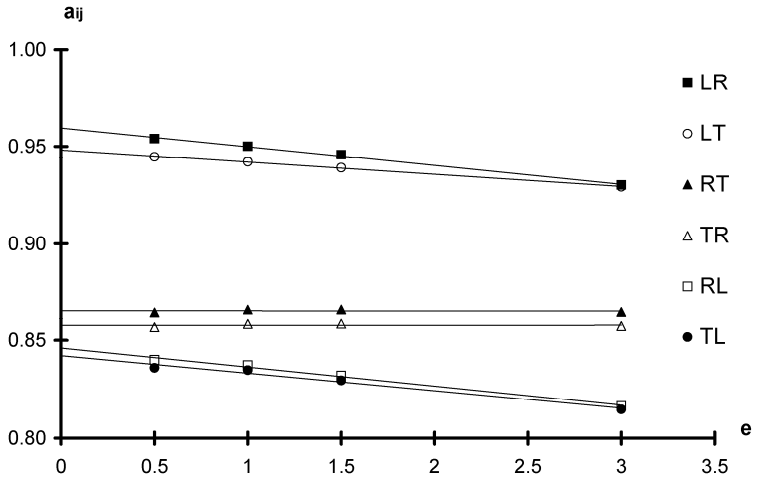


**Fig. 13** Modifications factors $a_{ij}$ plotted against numerical element-size $e$ (mm)

It can be seen that the two configurations with the stress oriented in the longitudinal directions (*LR* and *LT*) show a similar trend. This is also the case for the resembling configurations *RL* and *TL*, and the two rolling shear configurations *RT* and *TR*. As opposed to the others, both rolling shear configurations demonstrate a slightly decreasing trend with decreasing $e$. This can be explained by nonuniform strain fields in the outer range of the measurement area, overestimating the strain for increasing $e$, and thus contributing to a too high average shear strain.

**Table 4** Modification factors $a_{ij}$ for shear moduli estimate $\hat{G}_{ij}$ extrapolated for $e \approx 0$

| *LR* | *RL* | *LT* | *TL* | *RT* | *TR* |
|---|---|---|---|---|---|
| 0.960 | 0.846 | 0.948 | 0.842 | 0.866 | 0.858 |

Different numerical models are shown in Fig. 14 and Fig. 15 with mesh sizes $e$ = 3 mm and $e$ = 0.5 mm, respectively. It can be noted that the notch was modelled with a fillet radius of 1 mm to avoid stress singularities.

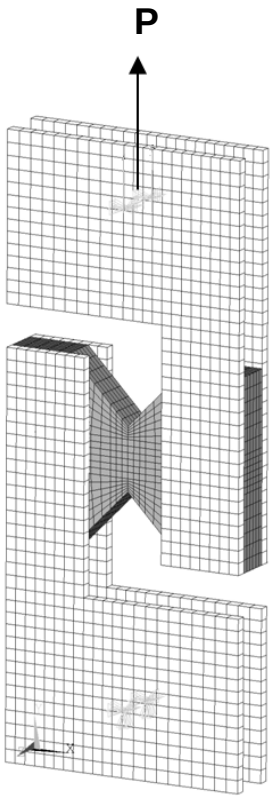


**Fig. 14** Numerical model of the test ($e$ = 3 mm)

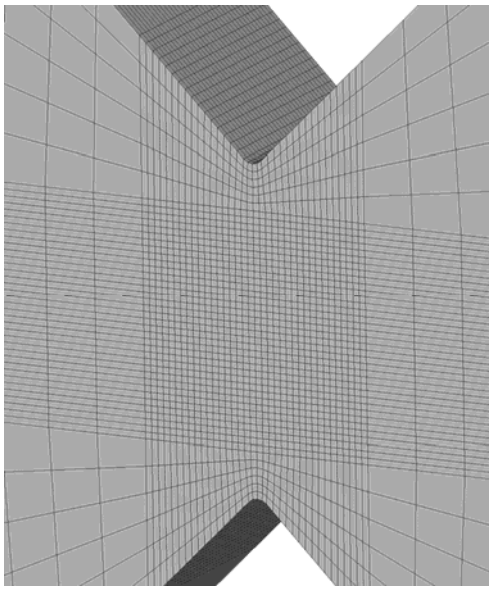

**Fig. 15** Close-up of specimen ($e$ = 0.5 mm)

By multiplying the experimentally based apparent shear moduli estimates $\hat{G}_{ij}$ by the modifications factors in Table 4 , improved shear moduli values $G_{ij}$ are obtained:

$$G_{ij} = \hat{G}_{ij} \cdot a_{ij} \tag{5}$$

Hence, the modification accounts not only for the measurement technique, but also for the test configuration in general, including effects from geometry, orthotropic material properties and boundary conditions. An inherent assumption made by the modification strategy is that the configuration behaves linearly, which is reasonable as long as no material yielding takes place, although the correction in principle could have been undertaken in an iterative manner. However, this methodology would have been hard to carry out in a sufficient way, since the number of elements in the critical section with this approach ideally should have approached infinite for an accurate prediction of the nonuniform strain fields. Simulations with modified shear moduli $G_{ij}$ and $e$ = 0.5 mm resulted in numerical $\overline{\gamma}$ values deviating less than 0.3% from the experimental average $\overline{\gamma}$ values, which supports the applicability of the approach used herein. With a smaller $e$-value, the deviation could have been expected to be even smaller. Moreover, it should be noted that similar modification factors for the analogous Iosipescu test have been proposed by Pierron and Vautrin (1994), Pierron (1998), Dumail et al. (2000) and Xavier et al. (2004). Oliveira (2004) studied three

of the Arcan configurations with application to pine, and found somewhat less corrective factors than determined herein, especially for *ij* = *TR*. This is presumably due to the fact that Oliveira used strain gauges measuring a smaller area than the video extensometer, which in particular results in differences for the very soft rolling shear plane.

It was assumed that the material axes *LRT* in general coincided with the Cartesian geometry axes of the various configurations, i.e. that no off-axis loading occurred. It is clear that this is an idealization since material variation, annual ring curvature and carpentry makes it difficult to obtain specimens with a Cartesian material system unidirected with the geometric specimen axes. Study of the two numerically based in-plane normal strain components showed that the vertically oriented strain $\varepsilon_{ii}$ was very small for all configurations *ij*, while the horizontal strain $\varepsilon_{jj}$ on average could approach values close to 10% of the shear strain level $\gamma_{ij}$, particularly for the *LR* and *LT* configurations. This corresponds well with the overall tendencies of the experimental data. It should be noted that the experimental normal strain components could have been analyzed with a similar *SSE* technique as used for the shear strain. Comparison between the numerically and experimentally based strain responses would then have enabled determination of possible off-axis loading due to fibre inclination, which subsequently could have been used to improve the $G_{ij}$ estimates. This potential was not exploited herein since most tests showed very little normal strain.

## Shear moduli

Each shear modulus estimate given in Table 2 was modified according to Eq. (5) for configuration and measurement effects. Mean values and coefficients of variation CV of the resulting moduli $G_{ij}$ are given in Table 5 with averaging between *ij* and *ji* estimates according to orthotropic theory.

**Table 5** Modified experimental shear moduli $G_{ij}$ (MPa) from *n* tests measured at plane *ij* and *ji*

| | *ij* | Loading | | Unloading | | Reloading | | All | Total | CV | r |
|---|---|---|---|---|---|---|---|---|---|---|---|
| | | Mean | *n* | Mean | *n* | Mean | *n* | Mean | Mean | | |
| $G_{LR}$ | *LR* | 624 | 7 | 642 | 8 | 724 | 12 | 674 | 641 | 0.24 | 0.13 |
| | *RL* | 543 | 17 | 701 | 19 | 621 | 20 | 625 | | | |
| $G_{LT}$ | *LT* | 566 | 7 | 665 | 8 | 555 | 7 | 599 | 582 | 0.37 | -0.08 |
| | *TL* | 567 | 13 | 605 | 13 | 553 | 15 | 574 | | | |
| $G_{RT}$ | *RT* | 26.4 | 9 | 32.7 | 9 | 27.7 | 10 | 28.9 | 30.7 | 0.28 | 0.26 |
| | *TR* | 29.4 | 12 | 35.6 | 12 | 31.5 | 12 | 32.2 | | | |

The modified moduli are compared to values from the literature in Fig. 16 using the same references as stated for Table 3. It can be seen that the three experimental averages are within the minimum and maximum values of literature assignments, although they generally are somewhat lower than the literature averages, particularly $G_{RT}$. The overall agreement is, however, quite good. The credibility of the three linear moduli is promising for subsequent assessment of nonlinear and failure parameters, which are certainly more difficult to detect and obscure to verify since hardly any literature references exist for such data.

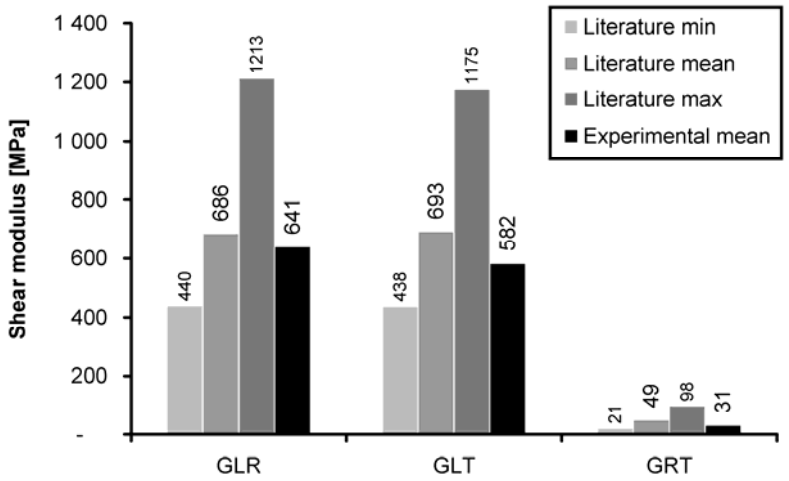


**Fig. 16** Literature values and modified experimental averages

The determined shear moduli are plotted against specimen density in Fig. 17 to Fig. 19. The values exhibit generally low correlation with density. Analysis of the Pearson's product-moment coefficient by statistical software Minitab (2006) resulted in significant correlation ($p < \alpha = 0.05$) only for the rolling shear $G_{RT}$, while $G_{LR}$ and $G_{LT}$ were uncorrelated. The determined correlation coefficients $r$ are given in Table 5. By way of comparison, the literature values result in correlation coefficients of –0.05 for $G_{LR}$, 0.25 for $G_{LT}$ and –0.46 for $G_{RT}$, which are in poor agreement with the tabulated values. Hence, the overall sensitivity to density is low for both experimental and literature shear moduli values. JCSS (2006) reports correlation of 0.6 which, by comparison, seems very high.

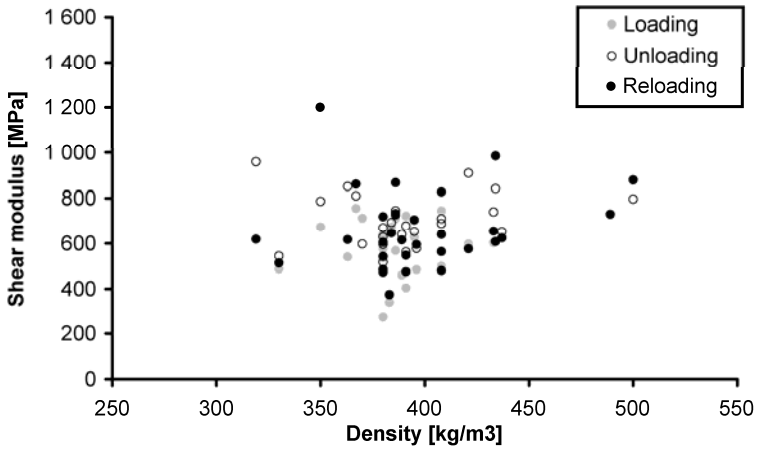


**Fig. 17** Shear modulus $G_{LR}$ based on modified experimental data

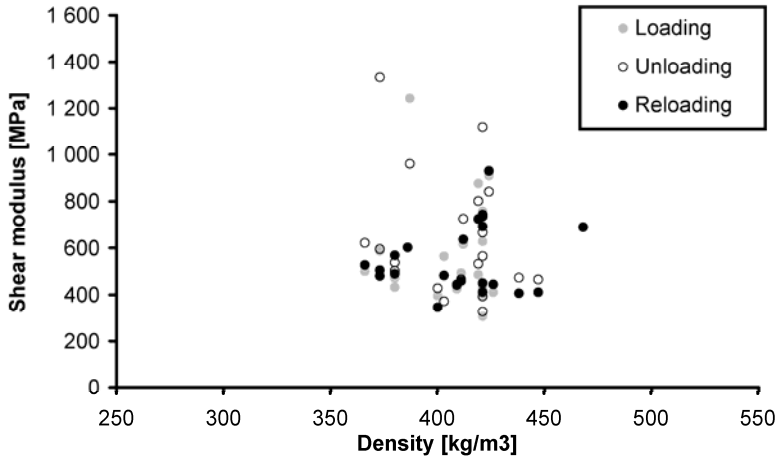


**Fig. 18** Shear modulus $G_{LT}$ based on modified experimental data

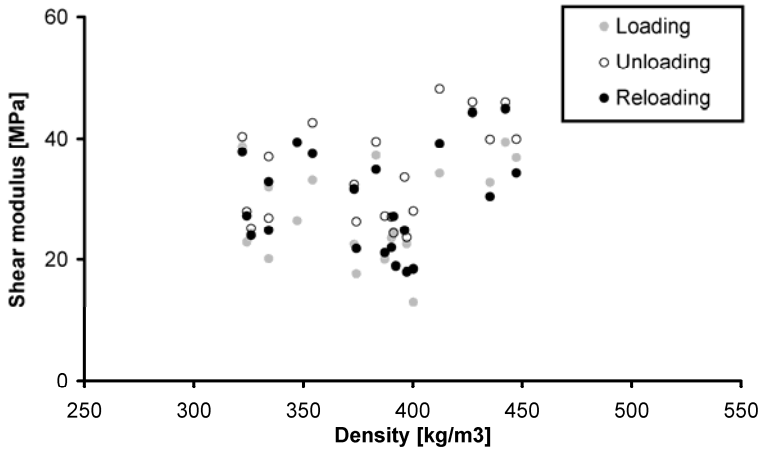


**Fig. 19** Shear modulus $G_{RT}$ based on modified experimental data

The non-parametric Mann-Whitney test (Minitab 2006) was used to investigate if any difference exists between *ij* and *ji* determined $G_{ij}$ values. No significant difference was found ($\alpha = 0.05$), neither for the modified nor the unmodified values. The two groups within the *LT*-plane, in particular, may be regarded as equal. According to the Mann-Whitney test, the differences were larger for the unmodified than the modified samples for each of the three moduli. This indicates that the modification procedure is viable. In summing up, it can therefore be concluded that both configuration types *ij* and *ji* are governed by the same modulus $G_{ij}$, and hence satisfying orthotropic theory assumptions.

The Mann-Whitney test was also used to investigate possible differences in shear moduli determined from the three loading sequences. In particular, the difference between loading and unloading was of interest since this could indicate creep or strain rate effects. Data from *ij* and *ji* configurations were treated as one sample in this context. The rolling shear resulted in significant difference in $G_{RT}$ between loading and unloading ($p = 0.01 < \alpha$), with an unloading modulus median nearly 24% higher than the median determined from loading. However, no significant differences could be found for the other two moduli, $G_{LR}$ and $G_{LT}$, even if the unloading sequences had the highest shear moduli with median values about 10% higher than obtained by loading. Except for the

rolling shear modulus $G_{RT}$, averaging of the respective shear moduli between the different loading sequences was therefore deemed reasonable.

The Mann-Whitney test also revealed that $G_{LR}$ and $G_{LT}$ are significantly different ($p = 0.001 < \alpha$). Hence, none of the three orthotropic shear moduli of wood can be deemed equal, as opposed to assumptions made in many standards and simplified procedures.

## Statistical distributions

The relatively high number of specimens enabled a probabilistic quantification of the shear moduli estimates. This effort was strongly motivated by the fact that wood is characterized by large variation in its parameter values, making a probabilistic approach desirable.

The Anderson-Darling (AD) test was used to assess to what extent the samples corresponded to the various distributions. This is a powerful empirical distribution function test, which can be used even for small samples with $n \leq 25$ (Anderson and Darling 1952). The test can be visualized through probability plots with percentile points for corresponding probabilities of the experimental data set. The linear middle line is the expected percentile from the distribution, and enclosing lines on each side represent the lower and upper bounds for the confidence intervals of each percentile (Minitab 2006). The closer the experimental points lie to the linear line, the closer the data follow the specified distribution. Probability plot and histogram for the $G_{RT}$ values are shown in Fig. 20 with adaptation to the three-parameter Weibull distribution.

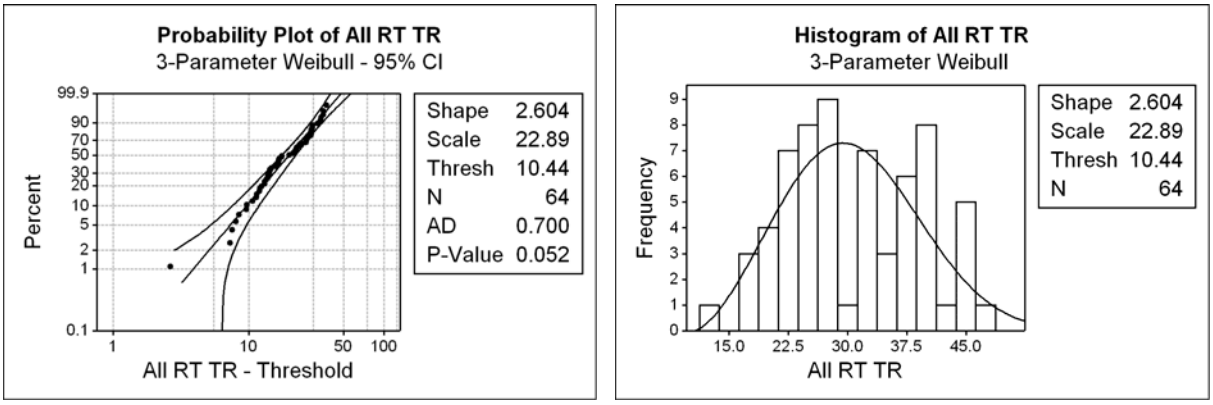


**Fig. 20** Rolling shear modulus $G_{RT}$ values (MPa) adapted to the Weibull distribution

The AD test uses the hypotheses:

- $H_0$ - The specified distribution adequately fit the data
- $H_1$ - The specified distribution does not fit the data

$H_0$ is rejected if the $p$-value, i.e. the probability of incorrectly rejecting $H_0$, is less than a critical level, say $\alpha = 5\%$, while a $p$-value larger than $\alpha$ indicates that the data follow the distribution. Different distributions can hence be quantitatively compared by means of the AD value, where the lowest value indicates the best correspondence, although any distribution with a nonsignificant $p$-value is acceptable.

The normal, lognormal and Weibull distributions were considered as the most pertinent distributions to investigate, partly based on assignments for timber by JCSS (2006) and partly based on histogram plots. Each of the three shear moduli was analysed in MINITAB 15 and the results are summarized in Table 6. Loading and unloading data from both *ij* and *ji* configurations are treated as one sample for *LR* and *LT* since the aforementioned Mann-Whitney analyses indicated no difference between the underlying samples. *RT* characteristics are, on the other hand, treated both as one sample and isolated for loading (+) and unloading (–) since the behaviour was found to differ significantly. The probability density functions for the Lognormal and Weibull distributions are given in Appendix, defining the parameters used in Table 6.

**Table 6** Statistical distribution characteristics for the experimentally based shear moduli $G_{ij}$ (MPa)

| | | *Normal* | | | | *Lognormal* | | | | *Weibull* | | | | |
|---|---|---|---|---|---|---|---|---|---|---|---|---|---|---|
| | *n* | *Mean* $\mu$ | *StDev* $\sigma$ | *AD* | *p* | *Mean* $\xi$ | *StDev* $\delta$ | *AD* | *p* | *Shape* $k$ | *Scale* $m$ | *Location* $x_0$ | *AD* | *p* |
| $G_{LR}$ | 83 | 640.6 | 152.4 | 0.487* | 0.22 | 6.434 | 0.244 | 0.49 | 0.21 | 2.856 | 462.0 | 227.5 | 0.62 | 0.08 |
| $G_{LT}$ | 63 | 582.4 | 213.4 | 2.80 | <0.005 | 6.313 | 0.321 | 1.03 | 0.01 | 1.391 | 306.5 | 303.7 | 0.70* | 0.08 |
| $G_{RT}$ | 64 | 30.74 | 8.55 | 0.91 | 0.02 | 3.386 | 0.290 | 0.72 | 0.06 | 2.604 | 22.89 | 10.44 | 0.70* | 0.05 |
| $G_{RT}^{+}$ | 43 | 28.99 | 8.31 | 0.78 | 0.04 | 3.325 | 0.297 | 0.59 | 0.12 | 2.38 | 20.55 | 10.80 | 0.59* | 0.11 |
| $G_{RT}^{-}$ | 21 | 34.34 | 8.05 | 0.80 | 0.03 | 3.510 | 0.236 | 0.81 | 0.03 | 1.177 | 11.41 | 23.47 | 0.77* | 0.05 |

*) Lower AD-value

The lower AD values are marked with asterisks (*), indicating the distribution with best correspondence to the experimental values for each modulus. The Weibull distribution gives the lowest values for $G_{LT}$ and $G_{RT}$, and almost the same value as the normal distribution for $G_{LR}$. Based on the *p*-values, the Weibull distribution is acceptable for all moduli, while the normal distribution is acceptable only for $G_{LR}$. Histograms with adaptation to the Weibull distribution are given in Fig. 21 and Fig. 22 for the two longitudinally oriented shear moduli.

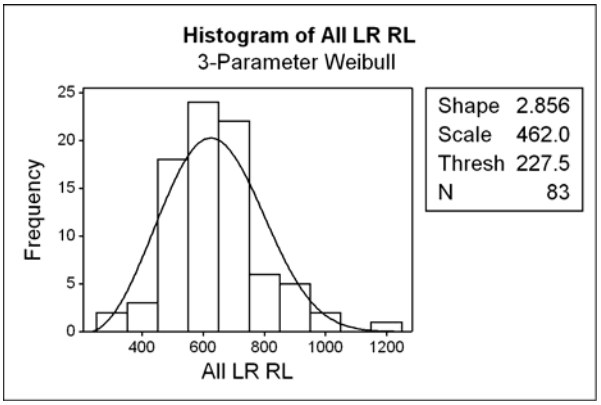


**Fig. 21** Shear modulus $G_{LR}$ (MPa)

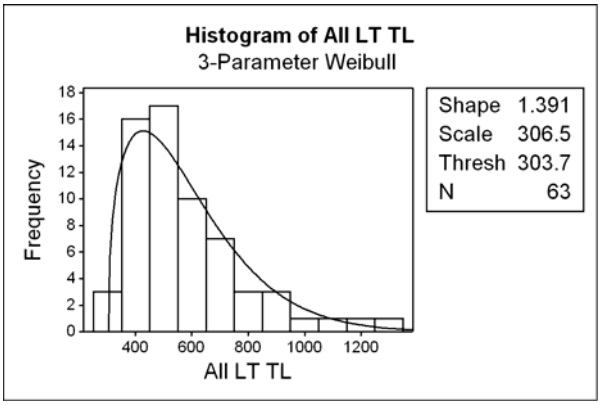


**Fig. 22** Shear modulus $G_{LT}$ (MPa)

## Concluding remarks

Design of structural applications of wood has traditionally been based on hand calculations. Numerical calculations, which to some extent have been used, have typically been focusing on the global behaviour and not on the detailed performance of e.g. connections. Consequently, the need for more accurate constitutive relationships suited for numerical implementation has been small. However, as the use of numerical methods is increasing within structural design of wood constructions, such knowledge is required on a more detailed level. The aim of this study has thus been to provide parameters characterizing the linear shear behaviour of Norway spruce for each of the three orthotropic planes. Nonlinear and failure characteristics will be treated in a later study.

Based on a rather thorough study of various shear tests used in the past for clear wood, it was concluded that the so-called Arcan specimen was the most promising, even if only three studies have been reported on this particular type of test. The resemblance to the somewhat more frequently used Iosipescu specimen, as well as the simplicity of the test setup, supported the choice of the Arcan test. A strong motivation was the ability to provide data for both the linear and nonlinear range, including failure parameters, and also the fact that the test configuration can be used for all three shear types in an orthotropic material.

The practical side of the testing worked well. Specimens were easy to produce, even if the deliberate correspondence between material and geometry axes required extra work and resulted in quite a few rejected specimens. By means of hot melt adhesives and clamps, the mounting to the brackets turned out to be both practical and efficient. The application of load worked well without hardly any occurrence of improper failure, even if some specimens broke during the first loading sequence. Deformation was measured by means of video extensometry, which eliminated physical contact with the specimen. A relatively large portion of the critical specimen section could thereby be measured for the three in-plane strain components, enabling a good basis for stiffness assessments. The values were evaluated by FEM simulations.

The average shear moduli were found to be $G_{LR} = 640$, $G_{LT} = 580$ and $G_{RT} = 30$ MPa. These values are somewhat lower than similar values reported in the literature, but the overall correspondence is quite good. The difference in average density between the two samples is low (390 vs. 398 kg/m$^3$) and cannot explain discrepancies. However, some deviations can be due to the fact that the literature values are not based on Norway spruce specifically, but spruce in general. The testing method can be another cause of differences. This is; however; hard to assess, since a statistical approach is hampered by the fact that the values reported in the literature are average values, whereas the experimental values are based on a set of free-standing tests.

Two different configurations *ij* were tested for each shear modulus. No significant difference could be found between corresponding samples *ij* and *ji* for any of the moduli. This agrees well with the findings for the *LR* plane for Sitka spruce by Yoshihara et al. (2001). Furthermore, it is interesting to note that the numerically based modification reduced the difference between the respective samples. These findings clearly support the assumption of the orthotropic theory that the same shear modulus $G_{ij}$ governs the shear deformation independent of *i* or *j* oriented driving shear load. Parameters determined by unloading resulted in higher values for all moduli compared to loading, but only $G_{RT}$ showed a significant difference. The correlation between density and the various moduli was found to be low, with a maximum determination coefficient $r^2$ of about 7% for $G_{RT}$. The coefficients of variation CV was found to equal 0.24 for $G_{LR}$, 0.28 for $G_{RT}$ and 0.37 for $G_{LT}$. The

difference in CV between corresponding *ij* and *ji* samples seems to be small. It should be noted that the variation may in fact be less than the stated CV values, since any unintended deviation between a specimen's material and geometric coordinate systems certainly contribute to variation. The CV corresponds well with results from Iosipescu tests on spruce, reporting CV values of 0.20 for $G_{LR}$ (Yoshihara et al. 2001) and 0.27 for $G_{RT}$ (Dumail et al. 2000).

The tests indicated that each of the three orthotropic shear moduli is significantly different. The $G_{LR}$ average was found to be approximately 10% higher than $G_{LT}$ and about 20 times the value of $G_{RT}$. The former difference corresponds quite well with a difference of 15% reported by Xavier et al. (2004) for maritime pine tested by the Iosipescu test; as opposed to a difference of about 1% in Fig. 16 for literature values.

A reasonably high number of specimens enabled a statistical quantification of the moduli values. It was found that the three-parameter Weibull distribution was most appropriate to fit the moduli, with nonsignificant *p*-values for all three types. JCSS (2006) states that the shear modulus of European softwood is lognormal distributed. According to the results presented herein, this is not statistically adequate for $G_{LT}$. On the other hand, $G_{LR}$ satisfies both the lognormal and particularly the normal distribution well.

## Appendix

The (3 parameter) Weibull probability density function *f* for *x* is given by

$$f\left(x,k,m,x_0\right)=\frac{k}{m}\cdot\left(\frac{x-x_0}{m}\right)^{k-1}\cdot e^{\left(-\left(\frac{x-x_0}{m}\right)^{k}\right)},\quad x\geq 0 \text{ and } f\left(x,k,m,x_0\right)=0,\quad x<0$$

The parameter $k$ (> 0) is the so-called shape parameter, $m$ (> 0) is the scale parameter and $x_0$ is the location parameter assigning the absolute lower limit of $x$.

The (2 parameter) lognormal probability density function *f* for *x* is given by

$$f\left(x,\xi,\delta\right)=\frac{1}{\sqrt{2\pi}\cdot x\cdot\partial}\cdot e^{\left(-\frac{1}{2}\left(\frac{\ln(x)-\xi}{\delta}\right)^{2}\right)},\quad x\geq 0 \text{ and } f\left(x,\xi,\delta\right)=0,\quad x<0$$

The parameter $\xi$ is the logarithmic mean value equal to the mean of ln($x$), and $\delta$ is logarithmic deviation equal to the standard deviation of ln($x$).

# References

Anderson T. W., Darling D. A. (1952) Asymptotic theory of certain "goodness-of-fit" criteria based on stochastic processes. Annals of Mathematical Statistics 23: 730-737.

Arcan M. (1984) The Iosipescu shear test as applied to composite materials. Experimental mechanics 24 (1): 66-67.

Arcan M., Hashin Z., Voloshin A. (1978) A method to produce uniform plane-stress states with application to fiber-reinforced materials. Experimental mechanics 18 (4): 141-146.

ASTM D143 (1984) Standard Methods of Testing Small Clear Specimens of Timber. American Society for Testing and Materials, p. 42.

ASTM D2718 (1995) Standard Test Method for Structural Panels in Planar Shear (Rolling Shear). American Society for Testing and Materials, p. 5.

ASTM D3044 (1986) Standard Test Method for Shear Modulus of Plywood. American Society for Testing and Materials, p. 3.

ASTM D5379 (1998) Standard Test Method for Shear Properties of Composite Materials by the V-Notched Beam Method. American Society for Testing and Materials, p. 13.

Bodig J., Goodman J. R. (1973) Prediction of elastic parameters for wood. Wood Science (5): 249-264.

Carrington H. (1923) The Elastic Constants of Spruce. Phil. Mag., London (45 (269)): 1055-1057.

Dahl K. B. (2008) Testing of Shear Properties of Spruce Softwood, Report R-14-08, Department of Structural engineering, Norwegian University of Science and Technology, Trondheim, Norway, p. 10.

Dahl K. B., Malo K. A. (2009) Planar strain measurements on wood specimens. Experimental mechanics 49: 575-586, (DOI 10.1007/s11340-008-9162-0).

Doyle D. V., Drow J. T., McBurney R. S. (1945) Elastic Properties of Wood. Report 1528 A+B, Report 1528, 1528-A, 1528-B, Forest Products Laboratory, Madison Wisconsin, p. 41+15+38.

Dumail J. F., Olofsson K., Salmén L. (2000) An Analysis of Rolling Shear of Spruce Wood by the Iosipescu Method. Holzforschung 54: 420-426.

FPL (1999) Wood Handbook. Wood as an Engineering Material. Gen. Tech. Rep. FPL-GTR-113, United States Department of Agriculture, Forest Products Laboratory, p. 463.

Goodman J. R., Bodig J. (1970) Orthotropic Elastic Properties of Wood. Journal of the Structural Division, Proceedings of the American Society of Civil Engineering ASCE 1 (1): 2301-2319.

JCSS (2006) Probabilistic Model Code. Part III - Resistance Models. Ch. 3.5 Properties of Timber, Joint Committee on Structural Safety, p. 16.

Jenkin C. F. (1920) Report on Materials Used in the Construction of Aircraft and Aircraft Engines, Report H.M. Stationery Office, London, p. 95-131.

Kollmann F. P., Côté W. A. (1968) Principles of Wood Science and Technology - Solid Wood (1st ed.), Springer Verlag, Berlin, p. 592.

Kubojima Y. (1997) Accuracy of the Shear Modulus of Wood Obtained by Timoshenko's Theory of Bending. Mokuzai Gakkaishi 43 (5): 439-443.

Liu J. Y. (1984) New Shear Strength Test for Solid Wood. Wood and Fiber Science 16 (4): 567-574.

Liu J. Y. (2000) Effects of shear coupling on shear properties of wood. Wood and Fiber Science 32 (4): 458-465.

Liu J. Y. (2002) Analysis of Off-Axis Tension Test of Wood Specimens. Wood and Fiber Science 34 (2): 205-211.

Liu J. Y., Flach D. D., Ross R. J., Lichtenberg G. J. (1999) An improved Shear Test Fixture using the Iosipescu Specimen. Mechanics of Cellulosic Materials 231/85: 139-147.

Liu J. Y., Floeter L. H. (1984) Shear strength in principal plane of wood. Journal of Engineering Mechanics 110 (6): 930-936.

Liu J. Y., Ross R. J. (1998) Wood property variation with grain slope. 12th Engineering Mechanics Conference, May 17-20, 1998, American Society of Civil Engineers, La Jolla, CA, USA.

Liu J. Y., Ross R. J., Rammer D. R. (1996) Improved Arcan Shear Test for Wood. International Wood Engineering Conference, October 28-31, 1996, New Orleans, LA, USA.

Minitab (2006). Minitab v.15 Help, Minitab Inc. Statistical Software, State College, Pennsylvania.

Moses D. (2001) The Notched Shear Block revisited. Research Highlights (2).

NS-EN 384 (2004) Structural timber - Determination of characteristic values of mechanical properties and density. European Committee for Standardization, p. 15.

NS-EN 408 (2003) Timber Structures - Structural timber and glued laminated timber. Determination of some physical and mechanical properties. European Committee for Standardization (2nd ed.), p. 27.

NS 3470 (1999) Norsk Standard. Design of timber structures. Design rules. Part 1: Common rules. Norges Standardiseringsforbund (5th ed.), p. 82.

Oliveira J. M. Q. (2004) Characterization of the shear behaviour of wood using the Arcan test (in Portugese). Universidade de Trás-os-Montes e Alto Douro. Master thesis, p. 164.
Pierron F. (1998) Saint-Venant Effects in the Iosipescu Specimen. Journal of Composite Materials 32 (22): 1986-2015.
Pierron F., Vautrin A. (1994) Accurate comparative Determination of the In-plane Shear Modulus of T300/914 by the Iosipescu and 45 Degree Off-axis Tests. Composites Science and Technology 52: 61-72.
SKOGFORSK (1992) Skandinaviske normer for testing av små feilfrie prøver av heltre, SKANORM, Dept. of Forestry, Agricultural University of Norway, p. 104.
Sliker A., Yu Y. (1993) Elastic constants for hardwoods measured from plate and tension tests. Wood and Fiber Science (25(1)): 8-22.
Stamer J. (1935) Elastizitätsuntersuchungen an Hölzern. Ingenieur-Archiv (6): 1-8.
Xavier J. C., Garrido N. M., Oliveira M., Morais J. L., Camanho P. P., Pierron F. (2004) A comparison between the Iosipescu and off-axis shear test methods for the characterization of Pinus Pinaster Ait. Composites: Part A 35: 827-840.
Yamasaki M., Sasaki Y. (2003) Elastic properties of wood with rectangular cross section under combined static axial force and torque. Journal of Materials Science 38: 603-612.
Yoshihara H., Furushima T. (2003) Shear strengths of wood measured by various short beam shear test methods. Wood Science and Technology 37: 189-197.
Yoshihara H., Kubojima Y. (2002) Measurement of the shear modulus of wood by asymmetric four-point bending tests. Journal of Wood Science 48: 14-19.
Yoshihara H., Matsumoto A. (2005) Measurement of the shearing properties of wood by in-plane shear test using a thin specimen. Wood Science and Technology 39: 141-153.
Yoshihara H., Ohhata O. (2003) Method of Measuring the Shear Strength of Wood by the Asymmetric Four-Point Bending Test using a Notched Beam Specimen. Journal of Testing and Evaluation 31 (4): 352-356.
Yoshihara H., Ohsaki H., Kubojima Y., Ohta M. (1999) Applicability of the Iosipescu shear test on the measurement of the shear properties of wood. Journal of Wood Science 45: 24-29.
Yoshihara H., Ohsaki H., Kubojima Y., Ohta M. (2001) Comparisons of Shear Stress/Shear Strain Relations of Wood obtained by Iosipescu and Torsion Tests. Wood and Fiber Science 33 (2): 275-283.
Yoshihara H., Ohta M. (1995a) Determination of the Shear Stress-Shear Strain Relationship of Wood by Torsion Tests. Mokuzai Gakkaishi 41 (11): 988-993.
Yoshihara H., Ohta M. (1995b) Shear Stress-Shear Strain Relationship of Wood in the Plastic Region. Mokuzai Gakkaishi 41 (6): 529-536.
Yoshihara H., Ohta M. (1996) Analysis of the Yield Behavior of Wood under Combined Shear Stresses in Torsion Tests. Mokuzai Gakkaishi 42 (6): 541-545.
Yoshihara H., Ohta M. (2000) Estimation of the shear strength of wood by uniaxial-tension tests of off-axis specimens. Journal of Wood Science 46: 159-163.
Yoshihara H., Satoh T. (2003) Examination of the off-axis tension test method for evaluating the shear properties of wood. Forest Products Journal 53 (5): 75-79.

# PAPER III

## Nonlinear Shear Properties of Spruce Softwood: Experimental Results

**K. B. DAHL[1], K. A. MALO[2]**

*Wood Science and Technology (2009) 43 (7): 539-558*

**Abstract**
Shear properties of clear softwood from Norway spruce were investigated by means of the Arcan shear test. The test enabled fairly detailed measurements of pure shear until failure in each of the three orthotropic shear planes, where video extensometry was used for strain measurements. A total number of 85 specimens were tested in 6 different configurations. A varying degree of nonlinearity was observed between the different configurations and material planes, especially for rolling shear. The stress–strain curves were adapted with linear, bilinear and Voce models. Compared to the linearized variant, it was found that the bilinear model generally increases the model accuracy by a factor of approximately two, whereas the Voce model shows even higher accuracy, although its adaptive robustness is somewhat lower. The parameters demonstrated low correlations with density, whereas the correlations with the initial shear moduli in many cases were considerably higher and significant. The correspondence with similar values reported in literature was found to be fairly good.

**Keywords** – Norway spruce, Orthotropy, Arcan shear test, Nonlinear behaviour

[1] Ph.D-student, Dept. of Structural Engineering, Norwegian University of Science and Technology NTNU, M.Sc. Structural and Civil Engineer, Multiconsult AS, Boks 265 Skøyen, N-0213 Oslo, Norway.
[2] Professor, Dept. of Structural Engineering, Norwegian University of Science and Technology NTNU

## Introduction

Wood is normally assumed to behave linearly in shear, followed by brittle failure. This is an assumption which partly stems from standardized shear tests, which are less appropriate for assessing the shear behaviour near ultimate capacity. Moreover, the difficulty in measuring pure shear has probably contributed to the assumption of a linear elastic material model, for lack of more detailed knowledge. This idealization has proved to be sufficient for the conventional design of wooden constructions, where the design is mainly based on hand calculation procedures. However, for design based on numerical methods, a more thorough characterization of the shear behaviour is required. In order to enable applicable three-dimensional models, the characterization must naturally comprise the three principal material planes *LR*, *LT* and *RT* of wood, as well as possible non-linear shear behaviour and interaction between shear and normal stress components in failure. Such knowledge can only be achieved by means of experimental shear testing, of which several procedures are standardized for wood. It is crucial that test configuration effects like stress concentrations and other governing failure modes than pure shear are taken into consideration. Any results from numerical simulation based on crude experimental values can otherwise be severely corrupted. As an example, Ukyo and Masuda (2006) showed that the apparent shear strength of the frequently used ASTM D143 (1984) shear block test should be modified upwards, and that the assumed linear stress–strain relationship for shear in reality is nonlinear. Another standardized test is the plate twist test described by ASTM D3044 (1986). While the notched block can be used both for strength and stiffness evaluations, the plate twist test is mainly suited for measuring linear behaviour, and can hardly be used for assessment of ultimate shear capacities. This is also the case for methods based on short beam bending tests. NS-EN 384 (2004) states that the shear strength can be tested by displacing one steel plate relative to another with a wood specimen glued in-between, but so far it seems like the test has received limited use.

It may be commented that none of the standardized methods seem particularly suited for producing a pure and uniform state of shear, which is required for a more detailed assessment of shear properties. Neither do they reflect the whole loading range; nor the rolling shear behaviour. It is moreover desirable that the normal stresses do not exceed their linear stress limits throughout loading, since any assessment of nonlinear shear otherwise requires that the nonlinearity of the normal stress components are known. The capability of testing a combination of shear and normal stress components in a uniform stress field is furthermore a desirable quality for evaluation of failure interaction effects. None of the aforementioned standardized methods seem to meet these demands in a sufficient way.

Several non-standardized shear tests used for wood is examined by Dahl and Malo (2009a), including the off-axis tensile test, torsion tests, and the Iosipescu and Arcan shear tests. In particular, several interesting studies have emerged from torsion studies, i.a. by Yamasaki and Sasaki (2003, 2004) who documented linear and nonlinear properties including failure of different wood species. Shear proportional limits/yield values as low as 40% of the ultimate shear stresses were found. Combinations of axial and torsional loading proved that the Hill criterion and in particular the Tsai-Wu criterion were in good agreement with both yield and failure data. Similar results have also been presented by Yoshihara and Ohta (1995a, b, 1996) and Yoshihara et al. (1997), although numerical simulations indicated that the real yield values were 20–30% lower than the apparent values observed. Moreover, it should be noted that the underlying theory for obtaining

orthotropic shear characteristics by means of torsion is quite complex, and that nonuniform strain fields and the presence of normal stress components complicate the assessments.

The Iosipescu shear test, consisting of a notched beam loaded so that the bending moment over the notch is zero, has been applied to clear wood in several studies. Even if this results in adequate shear moduli, it seems like the failure shear stresses can be somewhat encumbered by improper failure due to bending moment beside the critical section. In particular radially and tangentially oriented specimens are vulnerable due to low tensile capacities in these directions. It is interesting to note that Yoshihara et al. (1999, 2001) and Yoshihara and Matsumoto (2005) found yield and failure values approximately 30% lower than the apparent values obtained by torsion, corresponding well with numerical results for the torsion test.

The much resembling Arcan test has also been applied to clear wood in some studies. Its shear moduli are reported to correspond well with the notched shear block, although somewhat lower shear strengths were found. Liu and Ross (1998) asserted it to be the most reliable shear test for wood. Oliveira (2004) tested shear strength and stiffness by the Arcan method in each of the three orthotropic material planes of pine, and found reasonable results. Yoshihara and Matsumoto (2005) used a slightly modified version, and found good accordance with results from the Iosipescu test. The Arcan test is consequently regarded to be the most suited test for a general study of the shear properties of wood, comprising all material planes and the complete loading ranges. The simplicity of the test setup, and the relatively pure and uniform shear stress and strain situation is particularly appealing. Improper failure reported for the Iosipescu specimen can moreover be avoided by means of test bracket design. The test was consequently used by Dahl and Malo (2009a), wherein linear shear properties are treated, whilst the nonlinear and failure properties are reported herein.

## Materials and methods

Arcan specimens were made of Norway Spruce (*Picea Abies* (L.) Karst.) taken from eight different trees collected at four different locations in Norway, with log diameters as large as possible to obtain material with a minimum of annual ring curvature. The material was conditioned to approximately 12% moisture content and 20˚C, with densities ranging between 300 and 500 kg/m$^3$ with an average of 398 kg/m$^3$ and a coefficient of variation (CV) of 9%. The specimen geometry is shown in Fig. 1.

Six different specimen types were produced, each designated by *ij* where $i \neq j$ and $\{i, j\} = \{L, R, T\}$, see Fig. 2. The first index *i* assigns the direction of the component load *P* relative to the material orientation, while the second index *j* equals the direction of the normal vector of the loaded plane. Specimen type *ij* corresponds thus to testing of $\sigma_{ij} - \gamma_{ij}$ shear. Six configurations were chosen instead of three in order to investigate if *i* or *j* oriented load *P* possibly could affect the *ij* shear properties. The specimens were cut from the outer part of the stems in order to obtain specimens with a Cartesian material axis system coinciding with the geometry axis. Any fibre inclination to load orientation was thus tentatively avoided. Inhomogeneities and macroscopic defects such as knots and resin pockets were kept at a minimum.

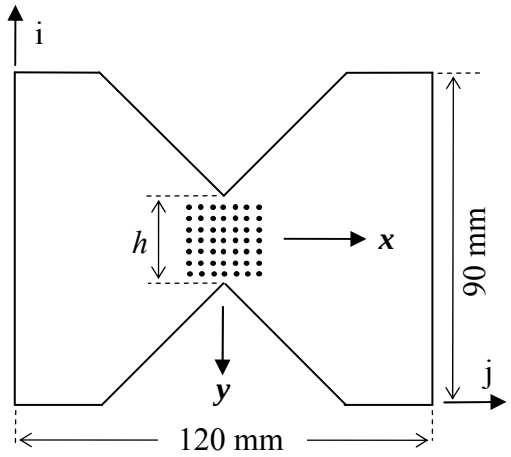


**Fig. 1** Specimen *ij* with dots and local axes *xy* for strain measurements (Dahl and Malo 2009a)

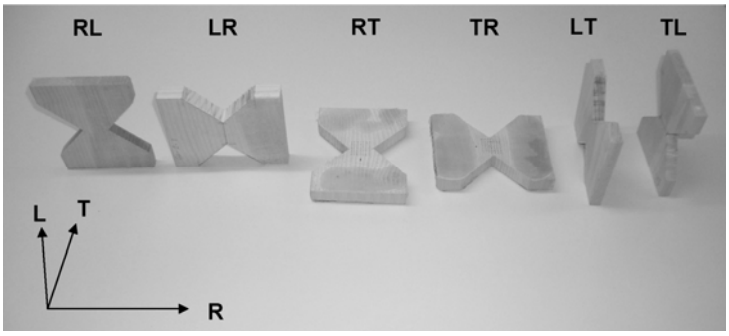


**Fig. 2** Shear specimen types *ij* oriented with principal material axes (Dahl and Malo 2009a)

In order to account for different shear strengths of the three material planes, different cross section thickness $t$ and height $h$ were used for the various specimen categories. Between 20 and 30 specimens were manufactured for each plane, and a total number of 85 specimens were tested. Compared to the original Arcan test, a somewhat modified fixture was used, consisting of L-shaped aluminium brackets glued to the specimen with hot melt adhesives and strengthened with clamps. The brackets were provided with a hole for pin loading. A loading rate of 0.3 mm/min was chosen for all tests, resulting in maximum capacities typically reached between 200 and 400 s. The tests were run in an acclimatized atmosphere of 20˚C and 65% relative humidity. For more details see Dahl and Malo (2009a).

Deformation was measured by means of video extensometry technique described by Dahl and Malo (2009b). A grid of target dots was prior to the test applied on the wood surfaces at the critical section as Fig. 1 illustrates, and in-plane $xy$ coordinates were continuously measured by the camera throughout loading until failure. A post processing routine calculated normal and shear strain based on the coordinate values, where the dots were interpreted as the nodes of an array of 36 quadratic elements, and a FEM formulation was utilized for the strain calculation. Estimates of the three in-plane strain components $\varepsilon_{ii}$, $\varepsilon_{jj}$ and $\gamma_{ij}$ averaged over the measurement area could thus be held together with the contemporary nominal shear stress estimate $\hat{\sigma}_{ij}$ for evaluation of the overall experimental material behaviour. Each specimen was exposed to loading till 40% of assumed component capacity, followed by unloading and finally reloading until failure. The latter sequence, comprising nonlinearity and failure, is reported herein.

The nominal shear stress $\hat{\sigma}_{ij}$ was estimated for each experimental timestep by

$$\hat{\sigma}_{ij} = \frac{P}{A_0} \cong \frac{P}{(h \cdot t)} \tag{1}$$

where $h$ and $t$ are the measured cross section dimensions at the initial configuration and $P$ is the load level. The nominal stress estimate implies a uniform distribution over the cross section, and is estimated analogously as for the resembling Iosipescu test by Yoshihara et al. (1999) and Dumail et al. (2000).

Experimental stress–strain curves for the various configurations are shown in Fig. 3. It can be seen that several configurations exhibit nonlinearities. Moreover, the initial stiffness as well as the nonlinear behaviour and ultimate stresses vary considerably between the three different shear types *ij*, and also between specimens of the same test type. It should be emphasized that the stress–strain curves reflect nominal stress data versus averaged strain over the measurement area, and thus represent apparent values, which implies that the real material behaviour not necessarily corresponds exactly with the indicated progress. The curves must therefore be assessed as apparent behaviour possibly influenced by configuration effects.

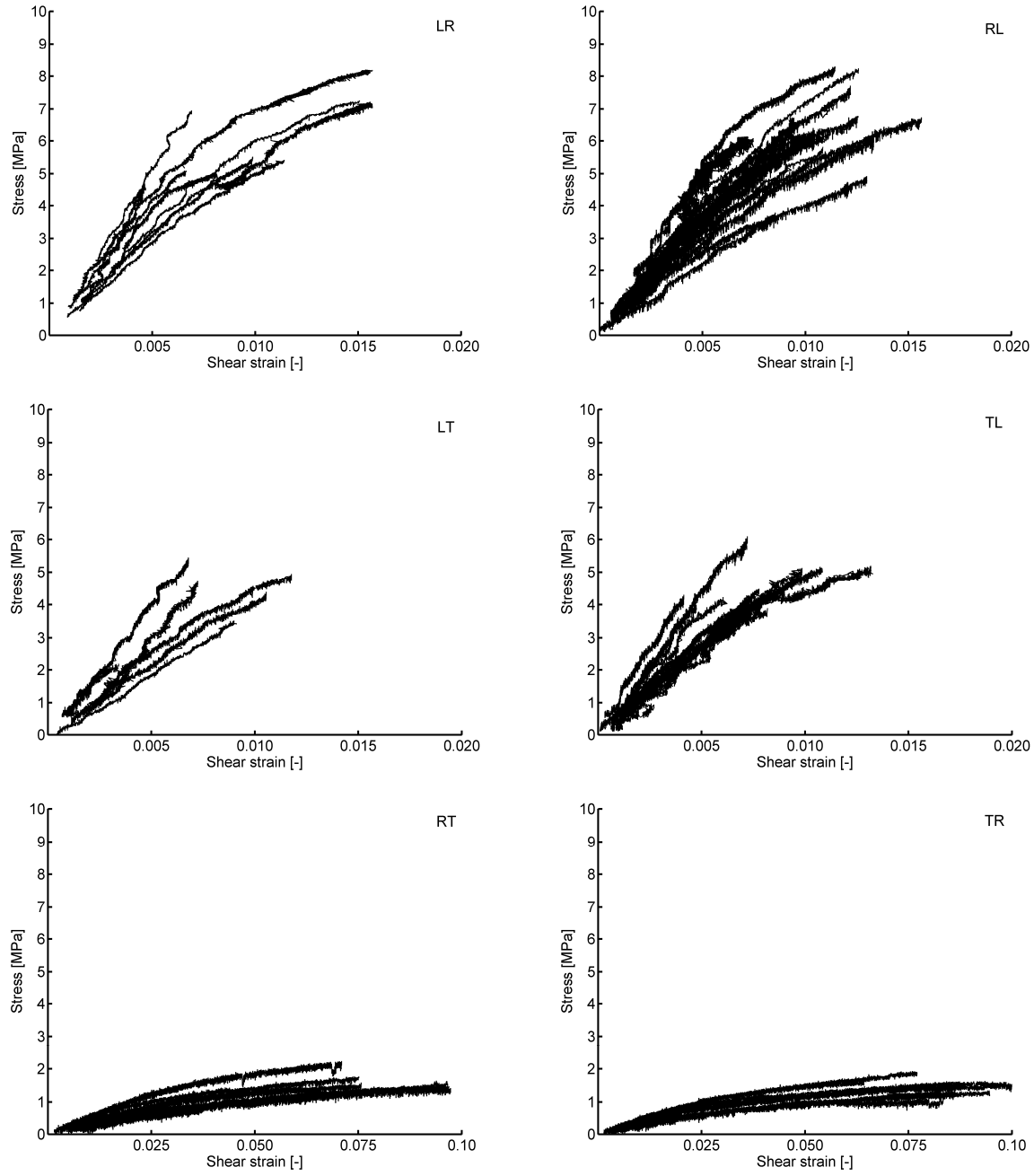


**Fig. 3** Experimental shear stress–strain curves for the various configuration types *ij* (Dahl and Malo 2009a)

## Linear and nonlinear material models

Estimates $\hat{G}_{ij}$ for the three linear elastic shear moduli were reported in Dahl and Malo (2009a). The determination was based on a least sum square error method of the experimental stress–strain curves confined to maximum 40% of the ultimate capacities. The estimates $\hat{G}_{ij}$ were subsequently modified by means of finite element calculations in order to obtain improved values for $G_{ij}$ independent of configuration effects. The available $\hat{G}_{ij}$ values are used in the subsequent treatment herein to secure consistency between the linear and the nonlinear regimes.

In order to characterize the nonlinear behaviour, the bilinear and the Voce models were chosen for the nonlinear range. While the former has a linear progress after the linear elastic stress limit, the latter increases with a descending exponential progress. In addition, a completely linearized model over the whole stress range was investigated.

## Bilinear model

Given that the stress level $\sigma_{ij}$ has reached some level above the linear limit stress $\sigma_{ij}^{\text{lin}}$, the elastic and plastic strain increments $d\gamma_{ij}^{\text{e}}$ and $d\gamma_{ij}^{\text{p}}$, respectively, can be related to the stress increment $d\sigma_{ij}$ by the shear modulus $G_{ij}$ and the tangent shear modulus $G_{ij}^{\text{T}}$; or the plastic modulus $G_{ij}^{\text{P}}$; as illustrated in Fig. 4 (not sum over indices), where

$$d\gamma_{ij} = d\gamma_{ij}^{\text{e}} + d\gamma_{ij}^{\text{p}} \quad \Rightarrow \quad \frac{d\sigma_{ij}}{G_{ij}^{\text{T}}} = \frac{d\sigma_{ij}}{G_{ij}} + \frac{d\sigma_{ij}}{G_{ij}^{\text{P}}} \quad \Rightarrow \quad \frac{1}{G_{ij}^{\text{T}}} = \frac{1}{G_{ij}} + \frac{1}{G_{ij}^{\text{P}}} \tag{2}$$

By rearranging, an explicit expression for the plastic modulus $G_{ij}^{\text{P}}$ appears as

$$G_{ij}^{\text{P}} = \frac{G_{ij}^{\text{T}} \cdot G_{ij}}{G_{ij} - G_{ij}^{\text{T}}} \tag{3}$$

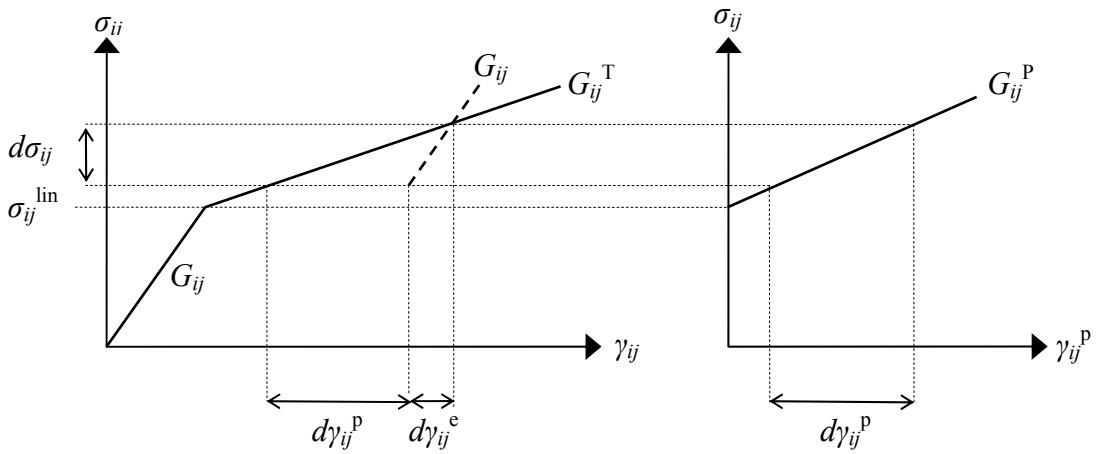


**Fig. 4** Bilinear shear stress–strain relationship for configuration and shear type *ij*

With $\{i,j\} = \{L, R, T\}$ for $i \neq j$, the three orthotropic shear stresses can be expressed by

$$\sigma_{ij} = \begin{bmatrix} G_{ij} \cdot \gamma_{ij} & for \quad \left|\gamma_{ij}\right| < \gamma_{ij}^{\text{lin}} \\ \sigma_{ij}^{\text{lin}} + G_{ij}^{\text{T}} \cdot \left(\gamma_{ij} - \gamma_{ij}^{\text{lin}}\right) = \sigma_{ij}^{\text{lin}} + G_{ij}^{\text{P}} \cdot \left(\gamma_{ij}^{\text{p}}\right) & for \quad \left|\gamma_{ij}\right| > \gamma_{ij}^{\text{lin}} \end{bmatrix} \tag{4}$$

where

$$\gamma_{ij}^{\text{lin}} = \frac{\sigma_{ij}^{\text{lin}}}{G_{ij}} \qquad \text{and} \qquad \gamma_{ij}^{\text{p}} = \gamma_{ij} - \left(\frac{\sigma_{ij}}{G_{ij}}\right) \tag{5}$$

## Voce model

The Voce model is formulated exponentially by the plastic strain:

$$\sigma_{ij} = \begin{bmatrix} G_{ij} \cdot \gamma_{ij} & for \quad \left|\gamma_{ij}\right| < \gamma_{ij}^{\text{lin}} \\ \sigma_{ij}^{\text{lin}} + R_{ij} \cdot \left(1 - e^{\left(-H_{ij} \cdot \gamma_{ij}^{p}\right)}\right) & for \quad \left|\gamma_{ij}\right| > \gamma_{ij}^{\text{lin}} \end{bmatrix} \tag{6}$$

where $i, j$, $\gamma_{ij}^{\text{p}}$ and $\gamma_{ij}^{\text{lin}}$ are as denoted for the bilinear model; and $\sigma_{ij}^{\text{lin}}$, $R_{ij}$ and $H_{ij}$ are material parameters referring to material plane $ij$, see Fig. 5.

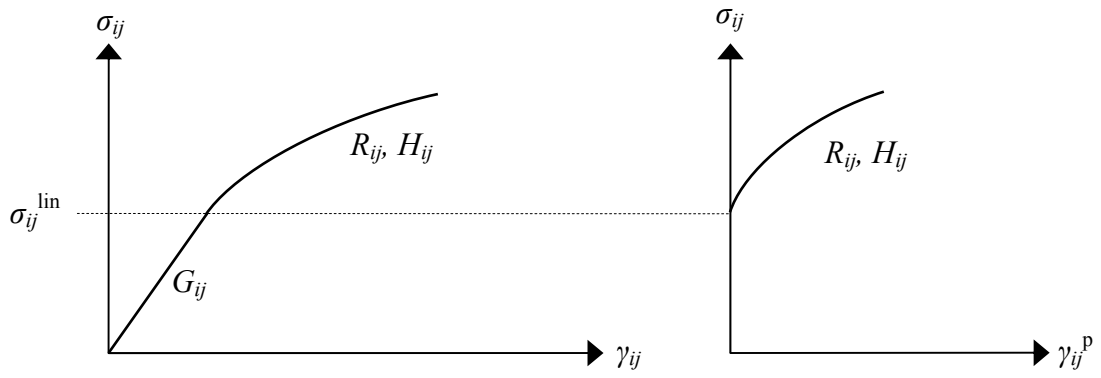


**Fig. 5** Voce shear stress–strain relationship for configuration and shear type $ij$

## Parameter determination

The bilinear and Voce material parameters were determined by a SSE minimization for each specimen, writing

$$SSE = \sum_{t=1}^{k} \left[\hat{\sigma}_{ij-t} - \sigma_{ij-t}^{\text{mod}}\right]^2 \tag{7}$$

where $\sigma_{ij-t}^{\mathrm{mod}}$ was calculated for each experimental timestep according to Eqs. (4) and (6) for the bilinear and Voce models, respectively, wherein the specimen specific $\hat{G}_{ij}$ values reported in Dahl and Malo (2009a) were utilized. The experimental average shear strain modified for strain paths deviating from the origin by coefficients $A_g$ was used, writing

$$\overline{\gamma}_{ij-t} = \overline{\gamma}'_{ij-t} + \left( \frac{A_g}{\hat{G}_{ij}} \right), \qquad \overline{\gamma}^{\mathrm{p}}_{ij-t} = \overline{\gamma}'_{ij-t} - \left( \frac{\hat{\sigma}_{ij-t}}{\hat{G}_{ij}} \right) \tag{8}$$

A subset consisting of $k$ timesteps was analysed, upwards limited by the ultimate load, whereas steps in the lower range showing initial disturbances were removed. Typically, $k$ contained between 2000 and 5000 steps. It can be noted that the linear part was included to enable flexibility of the $A_g$ coefficient values, and required adaptation on a total strain basis. This was deliberately done to account for possible shifted linear parts above the 40% limit confining the linear parameter determination range. Different values of $A_g$ and linear limit stresses $\hat{\sigma}_{ij}^{\mathrm{lin}}$ were allowed for the Voce and the bilinear models, although the $A_g$ values turned out to be quite similar between the models. The nonlinear parameter values were restricted as stated in Table 1, and no values were pursued in cases where fulfilment of the constraints led to unfeasible results.

**Table 1** Restrictions in determination of nonlinear shear material parameters

| Model | Parameters | | Restriction |
|---|---|---|---|
| Bilinear | $\hat{\sigma}_{ij}^{\mathrm{lin}}$ | Linear limit stress | $\hat{\sigma}_{ij}^{\mathrm{lin}} < \hat{\sigma}_{ij}^{\mathrm{ult}}$ |
| | $\hat{G}_{ij}^{T}$ | Tangent shear modulus | $0 < \hat{G}_{ij}^{T} < \hat{G}_{ij}$ |
| | $A_g$ | Initial stress offset | $A_g < \hat{\sigma}_{ij}^{\mathrm{lin}}$ |
| Voce | $\hat{\sigma}_{ij}^{\mathrm{lin}}$ | Linear limit stress | $\hat{\sigma}_{ij}^{\mathrm{lin}} < \hat{\sigma}_{ij}^{\mathrm{ult}}$ |
| | $\hat{H}_{ij}$ | Plastic exponent | $\hat{H}_{ij} > 0$ |
| | $\hat{R}_{ij}$ | Plastic multiplier | $\hat{R}_{ij} > 0$ |
| | $A_g$ | Initial stress offset | $A_g < \hat{\sigma}_{ij}^{\mathrm{lin}}$ |

The relationships resulting from the determined parameters were automatically plotted together with the experimental data, as visualized in Fig. 6, allowing an efficient reasonability check of parameters. Note that both total strain and plastic shear strain are shown.

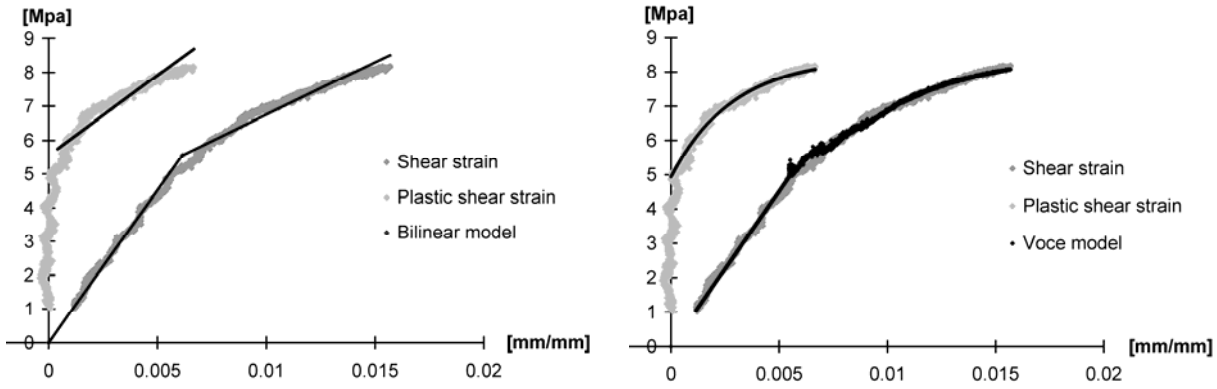


**Fig. 6** Bilinear (left) and Voce adaptation of experimental shear stress–strain curve ($ij = LR$)

Since many specimens followed an almost pure linear behaviour, it was moreover relevant to adapt the whole stress–strain progress by means of a completely linear model, as indicated in Fig. 7. This was in particular pertinent for the very linear *LT* and *TL* configurations; as opposed to the rolling shear *RT* and *TR*, which clearly show nonlinear behaviour for all specimens, see Fig. 3.

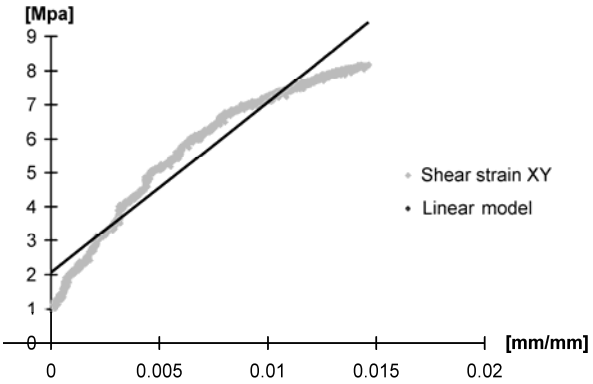


**Fig. 7** Linearized adaptation $G_{ij}^{\mathrm{LIN}}$ of the complete experimental shear stress–strain curve ($ij = LR$)

## Results

Average parameter values, coefficients of variation (CV) and correlations with density $r(\rho)$ are tabulated for all configuration types *ij* in Table 2. The number of values each estimate is based on *n* is moreover included to give an indication of the respective models suitability. Estimates of the plastic moduli $\hat{G}_{ij}^{\mathrm{P}}$ and the linear strain limits $\hat{\gamma}_{ij}^{\mathrm{lin}}$ are not included since they explicitly are given by Eqs. (3) and (5), respectively. The ultimate stress $\hat{\sigma}_{ij}^{\mathrm{ult}}$ and the corresponding ultimate strain $\hat{\gamma}_{ij}^{\mathrm{ult}}$ observed are stated as the determined interrelation is less evident, and both can be used for restricting the elastoplastic domain, i.e. in an enveloping surface for failure prediction. The initial stress offset $A_g$ from the bilinear model is used for the determination of $\hat{\gamma}_{ij}^{\mathrm{ult}}$. It should be emphasized that the tabulated parameters are apparent estimates based on averaged strains and nominal stresses, and that the suitability judgements to some extent were subjective, as rejection was done manually. Results for each specimen are to be found in Dahl (2008).

**Table 2** Shear parameter estimates for each configuration *ij*

| Type *ij* | | Density (kg/m³) | Linear | | Bilinear | | Voce | | | $\hat{\sigma}_{ij}^{\mathrm{ult}}$ | $\hat{\gamma}_{ij}^{\mathrm{ult}}$ |
|---|---|---|---|---|---|---|---|---|---|---|---|
| | | | $\hat{G}_{ij}$ | $\hat{G}_{ij}^{\mathrm{LIN}}$ | $\hat{\sigma}_{ij}^{\mathrm{lin}}$ | $\hat{G}_{ij}^{\mathrm{T}}$ | $\hat{\sigma}_{ij}^{\mathrm{lin}}$ | $\hat{R}_{ij}$ | $\hat{H}_{ij}$ | | |
| *LR* | Mean | 388 | 754 | 614 | 4.08 | 406 | 4.33 | 2.50 | 794 | 6.06 | 0.0120 |
| | CV | 0.05 | 0.30 | 0.42 | 0.29 | 0.28 | 0.15 | 0.28 | 0.36 | 0.25 | 0.33 |
| | r(ρ) | - | 0.03 | 0.00 | 0.11 | 0.40 | 0.05 | 0.20 | -0.28 | 0.33 | -0.05 |
| | n | 12 | 12 | 12 | 10 | 10 | 8 | 8 | 8 | 12 | 10 |
| *RL* | Mean | 400 | 734 | 604 | 4.26 | 434 | 4.09 | 2.59 | 749 | 6.12 | 0.0106 |
| | CV | 0.10 | 0.20 | 0.23 | 0.27 | 0.21 | 0.27 | 0.42 | 0.39 | 0.20 | 0.24 |
| | r(ρ) | - | 0.37 | 0.44 | 0.39 | -0.07 | 0.22 | -0.34 | 0.05 | 0.20 | -0.06 |
| | n | 23 | 20 | 21 | 19 | 19 | 16 | 16 | 16 | 23 | 19 |
| *LT* | Mean | 409 | 586 | 580 | 2.85 | 336 | 2.95 | 1.42 | 500 | 4.17 | 0.0086 |
| | CV | 0.06 | 0.27 | 0.31 | 0.42 | 0.30 | 0.37 | 0.31 | 0.00 | 0.24 | 0.53 |
| | r(ρ) | - | 0.30 | -0.03 | -0.52 | 0.43 | -0.46 | -0.99 | -1.00 | -0.50 | -0.61 |
| | n | 12 | 7 | 8 | 3 | 3 | 3 | 3 | 3 | 11 | 3 |
| *TL* | Mean | 415 | 657 | 607 | 3.09 | 469 | 3.75 | 2.10 | 484 | 4.54 | 0.0081 |
| | CV | 0.07 | 0.27 | 0.30 | 0.30 | 0.36 | 0.07 | 0.53 | 0.07 | 0.19 | 0.30 |
| | r(ρ) | - | 0.17 | 0.15 | -0.05 | 0.10 | 0.70 | 0.13 | -0.48 | -0.05 | -0.13 |
| | n | 15 | 15 | 15 | 13 | 13 | 5 | 5 | 5 | 15 | 13 |
| *RT* | Mean | 381 | 32.0 | 19.0 | 0.93 | 12.4 | 1.00 | 0.83 | 37 | 1.65 | 0.092 |
| | CV | 0.10 | 0.31 | 0.33 | 0.27 | 0.31 | 0.16 | 0.38 | 0.53 | 0.28 | 0.51 |
| | r(ρ) | - | 0.17 | 0.02 | 0.07 | 0.37 | 0.09 | 0.41 | -0.15 | 0.31 | 0.13 |
| | n | 10 | 10 | 10 | 10 | 10 | 8 | 8 | 8 | 10 | 10 |
| *TR* | Mean | 381 | 36.7 | 17.0 | 0.93 | 11.0 | 0.88 | 1.01 | 33 | 1.64 | 0.091 |
| | CV | 0.11 | 0.26 | 0.31 | 0.13 | 0.49 | 0.15 | 0.40 | 0.73 | 0.23 | 0.29 |
| | r(ρ) | - | 0.16 | 0.24 | 0.14 | 0.34 | 0.29 | 0.02 | 0.26 | 0.22 | -0.04 |
| | n | 12 | 12 | 12 | 12 | 12 | 11 | 11 | 11 | 12 | 12 |

$G_{ij}$, $\sigma_{ij}$ and $R_{ij}$ are given in MPa

The ultimate load $P^{ult}$ was followed by an immediate loss in component capacity. For the *LR*, *LT*, *RT* and about 60% of the *TR* configurations, the material separated completely by a vertical failure

at the critical section, and the capacity consequently dropped to zero. The cracks propagated very fast, and could not be perceived with the human eye. It was thus hard to assess where the crack was initiated along the critical section. The remaining *TR* specimens, in addition to *RL* and *TL* configurations, failed with a horizontal crack initiated at the notch root and propagating towards the loading brackets, which prevented further opening. Due to this and redistribution of stresses, the component capacity did not drop to zero, although the loss was considerable for all three types. For an idealized specimen not benefiting from the reinforcing effect of the brackets, a completely brittle failure would probably have been observed.

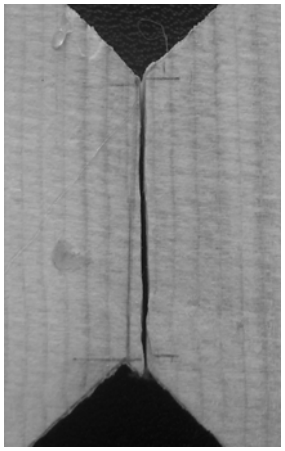

**Fig. 8** Typical failure for *LR* (left) and *RL* specimens

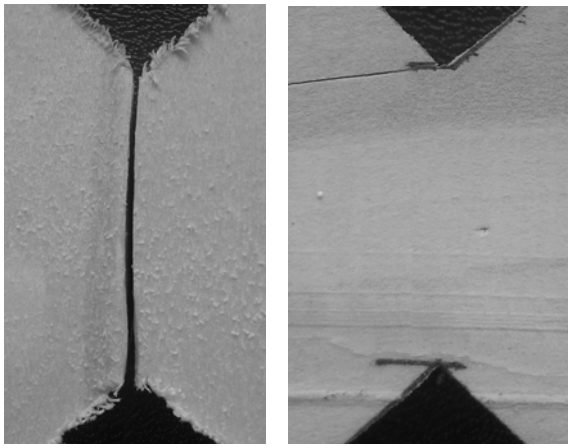

**Fig. 9** Typical failure for *LT* (left) and *TL* specimens

Typical failures for each of the four configuration types comprising the longitudinal direction (*L*) are shown in Fig. 8 and Fig. 9. It is noteworthy that the resembling configurations *LR* and *LT* both fail vertically, and correspondingly horizontally for *RL* and *TL*. Typical failures of the rolling shear configurations are shown in Fig. 10, where a characteristic *TR* specimen possessed by both failure types is depicted.

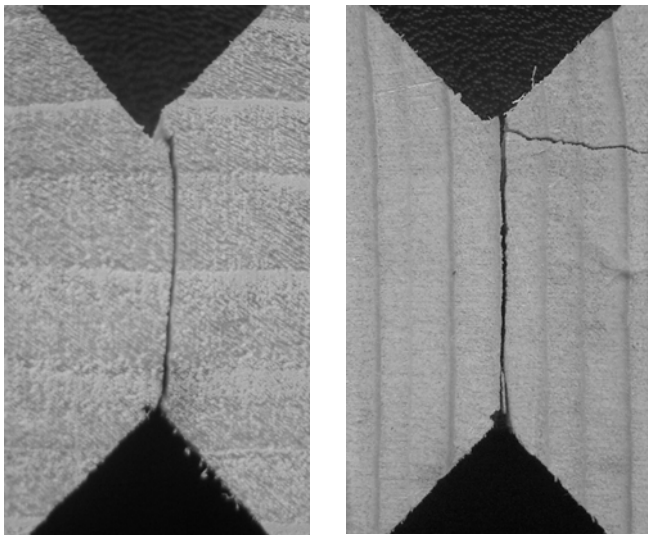

**Fig. 10** Typical failure for *RT* (left) and *TR* specimens

It is interesting to note that Xavier et al. (2004) reported exactly the same failure modes for *LR* and *TL* specimens of pine tested by the resembling Iosipescu test. For the *TR* configuration, they observed either a vertical failure outside the notched section; or failure oriented 45˚ from the notch root. As Fig. 10 shows, the horizontal *TR*–failure observed here is also somewhat inclined. Moreover, it should be noted that failures outside the critical section did not occur for any of the Arcan specimens used in this study, which hence are to be preferred to the Iosipescu setup for this particular configuration.

## Discussion

No significant differences between mutual configurations *ij* and *ji* could be found for any of the parameters stated in Table 2 by statistical analysis (Mann–Whitney test, *p*–values > $\alpha = 0.05$). This indicates that the material behaves symmetrically within each plane. The linear limit stresses $\hat{\sigma}_{ij}^{\text{lin}}$ for the bilinear model demonstrate particularly good correspondences (*p*–values > 0.87) between mutual configurations. This is also the case for the ultimate stresses $\hat{\sigma}_{ij}^{\text{ult}}$ with <1% difference in average stresses between both *LR* and *RL*, and between *RT* and *TR* (*p*–values > 0.35). Consequently, it was assessed as reasonable to treat parameter values from mutual configurations *ij*–*ji* as one sample. Mean values, CV and *p*–values for these samples are given in Table 3 together with correlations with densities $r(\rho)$ and with initial shear moduli $r(\hat{G})$.

**Table 3** Experimental shear parameter statistics

| | | Linear | | Bilinear | | Voce | | | | |
|---|---|---|---|---|---|---|---|---|---|---|
| | | $\hat{G}_{ij}$ | $\hat{G}_{ij}^{\text{LIN}}$ | $\hat{\sigma}_{ij}^{\text{lin}}$ | $\hat{G}_{ij}^{\text{T}}$ | $\hat{\sigma}_{ij}^{\text{lin}}$ | $\hat{R}_{ij}$ | $\hat{H}_{ij}$ | $\hat{\sigma}_{ij}^{\text{ult}}$ | $\hat{\gamma}_{ij}^{\text{ult}}$ |
| Mean | *LR–RL* | 742 | 608 | 4.20 | 424 | 4.17 | 2.56 | 764 | 6.10 | 0.0110 |
| | *LT–TL* | 634 | 598 | 3.04 | 444 | 3.45 | 1.85 | 490 | 4.38 | 0.0082 |
| | *RT–TR* | 34.6 | 17.9 | 0.93 | 11.7 | 0.93 | 0.94 | 34.4 | 1.64 | 0.0914 |
| CV | *LR–RL* | 0.24 | 0.31 | 0.27 | 0.23 | 0.23 | 0.38 | 0.38 | 0.21 | 0.28 |
| | *LT–TL* | 0.27 | 0.30 | 0.31 | 0.37 | 0.21 | 0.51 | 0.06 | 0.21 | 0.33 |
| | *RT–TR* | 0.28 | 0.32 | 0.20 | 0.40 | 0.16 | 0.39 | 0.63 | 0.25 | 0.39 |
| *p*–value | *LR–RL* | 0.95 | 0.32 | 0.87 | 0.32 | 0.31 | 0.93 | 0.88 | 0.96 | 0.35 |
| | *LT–TL* | 0.50 | 0.63 | 1.00 | 0.14 | 0.37 | 0.37 | 0.18 | 0.35 | 0.69 |
| | *RT–TR* | 0.25 | 0.49 | 0.92 | 0.62 | 0.23 | 0.34 | 0.90 | 0.62 | 0.77 |
| $r(\rho)$ | *LR–RL* | 0.21 | 0.24 | 0.33 | 0.02 | 0.18 | -0.28 | -0.01 | 0.22 | -0.08 |
| | *LT–TL* | 0.24 | 0.11 | -0.12 | 0.16 | -0.13 | -0.10 | -0.32 | -0.23 | -0.24 |
| | *RT–TR* | 0.16 | 0.14 | 0.09 | 0.34 | 0.22 | 0.12 | 0.13 | 0.26 | 0.05 |
| $r(\hat{G})$ | *LR–RL* | - | 0.85* | 0.51* | 0.34 | 0.40 | 0.07 | -0.06 | 0.31 | -0.12 |
| | *LT–TL* | - | 0.88* | -0.05 | 0.86* | -0.61 | -0.28 | 0.20 | 0.18 | -0.63* |
| | *RT–TR* | - | 0.56* | 0.51* | 0.56* | 0.37 | 0.40 | 0.17 | 0.49* | -0.18 |

$G_{ij}$, $\sigma_{ij}$ and $R_{ij}$ are given in MPa  *) Significant correlation (*p*–value < 0.05)

The linearized stiffness values $\hat{G}_{ij}^{\mathrm{LIN}}$ over the whole loading range comprise on average approximately 80% of the initial shear modulus $\hat{G}_{ij}$ for *LR–RL*. For the relatively soft rolling shear plane configurations *RT–TR* the values constitute roughly 50% of the initial modulus. For the *LT–TL* configurations, on the contrary, $\hat{G}_{ij}^{\mathrm{LIN}}$ attains approximately the same value as the initial modulus, which indicates little or no nonlinearity tendencies. This is moreover supported by the relatively few specimens from the *LT*–plane being adaptable by the nonlinear models. It can moreover be seen from Table 2 that the Voce model in general is somewhat less robust in describing the shear behaviour than the bilinear one.

The ratio between the apparent linear limit stress $\hat{\sigma}_{ij}^{\mathrm{lin}}$ and the ultimate shear stress $\hat{\sigma}_{ij}^{\mathrm{ult}}$ estimates is in the following referred to as the yield ratio. The rolling shear configurations *RT–TR* demonstrate in this sense most nonlinearity with yield ratios of 0.56 for the bilinear model. The other configurations (*LR–RL*, *LT–TL*) result in peculiarly similar ratios of 0.68, i.e. a somewhat smaller nonlinear portion than in the rolling shear plane. This is close a ratio of 0.60 obtained for the *LR*–plane by both torsion and Iosipescu tests of Sitka spruce by Yoshihara and Ohta (1995a, b, 1996), Yoshihara et al. (1999, 2001) and Yoshihara and Matsumoto (2005), and approximately in the middle of a yield ratio range of 0.40–0.90 obtained by torsion tests for the *LR* and *LT* planes of beech and cypress species (Yamasaki and Sasaki 2004). For the Voce model, the yield ratios are a bit more contradictory between mutual configurations. There does not seem to be any clear trend between the linear limit stress for bilinear versus Voce models. It should be noted that this is partly due to the fact that the Voce model; in its mathematical formulation; is quite flexible, so that the linear limit stress cannot necessarily be interpreted as the physical stress limit.

Similar to the yield ratio, a modulus ratio can be defined as the ratio between the estimated shear tangent modulus $\hat{G}_{ij}^{T}$ and the initial shear modulus $\hat{G}_{ij}$. In such sense, the rolling shear (*RT–TR*) has the lowest modulus ratios of 0.34. In combination with low yield ratios, this implies a relatively high degree of nonlinear strain when approaching ultimate capacity. The other configurations (*LR–RL*, *LT–TL*) have modulus ratios around 0.6, i.e. a relatively stiffer behaviour also beyond the linear limit.

The CV for the various parameters determined lie between 20–30%. It is interesting to note that the two shear strengths comprising the longitudinal direction both have relatively low CV's of 21%. By way of comparison, corresponding CV's obtained for spruce by means of the notched shear block test are reported to 16% by Foslie (1971), 20% by Liu et al. (1996) and 14% by FPL (1999). Yoshihara et al. (1999, 2001) obtained CV's of 23% for the *LR* and *LT* yield values of Sitka spruce by means of the Iosipescu test, which corresponds well with the values found herein.

It can be seen from the tabulated values that all correlations $r(\rho)$ to density are nonsignificant and with absolute values lower than 0.35, corresponding with a determination coefficient $r^2$ <12%. It should be noted that the *CV* of the densities $\rho$ are only about 10% or lower, and that higher correlations could have emerged in samples with higher density variation. It is, however, interesting to see that that several parameters attain high correlations $r(\hat{G})$ to the shear modulus $\hat{G}_{ij}$. All linearized moduli $\hat{G}_{ij}^{LIN}$ are significantly correlated to $\hat{G}_{ij}$, with determination coefficients $r^2$ of approximately 75% for the *LR* and *TL* material planes. Also the two bilinear parameters $\hat{\sigma}_{ij}^{\mathrm{lin}}$ and $\hat{G}_{ij}^{\mathrm{T}}$ demonstrate rather high correlation to $\hat{G}_{ij}$, as illustrated in Fig. 11, while the Voce parameters seem less predictable. It should be noted that due to the mathematical flexibility, several sets of the three

Voce parameters can satisfy adaptation to an experimental curve well, and that this can naturally reduce the correlation. The ultimate strains $\hat{\gamma}_{ij}^{\text{ult}}$ are typically negatively correlated to the shear modulus, which is logical since a higher modulus reduces the deformation. The ultimate shear stresses and strains demonstrate relatively low correlations with both density and initial shear moduli values.

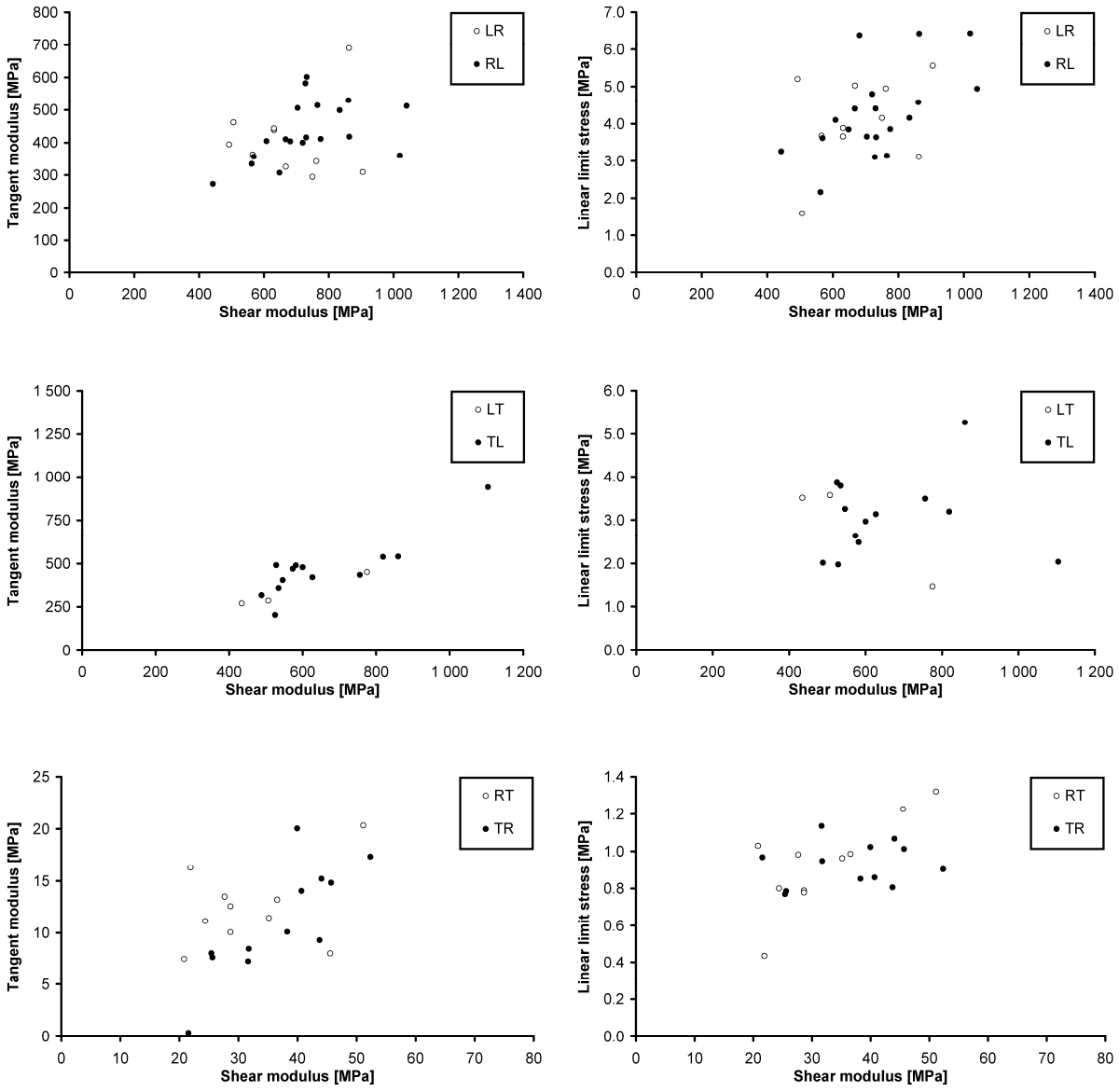


**Fig. 11** Bilinear parameter estimates $\hat{G}_{ij}^{T}$ and $\hat{\sigma}_{ij}^{lin}$ plotted against initial shear moduli $\hat{G}_{ij}$ for each *ij*

It is evident that the rolling shear configurations have considerably lower stiffness and strength than configurations from the two other material planes. Moreover, it is noteworthy that the *LR–RL* configurations have significantly higher values than the *LT–TL* for the shear modulus $\hat{G}_{ij}$, the bilinear stress limit $\hat{\sigma}_{ij}^{\text{lin}}$ and the ultimate stress and strain $\hat{\sigma}_{ij}^{\text{ult}}$ and $\hat{\gamma}_{ij}^{\text{ult}}$. The differences for linear

limits and ultimate stresses are both around 28%. This corresponds well with results from torsion tests of Sitka spruce, where differences for both stiffness and strength of approximately 10% are reported by Yoshihara and Ohta (1995a, b, 1996). The ultimate nominal stresses observed herein are plotted in Fig. 12 for each of the three planes.

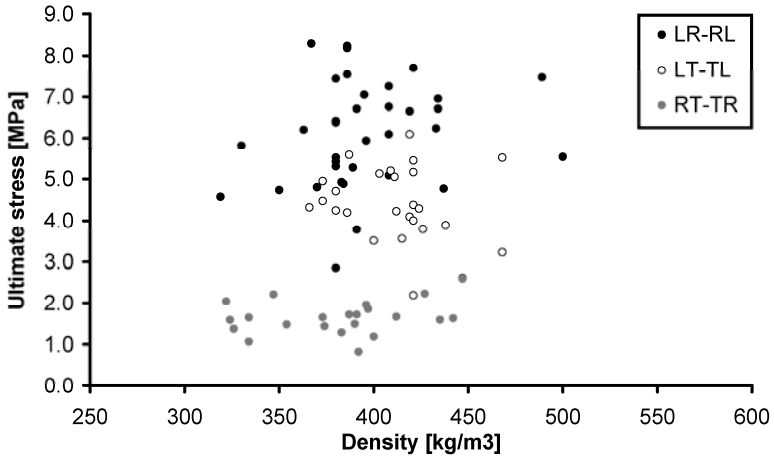


**Fig. 12** Ultimate shear stress estimates $\hat{\sigma}_{ij}^{\text{ult}}$ observed for the different material planes

The average shear strengths were found to equal 6.1 MPa for the *LR*–plane, 4.4 MPa for the *LT*–plane and 1.6 MPa for the *RT*–plane. The two former values are only about 80 and 60%, respectively, of the strengths obtained for Norway spruce by the notched shear block test by Foslie (1971). This trend corresponds to findings by Liu et al. (1996), who reported lower strengths for spruce by means of the Arcan test than by the notched shear block. When combining the *LR* and *LT* data herein into one sample, it was found that the strengths satisfied the normal distribution well with a mean value of 5.37 MPa and a standard deviation of 1.43 MPa. The corresponding 5% lower percentile of this distribution is 3.0 MPa, which is identical to the shear strength specified for grading class C30 in NS-EN 338 (2003).

## Model accuracy

The material parameters for each specimen represent average values in the sense that they are determined by optimization of experimentally data consisting of numerous stress–strain points. The parameters are thus a set of values describing a best fit of the overall behaviour.

In order to document strain prediction accuracy for the different material models applied to different shear types, the *SSE* values were collected for each optimization. By dividing by the number of steps *k* extracted for optimization from the stress–strain path, and taking the square root, the experimental mean stress residual $\Delta\sigma_{ij}$ can be estimated:

$$\Delta\sigma_{ij} = \sqrt{\frac{SSE_{\gamma_{ij}}}{k}} \qquad \{i, j\} = \{L, R, T\}\ ;\ i \neq j \tag{9}$$

This should be reasonable since the deviation from the optimized model behaviour in general seemed to be more or less randomly distributed over the stress range, see Fig. 13.

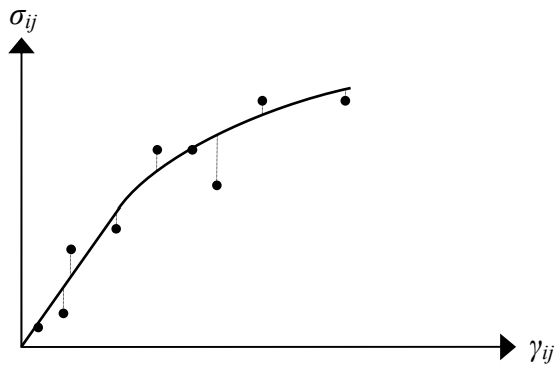


**Fig. 13** Stress residual contributions (MPa) for values adapted to the Voce model

The mean residuals were subsequently averaged over the *n* specimens of the same configuration type *ij* adapted to the models, and are presented in Table 4 for the various models and configuration types *ij*, where *N* assigns the total number of *ij* specimens. Comparisons between the linearized and the bilinear; and between the bilinear and the Voce models, are given as ratios in separate columns. It should be noted that the transformation from total strains $\gamma_{ij}$ to plastic strains $\gamma_{ij}^{p}$ in Eq. (5) removes some strain variation, affecting SSE comparison of the differently formulated models. The bilinear model is thus presented in dual columns comprising both total and plastic strain formulation to enable comparison with the Voce model; formulated by plastic strains only, and with the linearized model; formulated by total strains only. Comparison between the two bilinear variants is thus not of pertinent interest. The Voce model can, for the same reason, only be compared indirectly with the linearized model via the bilinear one.

**Table 4** Average stress residuals (MPa) for the different shear configuration types *ij*

| | | Linearization | | Bilinear (total) | | | Bilinear (plastic) | | Voce | | |
|---|---|---|---|---|---|---|---|---|---|---|---|
| *ij* | *N* | $\overline{\Delta\sigma_{ij}}$ | *n* | $\overline{\Delta\sigma_{ij}}$ | *n* | Ratio (%) | $\overline{\Delta\sigma_{ij}}$ | *n* | $\overline{\Delta\sigma_{ij}}$ | *n* | Ratio (%) |
| LR | 12 | 0.205 | 12 | 0.093 | 10 | 45 | 0.207 | 10 | 0.127 | 8 | 61 |
| RL | 23 | 0.244 | 21 | 0.140 | 19 | 57 | 0.351 | 19 | 0.199 | 16 | 57 |
| LT | 12 | 0.153 | 8 | 0.083 | 3 | 54 | 0.122 | 3 | 0.108 | 3 | 89 |
| TL | 15 | 0.149 | 15 | 0.106 | 13 | 71 | 0.332 | 13 | 0.158 | 5 | 48 |
| RT | 10 | 0.090 | 10 | 0.052 | 10 | 58 | 0.078 | 10 | 0.067 | 8 | 86 |
| TR | 12 | 0.132 | 12 | 0.053 | 12 | 40 | 0.105 | 12 | 0.064 | 11 | 61 |

It can be seen that the bilinear model holds average residuals between 40 and 71% compared to the linearized model residuals. The fraction (*n*/*N*) of specimens which feasibly could be adapted by the model is moreover high for all configuration types except *LT*, which turned out to be troublesome for nonlinear adaptation in general. By changing from a linearized model to a bilinear one, the overall accuracy of stress prediction can thus be considered to increase by a factor of approximately two. The bilinear model is thus quite robust and applicable, and relatively accurate for adapting shear behaviour of Norway spruce.

The Voce model holds average residuals between 48 and 89% compared to the bilinear model. Particularly the *LR*–plane show stable results around 60% with a relatively high adaptation fraction (*n*/*N*) near 0.7 for both configurations. Compared to the bilinear model, it is, however, noteworthy that (*n*/*N*) is lower for all material planes, particularly for the *LT*–plane. In general, the Voce model can thus be said to be less adaptive, but more accurate than the bilinear model in cases where it is applicable. The residuals are illustrated in Fig. 14, where the nonlinear *LT* and *TL* values are stippled to indicate their low *n*/*N* fraction.

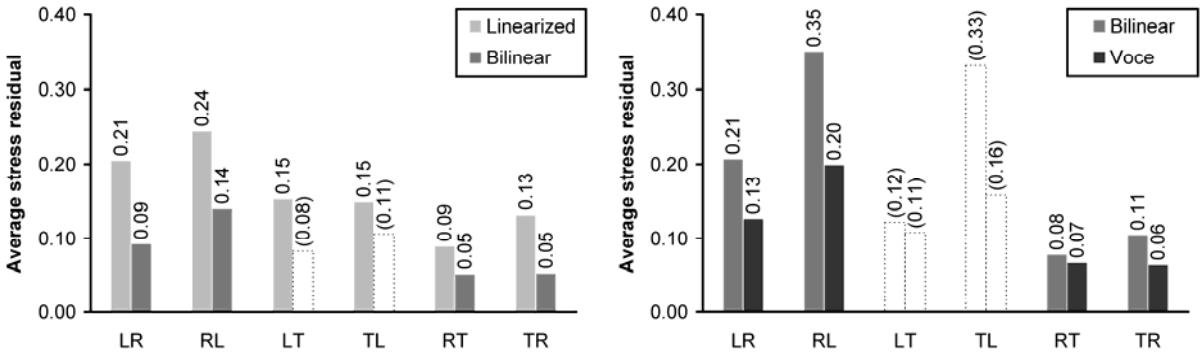


**Fig. 14** Average stress residuals $\overline{\Delta\sigma_{ij}}$ (MPa) for different models and shear types *ij*

Since the residual values can be interpreted as the expected deviation between modelled and experimentally based stress for a given strain level, the values, from a design viewpoint, express the uncertainty numerical results on average can be encumbered with. It should be noted that the experimental strain in this study is averaged over a measurement area of 18 mm ×18 mm. Any strain variation within the area is thus not reflected by this consideration. The residual values are, due to the same reason, only representative for areas and volumes of the same order of size as measured in the study, i.e. the representative volume element (RVE) of the utilized test.

## Concluding remarks

The Arcan shear test was used to investigate shear properties of softwood from Norway spruce. The tests comprised the three orthotropic material planes, and covered the load range up till failure. Six different configurations were used, comprising two mutual types within each material plane; with the test load oriented along either of the two inherent material axes. Linear and failure data in addition to nonlinear effects were observed. The linear elastic properties are treated in Dahl and Malo (2009a) where details and suitability of the test is assessed, while the observed nonlinear and failure data are reported herein.

No significant differences could be found between any of the parameters obtained by mutual tests within the same material plane. This indicates that the material behaves in a symmetric manner. Especially the linear limit stresses and the ultimate stresses proved to be equal between mutual configurations.

It was found that the stress–strain curves from the *LR*–plane, and in particular the rolling shear plane *RT*, exhibit nonlinear behaviour in shear, while the *LT*–plane follows a relatively linear progress. The bilinear and the Voce models were used to adapt the data, requiring two and three parameters, respectively, for each material plane. It was found that the model accuracy on average can be considered to increase by a factor of approximately two by using a bilinear model compared to a completely linear model. The Voce model improved the prediction accuracy even further, but was in some cases infeasible to adapt, and therefore less robust in characterizing the generalized shear behaviour of softwood.

For the bilinear model, the ratio between the observed linear limit and the ultimate shear stress was 0.56 for the *RT*–plane, and 0.68 for both the *LR* and *LT*–planes. The results for the Voce model seems a bit more contradictory between mutual configurations, which can be explained by the fact that the parameters cannot be separated and evaluated in the same straightforward manner. The ratio between the tangent and the initial shear modulus was in the range 0.3–0.4 for the rolling shear tests, while the other configurations resulted in ratios around 0.6.

The average shear strengths were 6.1 MPa for the *LR*–plane, 4.4 MPa for the *LT*–plane and 1.6 MPa for the *RT*–plane. The fact that the values are somewhat lower than values obtained by the notched shear test on the same subspecies corresponds well with other findings in the literature. The failures were oriented either vertically or horizontally depending on test type, and in all cases located at the critical section of the specimen. Improper failure types reported for similar tests were avoided, making the utilized Arcan setup attractive for shear studies of the whole loading range and the three orthotropic material planes.

It should be noted that the reported parameters herein are estimates not necessarily reflecting the true material behaviour. Configuration and measurement effects, including inhomogeneous and nonuniform stress and strain fields, can influence the determined values, which therefore must be considered as apparent. More detailed studies by means of numerical methods should therefore be undertaken in order to better understand the shear properties of softwood.

# References

ASTM D143 (1984) Standard Methods of Testing Small Clear Specimens of Timber. American Society for Testing and Materials, p. 42.

ASTM D3044 (1986) Standard Test Method for Shear Modulus of Plywood. American Society for Testing and Materials, p. 3.

Dahl K. B. (2008) Testing of Shear Properties of Spruce Softwood, Report R-14-08, Department of Structural engineering, Norwegian University of Science and Technology, Trondheim, Norway, p. 10.

Dahl K. B., Malo K. A. (2009a) Linear Shear properties of Spruce Softwood. Wood Science and Technology 43: 499-525, DOI 10.1007/s00226-009-0246-5.

Dahl K. B., Malo K. A. (2009b) Planar strain measurements on wood specimens. Experimental mechanics 49: 575-586, DOI 10.1007/s11340-008-9162-0.

Dumail J. F., Olofsson K., Salmén L. (2000) An Analysis of Rolling Shear of Spruce Wood by the Iosipescu Method. Holzforschung 54: 420-426.

Foslie M. (1971) Strength properties of Norwegian spruce (Picea Abies Karst.). Part 3: Strength properties of small, clear specimens, Report 42/317, Norwegian Institute of Wood Technology, Oslo, p. 12.

FPL (1999) Wood Handbook. Wood as an Engineering Material. Gen. Tech. Rep. FPL-GTR-113, United States Department of Agriculture, Forest Products Laboratory, p. 463.

Liu J. Y., Ross R. J. (1998) Wood property variation with grain slope. 12th Engineering Mechanics Conference, May 17-20, 1998, American Society of Civil Engineers, La Jolla, CA, USA.: 1351-1354.

Liu J. Y., Ross R. J., Rammer D. R. (1996) Improved Arcan Shear Test for Wood. International Wood Engineering Conference, October 28-31, 1996, New Orleans, LA, USA, Vol. 2: 85-90.

NS-EN 338 (2003) Structural timber Strength Classes. European Committee for Standardization (2nd ed.), p. 7.

NS-EN 384 (2004) Structural timber - Determination of characteristic values of mechanical properties and density. European Committee for Standardization, p. 15.

Oliveira J. M. Q. (2004) Characterization of the shear behaviour of wood using the Arcan test (in Portugese). Universidade de Trás-os-Montes e Alto Douro. Master thesis, p. 164.

Ukyo S., Masuda M. (2006) A new method for Measuring the True Shear Strength of Wood. 9th World Conference on Timber Engineering, Portland USA.

Xavier J. C., Garrido N. M., Oliveira M., Morais J. L., Camanho P. P., Pierron F. (2004) A comparison between the Iosipescu and off-axis shear test methods for the characterization of Pinus Pinaster Ait. Composites: Part A 35: 827-840.

Yamasaki M., Sasaki Y. (2003) Elastic properties of wood with rectangular cross section under combined static axial force and torque. Journal of Materials Science 38: 603-612.

Yamasaki M., Sasaki Y. (2004) Yield Behavior of Wood Under Combined Static Axial Force and Torque. Experimental mechanics 44 (3): 221-227.

Yoshihara H., Matsumoto A. (2005) Measurement of the shearing properties of wood by in-plane shear test using a thin specimen. Wood Science and Technology 39: 141-153.

Yoshihara H., Ohsaki H., Kubojima Y., Ohta M. (1999) Applicability of the Iosipescu shear test on the measurement of the shear properties of wood. Journal of Wood Science 45: 24-29.

Yoshihara H., Ohsaki H., Kubojima Y., Ohta M. (2001) Comparisons of Shear Stress/Shear Strain Relations of Wood obtained by Iosipescu and Torsion Tests. Wood and Fiber Science 33 (2): 275-283.

Yoshihara H., Ohta M. (1995a) Determination of the Shear Stress-Shear Strain Relationship of Wood by Torsion Tests. Mokuzai Gakkaishi 41 (11): 988-993.

Yoshihara H., Ohta M. (1995b) Shear Stress-Shear Strain Relationship of Wood in the Plastic Region. Mokuzai Gakkaishi 41 (6): 529-536.

Yoshihara H., Ohta M. (1996) Analysis of the Yield Behavior of Wood under Combined Shear Stresses in Torsion Tests. Mokuzai Gakkaishi 42 (6): 541-545.

Yoshihara H., Ohta M., Origuchi K. (1997) Yield Behavior of Wood under Compression-Shear Combined Stress Condition. J. Soc. Mat. Sci., Japan 46 (4): 385-389.

# PAPER IV

## Nonlinear Shear Properties of Spruce Softwood: Numerical Analyses of Experimental Results

**K. B. DAHL[1], K. A. MALO[2]**

*Composites Science and Technology (2009) 69:2144-2151*

**Abstract**

Determination of material parameters from experimental tests often rely on simplifying assumptions like the existence of uniform stress and strain fields within the considered part of the test specimen. However, more detailed analyses usually show that the stress and strain fields differ from the assumed (nominal) uniform distributions. In order to utilize the potential of numerical analyses of wooden structures by the FEM method, the nominal material parameters measured directly from tests need to be re-evaluated in order to make them more useful for FEM models and to make FEM models more reliable.

Experimental data from shear testing of clear wood from Norway spruce was analysed numerically with a bilinear material law in shear. The inherent material parameters were fitted to the experimental behaviour by means of optimization methods in conjunction with FEM analyses. The study included six Arcan test configurations comprising the three orthotropic material planes of wood, and covered the whole loading range until failure. Compared to numerical results, it was found that stiffness values measured were too high, and that downward adjustments in the range of 5–30% were required. Linear limit stresses between 40% and 60% of the nominal shear strengths were found, whilst the tangent moduli ranged between 30% and 70% of the linear elastic shear moduli. The rolling shear plane *RT* showed most nonlinearity and the *LT* plane least. Analyses with modified bilinear parameters showed good correspondence with experimental findings. The parameters were found to be relatively well adapted by Weibull distributions.

**Keywords** – Wood, Nonlinear behaviour, Orthotropy, Finite element analysis, Probabilistic methods

[1] Ph.D-student, Dept. of Structural Engineering, Norwegian University of Science and Technology NTNU, M.Sc. Structural and Civil Engineer, Multiconsult AS, Boks 265 Skøyen, N-0213 Oslo, Norway.
[2] Professor, Dept. of Structural Engineering, Norwegian University of Science and Technology NTNU

Is not included due to copyright

# PAPER V

## Shear Strengths of Spruce Softwood: Numerical Analyses of Experimental Results

**K. B. DAHL[1], K. A. MALO[2]**

*To be submitted*

**Abstract**
Experimentally based shear strengths of clear wood from Norway spruce were analysed numerically with an orthotropic material law comprising bilinearity in shear. The study included six Arcan shear test configurations covering all orthotropic material planes. Three configurations were found applicable for determination of shear strengths. The Tsai-Wu and the maximum stress criteria were assumed as failure functions. Analyses with the former showed that the nominal strengths are measured 15–25% too low depending on material plane. The modified shear strengths were on average found to equal 7.1 MPa (*LR*), 4.8 MPa (*LT*) and 2.0 MPa (*RT*). All quantities were adequately represented by normal distributions. High correlations with the linear shear stress limits were found.

**Keywords** – Wood, Orthotropy, Shear strength, Tsai-Wu, Finite element analysis, Probabilistic methods

[1] Ph.D-student, Dept. of Structural Engineering, Norwegian University of Science and Technology NTNU, M.Sc. Structural and Civil Engineer, Multiconsult AS, Boks 265 Skøyen, N-0213 Oslo, Norway.
[2] Professor, Dept. of Structural Engineering, Norwegian University of Science and Technology NTNU

Is not included due to copyright

# PAPER VI

## Linear Tensile and Compressive Properties of Spruce Softwood: Experimental Results

**K. B. DAHL[1], K. A. MALO[2]**

*To be submitted*

**Abstract**
The 3 moduli of elasticity and the 6 Poisson's ratios of Norway spruce were tested by compressive and tensile specimens of clear wood oriented in each of the three orthotropic directions *LRT* of the material. In-plane strains were measured by means of bi-dimensional video extensometry, and orthotropic parameters were determined for loading and unloading for each of the approximately 350 specimens. The average moduli equalled $E_{LL}$ = 9 040 MPa, $E_{RR}$ = 790 MPa and $E_{TT}$ = 340 MPa. $E_{LL}$ was significantly dependent on grading class, whereas the Poisson's ratios showed significant dependency on strain rate, and were somewhat higher than earlier reported. The two minor ratios were hardly measurable, and are probably obtained most conveniently by orthotropic symmetry considerations. Correlation with density was generally low, whereas the parameter variation was quite high. Many specimens showed a slight degree of shear strain, indicating fibre inclination in an orthotropic material like wood.

**Keywords** –Wood, Mechanical properties, Creep, Orthotropy, Elastic properties

[1] Ph.D-student, Dept. of Structural Engineering, Norwegian University of Science and Technology NTNU, M.Sc. Structural and Civil Engineer, Multiconsult AS, Boks 265 Skøyen, N-0213 Oslo, Norway.
[2] Professor, Dept. of Structural Engineering, Norwegian University of Science and Technology NTNU

Is not included due to copyright

# PAPER VII

## Linear Tensile and Compressive Properties of Spruce Softwood: Numerical Analyses of Experimental Results and Fibre Inclinations Effects

**K. B. DAHL[1], K. A. MALO[2]**

*To be submitted*

**Abstract**

Fibre inclination is one of the main causes of inhomogeneity in wood. Since wood has orthotropic characteristics, such deviations between principal material orientations and axial loads result in shear strains, which are rarely measured in on-axis testing of wood. Moreover, the fibre inclination may result in encumbered material parameter values. This study reports unintentional shear strains measured by bidimensional video extensometry in tensile and compressive specimens of clear softwood, tentatively oriented in each of the three principal orthotropic directions *LRT*. It was found that roughly 50% of the various specimens responded with shear strain, for which average inclination angles of approximately 3 degrees occurred. Probabilistic analyses were used to quantify the sensitivities between measured strains and inclination angles in and out of the measurement planes, and the potential deviations were outlined. Analytic theory in conjunction with numerically determined modification factors were used to modify apparent moduli of elasticity $E_{ii}$ and Poisson's ratios $\nu_{ij}$ for test configuration and inclination effects. The on-axis configuration effects were found to be relatively small (<2%), indicating suitable specimens, whereas effects from fibre inclinations were considerably higher. The modifications resulted in an increase of the 3 $E_{ii}$ of approximately 3%, whereas the 6 $\nu_{ij}$ changed within ±12%. Although the alterations are relatively small for a highly variable material like wood, it is worth being aware of the potential error, especially as unintentional shear strains are likely to be measured in wood specimens. The differences in parameter estimates from different specimen types were reduced in most cases. The 3 moduli of elasticity were found to be lognormal distributed, whereas the Poisson's ratios are relatively well adapted by normal distributions.

**Keywords** – Wood, Elasticity, Fibre inclination, Orthotropy, Finite element analysis, Probabilistic methods

[1] Ph.D-student, Dept. of Structural Engineering, Norwegian University of Science and Technology NTNU, M.Sc. Structural and Civil Engineer, Multiconsult AS, Boks 265 Skøyen, N-0213 Oslo, Norway.
[2] Professor, Dept. of Structural Engineering, Norwegian University of Science and Technology NTNU

Is not included due to copyright

# PAPER VIII

## Strengths and Nonlinear Properties of Spruce Softwood Tested in Tension and Compression: Experimental Results

**K. B. DAHL**[1]

*To be submitted*

**Abstract**

This paper reports nominal strengths and nonlinear behaviour of clear wood from Norway spruce tested in tension and compression in the three orthotropic directions. The tensile specimens responded relatively linearly with brittle failures, although some deflection could be found. The compressive specimens were ductile, especially perpendicular to grain, and were limited to small strains <2% at maximum. Approximately 350 specimens were tested in total. Bilinear models were adapted to active and passive strains observed, taking into account the different behaviour on the compressive and tensile sides. The tensile strengths were on average found to equal 63.4 MPa longitudinally, 4.9 MPa radially and 2.8 MPa tangentially. On the compressive sides, the strengths equalled 28.9 MPa longitudinally, 3.6 MPa radially and 3.8 MPa tangentially. It should be noted that the two latter are conditional on the small strain limitation, as no distinct ultimate stresses were observed perpendicularly. Linear limit stresses were found to lie at 65–70% of tensile strengths and at 63–80% of compressive strengths. The tensile tangent moduli range from 58–74% of the initial moduli, whereas all compressive lie at approximately 30%. Compared to completely linearized models (secants) for the various tensile configurations, the stress prediction accuracies increase 10–50% by applying bilinear models, with linearized moduli lying 5–10% lower than the initial moduli values. Except for the tangent moduli, the coefficients of variations were found to be lower than 0.3 for most parameters. Significant correlations between many parameters were found. The three-parametric Weibull distribution was found most applicable to represent the various parameters.

**Keywords** –Wood, Orthotropy, Nonlinearity, Ductility, Strengths, Experimental testing

[1] Ph.D-student, Dept. of Structural Engineering, Norwegian University of Science and Technology NTNU, M.Sc. Structural and Civil Engineer, Multiconsult AS, Boks 265 Skøyen, N-0213 Oslo, Norway.

Is not included due to copyright

**DEPARTMENT OF STRUCTURAL ENGINEERING**
**NORWEGIAN UNIVERSITY OF SCIENCE AND TECHNOLOGY**

N–7491 TRONDHEIM, NORWAY
Telephone: +47 73 59 47 00 Telefax: +47 73 59 47 01

"Reliability Analysis of Structural Systems using Nonlinear Finite Element Methods",
C. A. Holm, 1990:23, ISBN 82-7119-178-0.

"Uniform Stratified Flow Interaction with a Submerged Horizontal Cylinder",
Ø. Arntsen, 1990:32, ISBN 82-7119-188-8.

"Large Displacement Analysis of Flexible and Rigid Systems Considering Displacement-Dependent Loads and Nonlinear Constraints",
K. M. Mathisen, 1990:33, ISBN 82-7119-189-6.

"Solid Mechanics and Material Models including Large Deformations",
E. Levold, 1990:56, ISBN 82-7119-214-0, ISSN 0802-3271.

"Inelastic Deformation Capacity of Flexurally-Loaded Aluminium Alloy Structures",
T. Welo, 1990:62, ISBN 82-7119-220-5, ISSN 0802-3271.

"Visualization of Results from Mechanical Engineering Analysis",
K. Aamnes, 1990:63, ISBN 82-7119-221-3, ISSN 0802-3271.

"Object-Oriented Product Modeling for Structural Design",
S. I. Dale, 1991:6, ISBN 82-7119-258-2, ISSN 0802-3271.

"Parallel Techniques for Solving Finite Element Problems on Transputer Networks",
T. H. Hansen, 1991:19, ISBN 82-7119-273-6, ISSN 0802-3271.

"Statistical Description and Estimation of Ocean Drift Ice Environments",
R. Korsnes, 1991:24, ISBN 82-7119-278-7, ISSN 0802-3271.

“Properties of concrete related to fatigue damage: with emphasis on high strength concrete”,
G. Petkovic, 1991:35, ISBN 82-7119-290-6, ISSN 0802-3271.

"Turbidity Current Modelling",
B. Brørs, 1991:38, ISBN 82-7119-293-0, ISSN 0802-3271.

"Zero-Slump Concrete: Rheology, Degree of Compaction and Strength. Effects of Fillers as Part Cement-Replacement",
C. Sørensen, 1992:8, ISBN 82-7119-357-0, ISSN 0802-3271.

"Nonlinear Analysis of Reinforced Concrete Structures Exposed to Transient Loading",
K. V. Høiseth, 1992:15, ISBN 82-7119-364-3, ISSN 0802-3271.

"Finite Element Formulations and Solution Algorithms for Buckling and Collapse Analysis of Thin Shells",
R. O. Bjærum, 1992:30, ISBN 82-7119-380-5, ISSN 0802-3271.

"Response Statistics of Nonlinear Dynamic Systems",
J. M. Johnsen, 1992:42, ISBN 82-7119-393-7, ISSN 0802-3271.

"Digital Models in Engineering. A Study on why and how engineers build and operate digital models for decisison support",
J. Høyte, 1992:75, ISBN 82-7119-429-1, ISSN 0802-3271.

"Sparse Solution of Finite Element Equations",
A. C. Damhaug, 1992:76, ISBN 82-7119-430-5, ISSN 0802-3271.

"Some Aspects of Floating Ice Related to Sea Surface Operations in the Barents Sea",
S. Løset, 1992:95, ISBN 82-7119-452-6, ISSN 0802-3271.

"Modelling of Cyclic Plasticity with Application to Steel and Aluminium Structures",
O. S. Hopperstad, 1993:7, ISBN 82-7119-461-5, ISSN 0802-3271.

"The Free Formulation: Linear Theory and Extensions with Applications to Tetrahedral Elements with Rotational Freedoms",
G. Skeie, 1993:17, ISBN 82-7119-472-0, ISSN 0802-3271.

"Høyfast betongs motstand mot piggdekkslitasje. Analyse av resultater fra prøving i Veisliter'n",
T. Tveter, 1993:62, ISBN 82-7119-522-0, ISSN 0802-3271.

"A Nonlinear Finite Element Based on Free Formulation Theory for Analysis of Sandwich Structures",
O. Aamlid, 1993:72, ISBN 82-7119-534-4, ISSN 0802-3271.

"The Effect of Curing Temperature and Silica Fume on Chloride Migration and Pore Structure of High Strength Concrete",
C. J. Hauck, 1993:90, ISBN 82-7119-553-0, ISSN 0802-3271.

"Failure of Concrete under Compressive Strain Gradients",
G. Markeset, 1993:110, ISBN 82-7119-575-1, ISSN 0802-3271.

"An experimental study of internal tidal amphidromes in Vestfjorden",
J. H. Nilsen, 1994:39, ISBN 82-7119-640-5, ISSN 0802-3271.

"Structural analysis of oil wells with emphasis on conductor design",
H. Larsen, 1994:46, ISBN 82-7119-648-0, ISSN 0802-3271.

"Adaptive methods for non-linear finite element analysis of shell structures",
K. M. Okstad, 1994:66, ISBN 82-7119-670-7, ISSN 0802-3271.

"On constitutive modelling in nonlinear analysis of concrete structures",
O. Fyrileiv, 1994:115, ISBN 82-7119-725-8, ISSN 0802-3271.

"Fluctuating wind load and response of a line-like engineering structure with emphasis on motion-induced wind forces",
J. Bogunovic Jakobsen, 1995:62, ISBN 82-7119-809-2, ISSN 0802-3271.

"An experimental study of beam-columns subjected to combined torsion, bending and axial actions",
A. Aalberg, 1995:66, ISBN 82-7119-813-0, ISSN 0802-3271.

"Scaling and cracking in unsealed freeze/thaw testing of Portland cement and silica fume concretes",
S. Jacobsen, 1995:101, ISBN 82-7119-851-3, ISSN 0802-3271.

"Damping of water waves by submerged vegetation. A case study of laminaria hyperborea",
A. M. Dubi, 1995:108, ISBN 82-7119-859-9, ISSN 0802-3271.

"The dynamics of a slope current in the Barents Sea",
Sheng Li, 1995:109, ISBN 82-7119-860-2, ISSN 0802-3271.

"Modellering av delmaterialenes betydning for betongens konsistens",
Ernst Mørtsell, 1996:12, ISBN 82-7119-894-7, ISSN 0802-3271.

"Bending of thin-walled aluminium extrusions",
Birgit Søvik Opheim, 1996:60, ISBN 82-7119-947-1, ISSN 0802-3271.

"Material modelling of aluminium for crashworthiness analysis",
Torodd Berstad, 1996:89, ISBN 82-7119-980-3, ISSN 0802-3271.

"Estimation of structural parameters from response measurements on submerged floating tunnels",
Rolf Magne Larssen, 1996:119, ISBN 82-471-0014-2, ISSN 0802-3271.

“Numerical modelling of plain and reinforced concrete by damage mechanics”,
Mario A. Polanco-Loria, 1997:20, ISBN 82-471-0049-5, ISSN 0802-3271.

“Nonlinear random vibrations - numerical analysis by path integration methods”,
Vibeke Moe, 1997:26, ISBN 82-471-0056-8, ISSN 0802-3271.

“Numerical prediction of vortex-induced vibration by the finite element method”,
Joar Martin Dalheim, 1997:63, ISBN 82-471-0096-7, ISSN 0802-3271.

“Time domain calculations of buffeting response for wind sensitive structures”,
Ketil Aas-Jakobsen, 1997:148, ISBN 82-471-0189-0, ISSN 0802-3271.

"A numerical study of flow about fixed and flexibly mounted circular cylinders",
Trond Stokka Meling, 1998:48, ISBN 82-471-0244-7, ISSN 0802-3271.

“Estimation of chloride penetration into concrete bridges in coastal areas”,
Per Egil Steen, 1998:89, ISBN 82-471-0290-0, ISSN 0802-3271.

“Stress-resultant material models for reinforced concrete plates and shells”,
Jan Arve Øverli, 1998:95, ISBN 82-471-0297-8, ISSN 0802-3271.

“Chloride binding in concrete. Effect of surrounding environment and concrete composition”,
Claus Kenneth Larsen, 1998:101, ISBN 82-471-0337-0, ISSN 0802-3271.

“Rotational capacity of aluminium alloy beams”,
Lars A. Moen, 1999:1, ISBN 82-471-0365-6, ISSN 0802-3271.

“Stretch Bending of Aluminium Extrusions”,
Arild H. Clausen, 1999:29, ISBN 82-471-0396-6, ISSN 0802-3271.

“Aluminium and Steel Beams under Concentrated Loading”,
Tore Tryland, 1999:30, ISBN 82-471-0397-4, ISSN 0802-3271.

"Engineering Models of Elastoplasticity and Fracture for Aluminium Alloys",
Odd-Geir Lademo, 1999:39, ISBN 82-471-0406-7, ISSN 0802-3271.

"Kapasitet og duktilitet av dybelforbindelser i trekonstruksjoner",
Jan Siem, 1999:46, ISBN 82-471-0414-8, ISSN 0802-3271.

“Etablering av distribuert ingeniørarbeid; Teknologiske og organisatoriske erfaringer fra en norsk ingeniørbedrift”,
Lars Line, 1999:52, ISBN 82-471-0420-2, ISSN 0802-3271.

“Estimation of Earthquake-Induced Response”,
Símon Ólafsson, 1999:73, ISBN 82-471-0443-1, ISSN 0802-3271.

“Coastal Concrete Bridges: Moisture State, Chloride Permeability and Aging Effects”,
Ragnhild Holen Relling, 1999:74, ISBN 82-471-0445-8, ISSN 0802-3271.

”Capacity Assessment of Titanium Pipes Subjected to Bending and External Pressure”,
Arve Bjørset, 1999:100, ISBN 82-471-0473-3, ISSN 0802-3271.

“Validation of Numerical Collapse Behaviour of Thin-Walled Corrugated Panels”,
Håvar Ilstad, 1999:101, ISBN 82-471-0474-1, ISSN 0802-3271.

“Strength and Ductility of Welded Structures in Aluminium Alloys”,
Miroslaw Matusiak, 1999:113, ISBN 82-471-0487-3, ISSN 0802-3271.

“Thermal Dilation and Autogenous Deformation as Driving Forces to Self-Induced Stresses in High Performance Concrete”,
Øyvind Bjøntegaard, 1999:121, ISBN 82-7984-002-8, ISSN 0802-3271.

“Some Aspects of Ski Base Sliding Friction and Ski Base Structure”,
Dag Anders Moldestad, 1999:137, ISBN 82-7984-019-2, ISSN 0802-3271.

"Electrode reactions and corrosion resistance for steel in mortar and concrete",
Roy Antonsen, 2000:10, ISBN 82-7984-030-3, ISSN 0802-3271.

"Hydro-Physical Conditions in Kelp Forests and the Effect on Wave Damping and Dune Erosion. A case study on Laminaria Hyperborea",
Stig Magnar Løvås, 2000:28, ISBN 82-7984-050-8, ISSN 0802-3271.

"Random Vibration and the Path Integral Method",
Christian Skaug, 2000:39, ISBN 82-7984-061-3, ISSN 0802-3271.

"Buckling and geometrical nonlinear beam-type analyses of timber structures",
Trond Even Eggen, 2000:56, ISBN 82-7984-081-8, ISSN 0802-3271.

”Structural Crashworthiness of Aluminium Foam-Based Components”,
Arve Grønsund Hanssen, 2000:76, ISBN 82-7984-102-4, ISSN 0809-103X.

“Measurements and simulations of the consolidation in first-year sea ice ridges, and some aspects of mechanical behaviour”,
Knut V. Høyland, 2000:94, ISBN 82-7984-121-0, ISSN 0809-103X.

”Kinematics in Regular and Irregular Waves based on a Lagrangian Formulation”,
Svein Helge Gjøsund, 2000-86, ISBN 82-7984-112-1, ISSN 0809-103X.

”Self-Induced Cracking Problems in Hardening Concrete Structures”,
Daniela Bosnjak, 2000-121, ISBN 82-7984-151-2, ISSN 0809-103X.

"Ballistic Penetration and Perforation of Steel Plates",
Tore Børvik, 2000:124, ISBN 82-7984-154-7, ISSN 0809-103X.

"Freeze-Thaw resistance of Concrete. Effect of: Curing Conditions, Moisture Exchange and Materials",
Terje Finnerup Rønning, 2001:14, ISBN 82-7984-165-2, ISSN 0809-103X

“Structural behaviour of post tensioned concrete structures. Flat slab. Slabs on ground",
Steinar Trygstad, 2001:52, ISBN 82-471-5314-9, ISSN 0809-103X.

"Slipforming of Vertical Concrete Structures. Friction between concrete and slipform panel",
Kjell Tore Fosså, 2001:61, ISBN 82-471-5325-4, ISSN 0809-103X.

"Some numerical methods for the simulation of laminar and turbulent incompressible flows",
Jens Holmen, 2002:6, ISBN 82-471-5396-3, ISSN 0809-103X.

“Improved Fatigue Performance of Threaded Drillstring Connections by Cold Rolling”,
Steinar Kristoffersen, 2002:11, ISBN: 82-421-5402-1, ISSN 0809-103X.

"Deformations in Concrete Cantilever Bridges: Observations and Theoretical Modelling",
Peter F. Takâcs, 2002:23, ISBN 82-471-5415-3, ISSN 0809-103X.

"Stiffened aluminium plates subjected to impact loading",
Hilde Giæver Hildrum, 2002:69, ISBN 82-471-5467-6, ISSN 0809-103X.

"Full- and model scale study of wind effects on a medium-rise building in a built up area",
Jónas Thór Snæbjørnsson, 2002:95, ISBN82-471-5495-1, ISSN 0809-103X.

“Evaluation of Concepts for Loading of Hydrocarbons in Ice-infested water”,
Arnor Jensen, 2002:114, ISBN 82-417-5506-0, ISSN 0809-103X.

”Numerical and Physical Modelling of Oil Spreading in Broken Ice”,
Janne K. Økland Gjøsteen, 2002:130, ISBN 82-471-5523-0, ISSN 0809-103X.

”Diagnosis and protection of corroding steel in concrete”,
Franz Pruckner, 2002:140, ISBN 82-471-5555-4, ISSN 0809-103X.

“Tensile and Compressive Creep of Young Concrete: Testing and Modelling”,
Dawood Atrushi, 2003:17, ISBN 82-471-5565-6, ISSN 0809-103X.

“Rheology of Particle Suspensions. Fresh Concrete, Mortar and Cement Paste with Various Types of Lignosulfonates”,
Jon Elvar Wallevik, 2003:18, ISBN 82-471-5566-4, ISSN 0809-103X.

“Oblique Loading of Aluminium Crash Components”,
Aase Reyes, 2003:15, ISBN 82-471-5562-1, ISSN 0809-103X.

“Utilization of Ethiopian Natural Pozzolans”,
Surafel Ketema Desta, 2003:26, ISSN 82-471-5574-5, ISSN:0809-103X.

“Behaviour and strength prediction of reinforced concrete structures with discontinuity regions”,
Helge Brå, 2004:11, ISBN 82-471-6222-9, ISSN 1503-8181.

“High-strength steel plates subjected to projectile impact. An experimental and numerical study”,
Sumita Dey, 2004:38, ISBN 82-471-6282-2 (printed version), ISBN 82-471-6281-4 (electronic version), ISSN 1503-8181.

“Alkali-reactive and inert fillers in concrete. Rheology of fresh mixtures and expansive reactions”,
Bård M. Pedersen, 2004:92, ISBN 82-471-6401-9 (printed version), ISBN 82-471-6400-0 (electronic version), ISSN 1503-8181.

“On the Shear Capacity of Steel Girders with Large Web Openings”,
Nils Christian Hagen, 2005:9, ISBN 82-471-6878-2 (printed version), ISBN 82-471-6877-4 (electronic version), ISSN 1503-8181.

”Behaviour of aluminium extrusions subjected to axial loading”,
Østen Jensen, 2005:7, ISBN 82-471-6873-1 (printed version), ISBN 82-471-6872-3 (electronic version), ISSN 1503-8181.

”Thermal Aspects of corrosion of Steel in Concrete”,
Jan-Magnus Østvik, 2005:5, ISBN 82-471-6869-3 (printed version), ISBN 82-471-6868 (electronic version), ISSN 1503-8181.

”Mechanical and adaptive behaviour of bone in relation to hip replacement. A study of bone remodelling and bone grafting”,
Sébastien Muller, 2005:34, ISBN 82-471-6933-9 (printed version), ISBN 82-471-6932-0 (electronic version), ISSN 1503-8181.

“Analysis of geometrical nonlinearities with applications to timber structures”,
Lars Wollebæk, 2005:74, ISBN 82-471-7050-5 (printed version), ISBN 82-471-7019-1 (electronic version), ISSN 1503-8181.

“Pedestrian induced lateral vibrations of slender footbridges”,
Anders Rönnquist, 2005:102, ISBN 82-471-7082-5 (printed version), ISBN 82-471-7081-7 (electronic version), ISSN 1503-8181.

“Initial Strength Development of Fly Ash and Limestone Blended Cements at Various Temperatures Predicted by Ultrasonic Pulse Velocity”,
Tom Ivar Fredvik, 2005:112, ISBN 82-471-7105-8 (printed version), ISBN 82-471-7103-1 (electronic version), ISSN 1503-8181.

“Behaviour and modelling of thin-walled cast components”,
Cato Dørum, 2005:128, ISBN 82-471-7140-6 (printed version), ISBN 82-471-7139-2 (electronic version), ISSN 1503-8181.

“Behaviour and modelling of selfpiercing riveted connections”,
Raffaele Porcaro, 2005:165, ISBN 82-471-7219-4 (printed version), ISBN 82-471-7218-6 (electronic version), ISSN 1503-8181.

”Behaviour and Modelling og Aluminium Plates subjected to Compressive Load”,
Lars Rønning, 2005:154, ISBN 82-471-7169-1 (printed version), ISBN 82-471-7195-3 (electronic version), ISSN 1503-8181.

”Bumper beam-longitudinal system subjected to offset impact loading”,
Satyanarayana Kokkula, 2005:193, ISBN 82-471-7280-1 (printed version), ISBN 82-471-7279-8 (electronic version), ISSN 1503-8181.

“Control of Chloride Penetration into Concrete Structures at Early Age”,
Guofei Liu, 2006:46, ISBN 82-471-7838-9 (printed version), ISBN 82-471-7837-0 (electronic version), ISSN 1503-8181.

“Modelling of Welded Thin-Walled Aluminium Structures”,
Ting Wang, 2006:78, ISBN 82-471-7907-5 (printed version), ISBN 82-471-7906-7 (electronic version), ISSN 1503-8181.

”Time-variant reliability of dynamic systems by importance sampling and probabilistic analysis of ice loads”,
Anna Ivanova Olsen, 2006:139, ISBN 82-471-8041-3 (printed version), ISBN 82-471-8040-5 (electronic version), ISSN 1503-8181.

“Fatigue life prediction of an aluminium alloy automotive component using finite element analysis of surface topography”,
Sigmund Kyrre Ås, 2006:25, ISBN 82-471-7791-9 (printed version), ISBN 82-471-7791-9 (electronic version), ISSN 1503-8181.

”Constitutive models of elastoplasticity and fracture for aluminium alloys under strain path change”,
Dasharatha Achani, 2006:76, ISBN 82-471-7903-2 (printed version), ISBN 82-471-7902-4 (electronic version), ISSN 1503-8181.

“Simulations of 2D dynamic brittle fracture by the Element-free Galerkin method and linear fracture mechanics”,
Tommy Karlsson, 2006:125, ISBN 82-471-8011-1 (printed version), ISBN 82-471-8010-3 (electronic version), ISSN 1503-8181.

“Penetration and Perforation of Granite Targets by Hard Projectiles”,
Chong Chiang Seah, 2006:188, ISBN 82-471-8150-9 (printed version), ISBN 82-471-8149-5 (electronic version), ISSN 1503-8181.

“Deformations, strain capacity and cracking of concrete in plastic and early hardening phases”,
Tor Arne Hammer, 2007:234, ISBN 978-82-471-5191-4 (printed version), ISBN 978-82-471-5207-2 (electronic version), ISSN 1503-8181.

“Crashworthiness of dual-phase high-strength steel: Material and Component behaviour”,
Venkatapathi Tarigopula, 2007:230, ISBN 82-471-5076-4 (printed version), ISBN 82-471-5093-1 (electronic version), ISSN 1503-8181.

“Fibre reinforcement in load carrying concrete structures”,
Åse Lyslo Døssland, 2008:50, ISBN 978-82-471-6910-0 (printed version), ISBN 978-82-471-6924-7 (electronic version), ISSN 1503-8181.

“Low-velocity penetration of aluminium plates”,
Frode Grytten, 2008:46, ISBN 978-82-471-6826-4 (printed version), ISBN 978-82-471-6843-1 (electronic version), ISSN 1503-8181.

“Robustness studies of structures subjected to large deformations”,
Ørjan Fyllingen, 2008:24, ISBN 978-82-471-6339-9 (printed version), ISBN 978-82-471-6342-9 (electronic version), ISSN 1503-8181.

“Constitutive modelling of morsellised bone”,
Knut Birger Lunde, 2008:92, ISBN 978-82-471-7829-4 (printed version), ISBN 978-82-471-7832-4 (electronic version), ISSN 1503-8181.

“Experimental Investigations of Wind Loading on a Suspension Bridge Girder”,
Bjørn Isaksen, 2008:131, ISBN 978-82-471-8656-5 (printed version), ISBN 978-82-471-8673-2 (electronic version), ISSN 1503-8181.

“Cracking Risk of Concrete Structures in The Hardening Phase”,
Guomin Ji, 2008:198, ISBN 978-82-471-1079-9 (printed version), ISBN 978-82-471-1080-5 (electronic version), ISSN 1503-8181.

“Modelling and numerical analysis of the porcine and human mitral apparatus”,
Victorien Emile Prot, 2008:249, ISBN 978-82-471-1192-5 (printed version), ISBN 978-82-471-1193-2 (electronic version), ISSN 1503-8181.

“Strength analysis of net structures”,
Heidi Moe, 2009:48, ISBN 978-82-471-1468-1 (printed version), ISBN 978-82-471-1469-8 (electronic version), ISSN 1503-8181.

“Numerical analysis of ductile fracture in surface cracked shells”,
Espen Berg, 2009:80, ISBN 978-82-471-1537-4 (printed version), ISBN 978-82-471-1538-1 (electronic version), ISSN 1503-8181.

“Subject specific finite element analysis of bone – for evaluation of the healing of a leg lengthening and evaluation of femoral stem design”,
Sune Hansborg Pettersen, 2009:99, ISBN 978-82-471-1579-4 (printed version), ISBN 978-82-471-1580-0 (electronic version), ISSN 1503-8181.

“Evaluation of fracture parameters for notched multi-layered structures”,
Lingyun Shang, 2009:137, ISBN 978-82-471-1662-3 (printed version), ISBN 978-82-471-1663-0 (electronic version), ISSN 1503-8181.

“Modelling of Dynamic Material behaviour and Fracture of Aluminium Alloys for Structural Applications”,
Yan Chen, 2009:69, ISBN 978-82-471-1515-2 (printed version), ISBN 978-82-471-1516-9 (electronic version), ISSN 1503-8181.